RESISTIVITY STRUCTURE BENEATH SAKURAJIMA AND MERAPI VOLCANOES INFERRED FROM MAGNETOTELLURIC(MT) SURVEY(Dissertation_全文)

AUTHOR(S):

Aradiy, Edy Muhammad

RESISTIVITY STRUCTURE BENEATH SAKURAJIMA AND MERAPI VOLCANOES INFERRED FROM MAGNETOTELLURIC (MT) SURVEY

by

Edy Muhammad Arsadi

Department of Geology and Mineralogy
Kyoto University
1994

CONTENTS

ACKNOWLEDGMENTS

My first and most sincere thanks go to my advisor, Prof. Susumu Nishimura, for his encouragement, guidance and fatherly supervision. Despite his tight schedule, he has always been kind enough to share time with me to discuss this research work. I also wish to thank my home advisor, Mr. Suparka S., for his kind support during research in Indonesia. I would like to express my appreciation to Dr. Ikuo Katsura for his patient guidance, valuable discussion and great encouragement. I wish to thank Dr.Tohru Mogi for permitting me to use the MT program pertaining to this research work and for valuable discussion.

The field works both at Sakurajima and at Merapi volcanoes were completed through the effort of a number of people. Mr. A. Jomori and Dr. K. Kusunoki whose expertise in the field was a major factor in acquiring the data obtained during the field work at Sakurajima volcano. I am also indebted to Dr.Hery Harjono, Mr. H. Permana, Mr. Kamtono, Mr. B.Widoyoko and Mr. Yayat Sudrajat for their assistance in obtaining the data measuring at Merapi volcano. My thanks and regards also expressed to Prof. J. Nishida, Associate Prof. M. Torii and Dr. T. Tagami for discussion while writing this thesis. Prof. S. Banno and Prof. K. Chinzei are thankfully acknowledged for critical reading of this thesis and suggesting several points to improve it.

The author would like to thank the Government of Japan for the financial assistance through the Japan Society for the Promotion of Science (JSPS). I wish to thank the Department of Geology and Mineralogy, Sakurajima Volcanological Observatory and Data

Processing Center of Kyoto University for providing excellent services and facilities. I am also indebted to the Research and Development Center for Geotechnology, Indonesian Institute of Sciences, Volcanological Survey of Indonesia for their excellent support and understanding.

I wish to extend my gratitude and appreciation to all of the members of the Physical Geology Laboratory, librarian and administration staff of Kyoto University for their encouragement and cooperation. I am also indebted to all of the members of the Geophysical Laboratory, all of my colleagues at Research and Development Centre for Geotechnology-LIPI, especially Dr.Jan Sopaheluwakan, Mr. A.Subardja and Mr. Herryal Z.Anwar for their support and criticism for improving the manuscripts.

Finally, special thanks go to my wife Ilah and my sons Ari and Yuki for their patience and understanding during the research period.

ABSTRACT

Sakurajima volcano in Japan and Merapi volcano in Indonesia are very active volcanoes with different eruptive types at least since 1955. An Extremely Low Frequency Magnetotelluric (ELF-MT) survey has been applied to obtain the resistivity structures beneath the volcanoes related to their volcanic activities.

Sakurajima volcano shows highly inhomogeneous and anisotropic resistivity structure inferred from a tensor impedance analysis. Three main trends of the principal axis of apparent resistivity are recognized at the Sakurajima volcano; north-south, and east-west direction for the results using low frequency and concentric trend for high frequency MT. These trends correspond to the regional and local structure around the Sakurajima volcano.

Based on two-dimensional model analysis using finite element method, four layers of the resistivity structure beneath Sakurajima volcano are calculated. The resistivity down to the depths of 400 to 600 m varies between 50 and 3,000 ohm-m, representing various lithologies such as lava flows from Sakurajima volcano, unconsolidated pyroclastic deposits from the Aira caldera and the Kekura Formation. The Sakurajima volcano overlies a conductive basement layer obtained. The basement is evident in controlled source audio magnetotelluric (CSAMT) and time domain electromagnetic (TDEM) data, especially at the southern part of the volcano with resistivities less than 10 ohm-m. The conductive layer also represents the Kekura Formation. The heat related to magmatic activity or the presence of the minerals as results of

hydrothermal process is responsible for the low resistivities.

The resistivity of the conductive basement beneath Merapi volcano is 25-50 ohm-m. Groundwater, convective heat from a shallow magma reservoir and the presence of clay minerals may be the cause of the low resistivities. The volcanic body shows resistivities from 100 to 250 ohm-m, whereas the rocks just beneath the summit exhibit values of more than 1,000 ohm-m to the depths of 2 km. The resistivity structure of the volcano shows striking temporal changes in the ELF-MT data before and during the eruption in 1992. This suggests the MT method as a good tool for monitoring Merapi volcanic activity.

Different eruption types of Sakurajima and Merapi volcanoes may be due to the difference in viscosities related to their chemical compositions, variations in the content of potential volatiles, the presence of solid fragments in magma and temperature. The high resistivity at the summit of Merapi volcano down to the depth of 2 km suggests that the rocks filling in the vent contributes to the process increasing magma viscosity. Themal conditions beneath Sakurajima and Merapi volcanoes, which controls magma viscosity, may be different. The conductive basement of Sakurajima volcano shows lower resistivity than beneath Merapi volcano.

1. BACKGROUND AND OBJECTIVE OF THE MT SURVEY AT SAKURAJIMA AND MERAPI VOLCANOES

The presence of volcanoes has concerned mankind since the beginning of history. It gives invaluable natural resources or is a threat to human life. Among natural disasters, volcanic eruption cannot be neglected because it will cause socio-economical problems. The objective of the research on the prediction and prevention of the volcanic eruptions has gradually gained interest because of the increasing populations and economic developments in potentially dangerous areas. At present, application of geophysical methods makes significant contributions not only to the search geothermal part of, for energy but also to surveillance and prediction of volcanic eruptions.

The type of volcanic activities varies from one volcano to another. The types of activities may be related to the composition of magma, regional tectonic and geologic conditions of each volcano, and its adjacent area. Furthermore, the subsurface geologic condition of each volcano such as the presence of groundwater, fracture zones or faults on and around a volcano, thermal accumulation and the presence of magma chamber, plays a significant role in eruption process.

Study on the resistivity structure beneath an active volcanic area is useful for providing information about distribution of conductive zone which has strong relationship with magmatic activities. Investigating resistivity in active volcanic areas, however, encounters a serious barrier of topographic and eruptive conditions. Magnetotelluric (MT) method

promises to eliminate difficulties caused by topographic effects. The advantages of the application of the MT method in volcanic areas are the development of field equipments which are small, available at relatively low costs, and simple to operate in the field for acquiring data to depths of 3-5 km. By recent developments, measurement is made in relatively short time, therefore the MT method can be used for covering a wide area. However, the noise coming from artificial electromagnetic waves still remains a problem.

The application of MT method in volcanic area has mainly developed in two areas. One is to search for geothermal energy potential (e.g., Galanopoulos et al., 1991, Aiken et al., 1991, Takasugi et al., 1992, Ehara, 1992 and Mogi et al., 1993). The other is to study the subsurface resistivity structure to obtain better understanding of the geological structure beneath an active volcano and relation to its activities.

Ballestracci (1982) carried out MT profiling on Strombolian volcano. He found anomalies of resistivities at shallow depths which he associated with intrusive dikes and active lava channels. From these data he discussed the activity of a Strombolian volcano. Ortiz et al. (1986) were able to identify the presence of a shallow magma chamber beneath Timanfaya volcano, and the double depressions of Teide volcano. A water reservoir, fracture zone that containing meteoric water, fresh water lenses and sea water have been detected beneath Izu-Oshima volcano, Japan (Utada et al.,1990, Ogawa et al., 1990). Ogawa et al. (1992) made MT investigation at the same location after Izu-Oshima 1986 eruption. He found that resistivity of the basement differed before and after the eruption. Ingham (1992) carried out MT soundings on White Island

volcano, New Zealand. The result suggests that the acid hydrothermal system which is believed to underlie low-resistivity crater region coming up close to the surface near the active fumarole. All of the results show that the resistivity structure beneath an active volcano has strong relation with its activities, however, the main control of the resistivity values varies from one to another.

Sakurajima volcano is one of the highly active volcanos in Japan. It is situated in the Kagoshima Bay, southern Kyushu island. There are four calderas and the hypothetical Anraku cryptocaldera in southern Kyushu. The largest Aira caldera is located in the Kagoshima Bay. The Kagoshima Bay itself is characterized by graben-like topography and low gravity anomalies (Yokoyama and Ohkawa, 1986). Sakurajima volcano is a post caldera stratocone formed on the southern rim of the Aira caldera after the major collapse (Aramaki, 1984). The volcano is composed of two steep strato cones, Kita-dake (north-summit, 1118 m) and Minami-dake (south-summit, 1060 m) and is almost totally surrounded by sea. Sakurajima volcano had four major eruptions and produced large quantities of lava in 1476, 1779, 1914 and 1946. From time to time, Sakurajima volcano has repeated small eruptions, emitting a great quantity of volcanic ash, sand and many incandescent volcanic bomb. Except for minor activities in 1935, 1938 and 1939, Sakurajima volcano has remained quiet after the 1914 eruption until 1946. South summit is active at present, emitting ash and gas, occasionally accompanied by lithic blocks and pumice from summit craters but no lava flow were seen after eruption in 1955 (Yokoyama, 1986). The rocks of Sakurajima are pyroxene andesite and dacite with SiO_2 content from 57

to 67 weight percents (Fukuyama and Ono, 1981). Based on the data obtained by precise leveling and electronics distance meter (EDM) surveys at and around Sakurajima, the relation between the volcanic activity and vertical deformation has been studied and reveals significant changes in vertical deformation related to movement of magma in the volcano (Sakurajima Volcano Observatory, 1988).

Merapi volcano is located in Central Java, Indonesia. Tectonically, the volcano lies at the intersection of two faults, one runs from south-west to north-east and other from south to north. Merapi volcano represents an andesitic-strato volcano with altitude 2,986 meters above sea level and one of the most active volcanoes in the Sunda arc. Merapi volcano itself may be geologically divided into two groups. The older products of Merapi dominate the north, east and southeastern slopes of the volcano. The younger deposits which continued to develop until present are confined in the southwest portion of the volcano. The known history of eruptions of Merapi volcano goes back to the year 1006. This eruption was described in general by Bemmelen (1949). More detailed description of the periodicity of Merapi activities began in early 19th century (Bemmelen, 1949). It was concluded that the period of eruption ranges between 1 to 7 years, while the period of apparent dormancy is 1 to 12 years. During the last 50 years Merapi has had relatively similar eruptions which came to be classified as the "Merapi type". The "Merapi type eruptions" is characterized by collapse of the lava dome or parts of it (Merapi Volcano Observatory, 1990). During the lava dome development, the gravity sliding usually occur due to the position of the dome which overlies an inclined slope of Merapi summit. The sliding are usually

accompanied by the glowing cloud or "nuee ardante" of sliding. The rock composition is in general pyroxene-hornblende andesite. Silica contents ranges between 50 - 57 % (Merapi Volcano Observatory, 1990). The most recent Merapi eruption occurred on February 2, 1992.

The thermal effect of volcanic eruption is strongly dependent on the chemical components of magma and magmatic gas. Gas in volcanic system may be derived from the magma itself during differential process and expansion of volatile matters. Since 1955 eruption of Sakurajima volcano is generally characterized by emission of ash and gas occasionally accompanied by lithic block and pumice, while eruption of Merapi volcano is characterized by lava flows and lava dome building. Difference in thermal effect, chemical and magma volume characters between Sakurajima and Merapi volcanoes suggests different resistivity underground structures in both volcanoes.

Sponsored by Kyoto University, Japan, Research and Development Centre for Geotechnology, Indonesian Institute of Sciences (RDCG-LIPI) and Japan Society for the Promotion of Science (JSPS), a study on resistivity structure beneath active volcano using MT method has been carried out at Sakurajima and Merapi volcanoes. The objective of the research is to compare the resistivity structure between Sakurajima and Merapi volcanoes which have different eruptive types. At present the two volcanoes are very active and exist near or are surrounded by densely populated areas. Since both have volcano observatories, some information have been available from other survey methods. Hence these areas are ideal locations for a study of resistivity structure related to volcanic activities although the resistivity structure beneath both

volcanoes have not yet being well understood.

The main objectives of the present research are;

1) To outline conductivity anomalies beneath Sakurajima and Merapi volcanoes in which the conductivity anomalies have strong relation with geologic structure and thermal accumulation.
2) To obtain a better understanding about resistivity structure and to relate to the structure with different eruptive types of Sakurajima and Merapi volcanoes.

This is the first time that the MT method has been applied in the study of the resistivity structure especially in Merapi volcano. MT measurements at Sakurajima volcano was started in 1985 supported by Kyoto University and in 1989 at Merapi volcano supported by RDCG-LIPI. Data analyses and additional MT measurement at both volcanoes have been sponsored by JSPS since 1991. In 1992 and 1993 MT measurements were carried out during eruptive stage of Merapi volcano to reveal the changes of resistivity structure. Controlled source audio magnetotelluric (CSAMT) and time domain electromagnetic (TDEM) methods also have been done at Sakurajima volcano in 1987, 1989, 1990 and 1993. These data will be utilised in discussion of resistivity structure beneath Sakurajima volcano. Since information of subsurface geological structure underneath Merapi volcano is scarce, the gravity and magnetic methods have been applied simultaneously during MT survey (Arsadi, et al. 1991).

Since geologic setting, volcanic activity, instrumentation, data

acquisition and analyses have some differences between Sakurajima and Merapi volcanoes, the explanation of the research will be presented separately in Part 2 and Part 3. Subsurface volcanic structure which is reflected and interpreted from the resistivity structure is the main part of discussion of each part and each part is closed by a summary. In Part 4, comparisons are made between the resistivty structures of Sakurajima and Merapi volcanoes related to their eruptive activities and resistivity structure.

2. RESISTIVITY STRUCTURE BENEATH SAKURAJIMA VOLCANO

2.1. Introduction

The Sakurajima volcano is one of the most highly active volcano in Japan, located at Kagoshima Bay, southern Kyushu (Fig.1). The Sakurajima volcano is a post-caldera stratocone formed on the southern rim of the Aira caldera after the major collapse of the Aira caldera (Aramaki, 1984). Sakurajima volcano was originally a volcanic island. In 1914 the island was connected with the Osumi Peninsula by lava flows.

Several geophysical studies have been carried out on Sakurajima volcano using various methods, especially by Sakurajima Volcano Observatory, Kyoto University. Among them, Yokoyama (1961, 1986), Abe et al. (1975) and Nishimura et al. (1988, 1989a) made gravity surveys at and around the Sakurajima. The Bouguer anomaly pattern revealed shape of the Aira caldera and supported that Sakurajima volcano situated on the southern rim of caldera where the basement of the caldera has a funnel shape. Blank et al. (1966), Matsuzaki and Utashiro (1966) estimated a dipole source of magnetic anomaly at Sakurajima using the results of the aeromagnetic surveys. Ono et al. (1978) found out that a large attenuation of seismic wave occurs under Sakurajima volcano and the Aira caldera. It suggests the existence of high temperature rocks or a magma reservoir causing especially strong S-wave attenuation (Kamo et al., 1977, 1980).

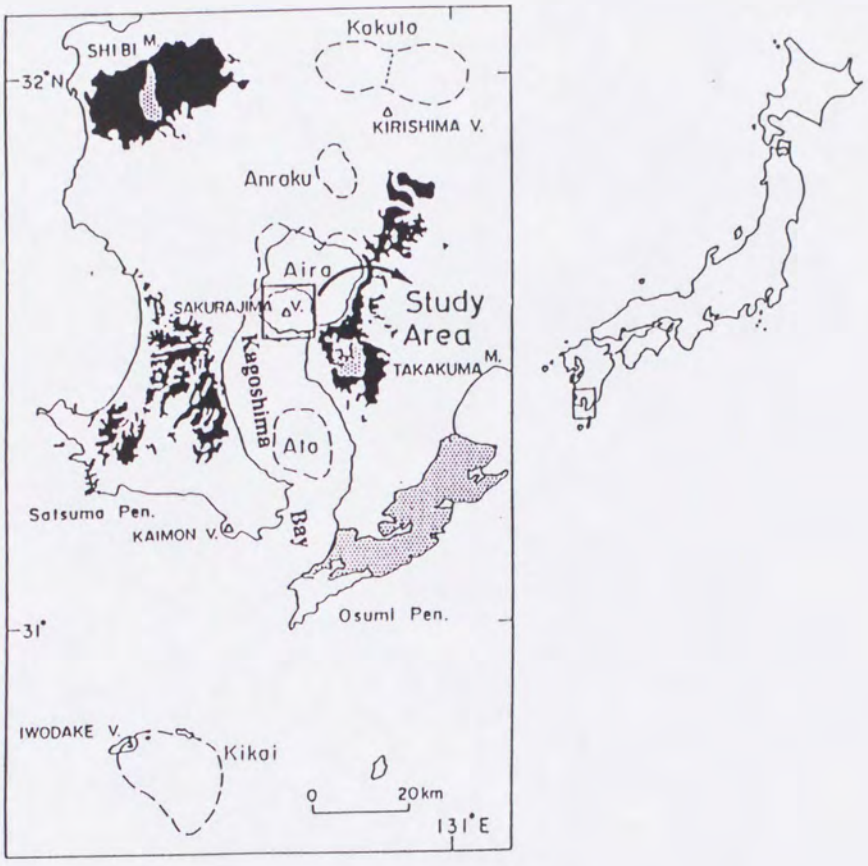

Fig.1. Location of study area. Black: Shimanto Group, dotted: granite, broken line: caldera boundary, triangle: volcano. Geological setting is based on Yokoyama and Ohkawa (1986).

The volcanic earthquakes of Sakurajima volcano have been monitored at Sakurajima Volcano Observatory, Kyoto University. The hypocenters especially of A-type earthquakes are distributed on a trend from the active vent toward SSW direction with increasing depth (Nishi, 1978). This trend is considered to be a pathway for ascending magma. Yokoyama (1986) discussed the pressure source of magma chamber from the geodetic data around Sakurajima. Ishihara (1988) proposed the exitence of a magma reservoir located deeper than 3 to 4 km below sea level beneath the south summit of volcano based on geodetic and seismological evidence. On the basis of drilling results, Hayasaka and Oki (1971) reported the subsurface geological structure of Kagoshima area.

The electrical survey was done by Yukutake et al. (1980) using Schlumberger array method and the dipole mapping around Sakurajima volcano. Another resistivity estimation was done by MT method using natural ELF electromagnetic waves (Nishimura and Mogi, 1986, Karaushi et al., 1989). They discussed the result mainly on the basis of resistivity value distribution without subsurface resistivity model. Therefore the resistivity structure beneath Sakurajima volcano has not been clear yet.

In this research, resistivity structure beneath Sakurajima volcano is presented based on two-dimensional (2-D) model derived from ELF-MT survey. Conjunction with the results of Controlled Source Audio Magnetotelluric (CSAMT) and Time Domain Electromagnetic (TDEM) surveys, the resistivity structure of Sakurajima volcano will be discussed.

2.2. Geologic setting and volcanic activity

There is a chain of large and small calderas and active volcanoes at the southern Kyushu island (Fig.1). One of the calderas is Aira caldera situated at Kagoshima Bay. The Kagoshima Bay itself is characterized by a graben-like topography and low-gravity anomalies (Yokoyama, 1986.a). According to Aramaki (1984), the basement complex called the Shimanto Group is made up of highly deformed Mesozoic to Paleogene sediment of shale, sandstone, conglomerate and minor pillow lava. The Shimanto Group is broken by step faulting and overlain by a densely welded pyroclastic flow deposits about 2.9 Ma in age (Shibata et al., 1978). This means that in the last 2.9 Ma, the western and eastern sides of the Kagoshima Bay were faulted by as much as 800 m. The N-S striking graben-like depression of the Kagoshima Bay was discovered by drilling and air-gun surveys (Hayasaka and Oki, 1971; Chujo and Murakami, 1976). The graben is horizontally filled up by the marine Kekura Formation mainly composed of volcanic materials.

Formation of Aira caldera and the building of Sakurajima volcano at southern rim of caldera were described by Aramaki (1984). Aira caldera is a Valles-type caldera covering an area about 20 km X 20 km. However, the underground structure of Aira caldera appears to be different from that of the typical Valles-type caldera. In Aira caldera, there is no evidence supporting the presence of a ring fracture such as ring fault or circular arrangement of lava dome, resurgent central dome, etc. Sakurajima volcano started to grow as an insular volcano, surrounded by the sea of the Kagoshima Bay, but during the 1914 eruption lava flows

buried the eastern strait and the volcano was connected to the Osumi Peninsula. At present the volcano is composed of two steep strato cones, Kita-dake (north summit, 1,118 m) and Minami-dake (south summit, 1,060 m) with a few parasitic cone at their flank and foot and surrounded by gently sloping foot hills. The major constituents of the two cones are coarse pyroclastic materials associated with lesser amount of lava flows and fan deposits (Aramaki, 1984).

Within the limits of the recorded history, Sakurajima volcano started its volcanic activity approximately 13,000 years ago and had 4 major eruptions, producing large quantities of lava in 1471-1476, 1779, 1914 and 1946. The unshaded areas are also covered with the lava flows of historically very old and different eras (Fig.2). The lava flows are of andesitic type with phenocrysts of mainly plagioclase, augite and hyperthene, and occasionally magnetite and olivine (Fukuyama, 1978). There are nodules of granodiorite in the Minami-dake ejecta. However, an 800 m borehole drilled at Koike did not reach the basement (Aramaki, 1984).

From time to time, Sakurajima volcano has repeated small eruptions and emitted a great quantity of volcanic ash, sand and many incandescent bomb. Except for minor activities in 1935, 1938, and 1939, the Sakurajima became quiet after 1914 eruption until 1946. In 1955 the Minami-dake burst into eruption. It has erupted intermittently until the present, emitting ash and gas, occasionally with lithic block and pumice, but no lava flow was seen (Yokoyama, 1986). During the period from 1955 to 1975, more than 10^8 tons of volcanic ash was ejected from the summit crater (Kamada, 1975).

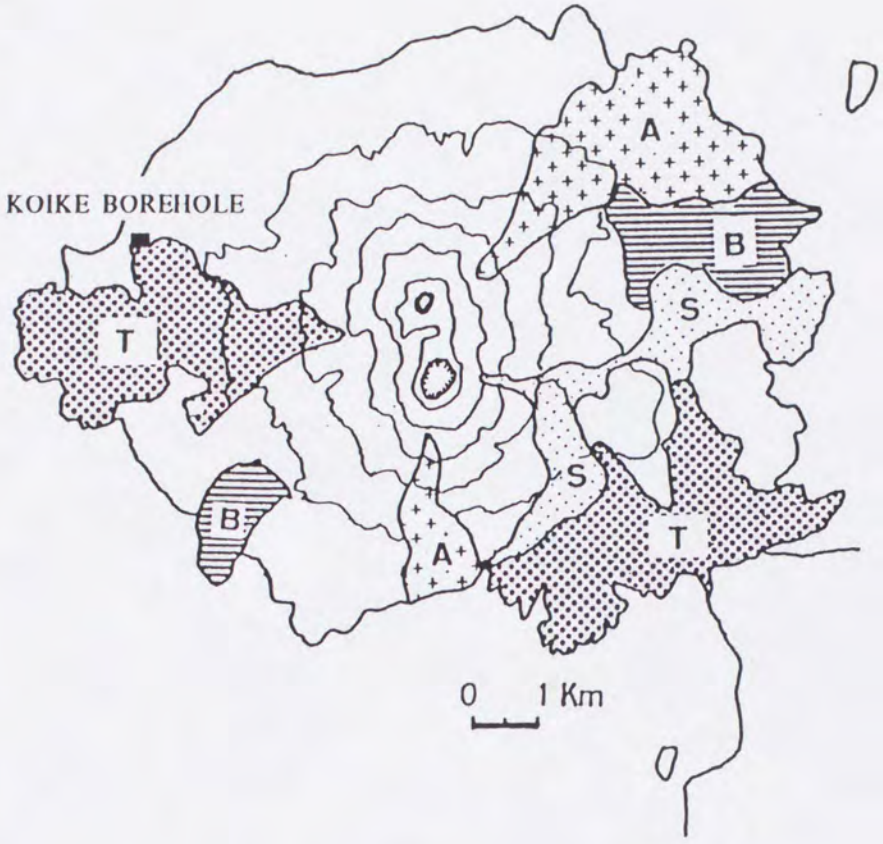

Fig.2. Simplified map of the lava flow distribution of Sakurajima volcano (from Fukuyama and Ono, 1981). Contour line interval is 200 m in altitude. B:Bunmei (AD. 1471, 1476 eruptions), A:An'ei (1779), T:Taisho (1914-15), S:Showa (1946) lava flows. The blank parts are also covered with the lava flows of historically very old and different eras.

2.3. ELF-MT survey

2.3.1. ELF-MT method and Instrumentation

The magnetotelluric (MT) method is an electromagnetic exploration techniques to estimate resistivity structure of subsurface layers by measuring both electric and magnetic fields at the surface. The method utilizes the physical relationships between magnetic field (micropulsation), telluric current and resistivity structure (Cagniard, 1953). The basic concept for the MT method is simple; at an observation site in which subsurface information will be estimated, tangential (horizontal) components of the electric and magnetic fields caused by natural energy sources are measured together. The ratio of intensity of the electric field to the magnetic field is a quantity which has the unit of the electrical impedance. This impedance is a function of electrical properties of the medium. Determination of the impedance at a series of frequencies provides information about the profile of electrical resistivity as a function of depth in the earth.

Since the earth's magnetic field varies with time, current may be induced in the earth which cannot be explained in terms of the direct current theory, using Maxwell's equations. There are two fundamental assumptions in the MT approach. First, the Earth is horizontally layered with each layer being electrically isotropic-homogeneous. Second, the natural electromagnetic waves are plane waves impinging to the earth. The basic equation for apparent resistivity measured by MT is,

$$\rho_a = \frac{1}{\varpi\mu}\frac{E_x}{H_y}^2 = \frac{1.26 \times 10^5}{f}\frac{E_x}{H_y}^2 \quad \text{ohm-m} \qquad (1)$$

where ρ_a is apparent resistivity in ohm-m, μ (H/m) is magnetic permeability of free space, ϖ (radian/s) is angular velocity, E_x is electric field in V/m, H_y is magnetic field in A/m and f is frequency in Hz (Cagniard, 1953).

The amplitude of the electromagnetic field when propagating into the earth will decrease with increasing depth, as a consequence of transformation of electromagnetic energy to heat. The depth in which amplitude of the field reduces to the fraction 1/e, is defined as skin depth. Relationship between skin depth, resistivity of the medium and frequency is,

$$\delta = 1/6.28\,[10\,\rho/f]^{1/2} = 503\,[\,\rho/f\,]^{1/2} \quad \text{meter} \qquad (2)$$

where δ is skin depth in meter, ρ is resistivity of medium in ohm-m and f is frequency in Hz. Skin depth as a function of resistivity and frequency can be seen in Fig.3.

The fluctuations of the natural electromagnetic field may occur over period ranging from millisecond to centuries. General characteristics, classifications and basic properties of the natural electromagnetic field, were described by Keller and Frischnecht (1966), Kaufmann and Keller (1981) and Parkinson (1983). The natural electromagnetic field of the earth arises from variety of causes. Variations with periods less than one millisecond are not usually used in resistivity

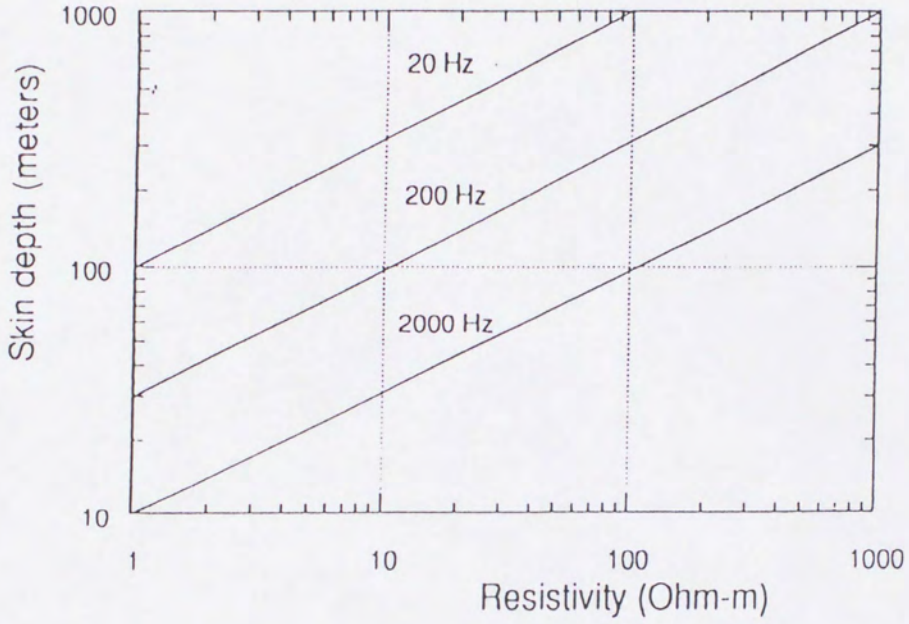

Fig.3. Skin depth as a function of resistivity and frequency.

determinations, since rapid variations do not penetrate very far into the earth and oscillation with periods longer than one day are usually excluded from the frequency range of interest.

The natural electromagnetic field with frequency less than one Hz appears from some interaction between radiation or particle matter emitted by the sun and the earth's atmosphere and magnetosphere. Frequencies of more than one Hz are contributed by meteorological activities, in particularly lightning associated with thunder (storm). Lightning which occurs far from measuring site provides a surprisingly uniform source for electromagnetic energy. The electromagnetic field that generated from lightning strokes propagates to greater distances at particular frequencies. The higher frequency components of the electromagnetic field are attenuated. The lower frequency components are enhanced by a wave-guide propagation, with energy being reflected back and forth between the conductive surface of the earth and the ionized layer of air in the ionosphere. This energy excites a resonance in the earth-ionosphere cavity, and the best known of these phenomena is called "Schumann resonance" (Parkinson, 1983). Its frequencies are:

$$f = 7.8\,(n(n+1)/2)^{1/2} \quad \text{Hz} \quad ; n = 1, 2, 3, \ldots\ldots \qquad (3)$$

An analysis of the orthogonal components of the magnetic field in the extremely low frequency (ELF) range, 4-60 Hz, was done by Ogawa et al. (1969, 1979) and Sentman (1987) with spectrum as shown in Fig.4. The MT method using electromagnetic field in ELF band is called the ELF-MT method.

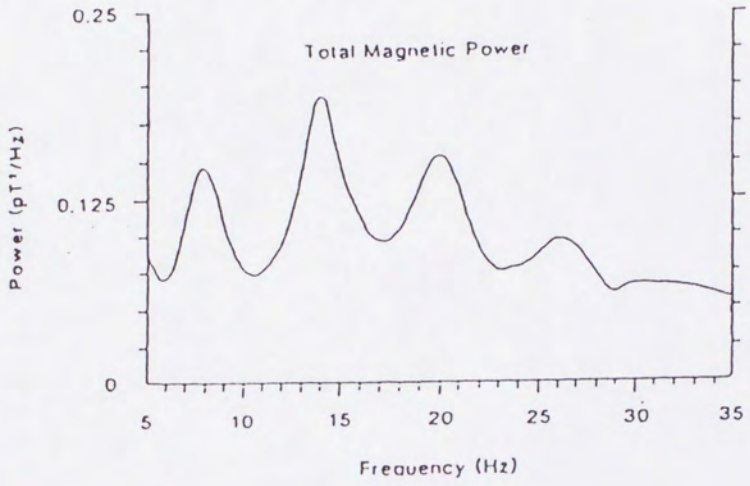

Fig.4. A one-hour average of the total horizontal magnetic power over the frequency range 5-35 Hz. At some frequencies appear the Schumann resonance peaks (after Sentmann, 1987).

The man-made portions contributing to frequencies above one Hz are from commercial power distribution system and radio station. If the source is far enough, it is conceivable that the field from these man-made source can be used effectively in studying resistivity (Handa, 1985., Utada et al., 1990), however, in many cases the sources are located too close to observation sites. It is difficult to handle their effects mathematically.

Eq.(1) is derived based on assumption that layers of the earth are homogeneous and isotropic. In the presence of lateral inhomogeneities, the impedance is usually represented by a function of electrical properties of medium, orientation of sensor axes, and direction of arrival of primary field. The tensor impedance method, which is independent of measuring direction, was discussed by Cantwell (1960), Swift (1967), Sims (1971), Vozoff (1972), and Reddy (1974).

Since the component of magnetic field in z direction (vertical) is neglected, the formulation of tensor impedance is:

$$\begin{bmatrix} Ex \\ Ey \end{bmatrix} = \begin{bmatrix} Zxx & Zxy \\ Zyx & Zyy \end{bmatrix} \begin{bmatrix} Hx \\ Hy \end{bmatrix} \qquad (4)$$

Where Zxx, Zxy, Zyx, and Zyy are elements of tensor impedance, Hx, Hy, Ex, and Ey are components of magnetic and electric fields in x and y direction.

Swift (1967) used auto-spectra, cross-spectra and coherency to calculate tensor elements with formulations:

Auto-spectra : $< ExEx^* >, < EyEy^* >$ (5)

$< HxHx^* >, < HyHy^* >$

Cross-spectra : $< ExEy^* >, < ExHx^* >, < ExHy^* >$ (6)

$< EyHx^* >, < EyHy^* >, < HxHy^* >$

and simplified form of coherency is :

$$\text{Coherency} \quad (AB) = \frac{< AB^* >}{(< AA^* >< BB^* >)^{1/2}} \qquad (7)$$

Where * is complex conjugate, and the coherency is a quantitative of linear relationship between two data series.

The tensor impedance element are :

$$Zxx = \frac{|Ex|}{|Hx|} \left(\frac{Coh(ExHx) - Coh(ExHy)\,Coh(HyHx)}{1 - |Coh(HxHy)|^2} \right) \qquad (8.a)$$

$$Zxy = \frac{|Ex|}{|Hy|} \left(\frac{Coh(ExHy) - Coh(ExHx)\,Coh(HxHy)}{1 - |Coh(HxHy)|^2} \right) \qquad (8.b)$$

$$Zyx = \frac{|Ey|}{|Hx|} \left(\frac{Coh(EyHx) - Coh(EyHy)\,Coh(HyHx)}{1 - |Coh(HxHy)|^2} \right) \qquad (8.c)$$

$$Zyy = \frac{|Ey|}{|Hy|} \left(\frac{Coh(EyHy) - Coh(EyHx)\,Coh(HxHy)}{1 - |Coh(HxHy)|^2} \right) \qquad (8.d)$$

Where $Ex = (<ExEx^* >)^{1/2}$ etc., are the Fourier spectra and Coh is coherency.

For a Cartesian coordinate rotation, when the new axes are rotated ϕ degrees clockwise as in Fig.5, the transformed field components are:

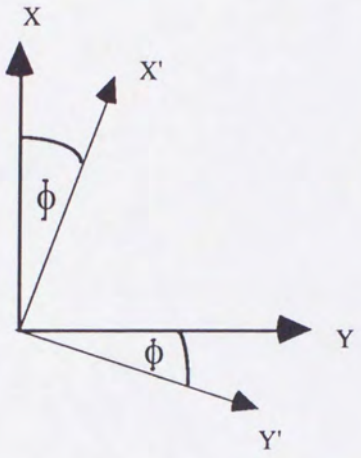

Fig.5 Axis rotation in the tensor impedance analysis

$$E' = \beta E \text{ and } H' = \beta H$$

Where

$$\beta = \begin{pmatrix} \cos\phi & \sin\phi \\ -\sin\phi & \cos\phi \end{pmatrix}$$

To transform z tensor, such that :

$$E' = Z' H'$$

Where Z' are (Vozoff, 1972);

$$2Z'xx(\phi) = (Zxx + Zyy) + (Zxx - Zyy)\cos 2\phi + (Zxy + Zyx)\sin 2\phi \quad (9.a)$$

$$2Z'xy(\phi) = (Zxy - Zyx) + (Zxy + Zyx)\cos 2\phi - (Zxx - Zyy)\sin 2\phi \quad (9.b)$$

$$2Z'yx(\phi) = -(Zxy - Zyx) + (Zxy + Zyx)\cos 2\phi - (Zxx - Zyy)\sin 2\phi \quad (9.c)$$

$$2Z'yy(\phi) = (Zxx + Zyy) - (Zxx - Zyy)\cos 2\phi - (Zxy + Zyx)\sin 2\phi \quad (9.d)$$

For an isotropic or layered earth,

$Zxx = Zyy = 0$ and $Zxy = -Zyx$

Then upon any rotation,

$Z'xx = Z'yy = 0$

For two-dimensional earth with the measuring axes aligned with the structure, the impedance tensor is characterized by;

$Zxx = Zyy = 0$ and $Zxy = Zyx$

The structural strike and the perpendicular direction are defined as the principal axes of tensor impedance. Upon rotational away from the principal directions, diagonal elements appear, but are such that;

$Z'xx = -Z'yy$

For obtaining principal axes of tensor impedance, the axes is rotated until the sum $Z'xx + Z'yy$ should vanish for an ideal two-dimensional impedance tensor. When analyzing impedance tensor from actual field data, however, a simple rotation of the impedance tensor does not always yield a direction where $Z'xx = Z'yy = 0$.

Vozoff (1972) proposed the formulation for obtaining direction of principal axes of tensor impedance is :

$$\tan 4\phi = \frac{(Zxx - Zyy)(Zxy + Zyx)^* + (Zxx + Zyy)^*(Zxy - Zyx)}{|Zxx - Zyy|^2 - |Zxy + Zyx|^2} \quad (10)$$

where ϕ is azimutal angle of principal axes, where Zxx + Zyy is minimum.

The apparent resistivities for two-dimensional structure can be calculated from the principal values of the impedance tensor.

$$\rho_a = \frac{1.26 \times 10^5}{f} |Z|^2 \qquad (11)$$

Where Z is principal value of impedance tensor.

Skew is a quantity to see the dimensional structure. If skew value is large, structure at the site should be three-dimensional in that frequency range (Vozoff, 1972). The Skew is defined by:

$$\text{Skew} = \frac{|Zxx + Zyy|}{|Zxy - Zyx|} \qquad (12)$$

In the present research, the natural electromagnetic field in the ELF-band, 4 - 60 Hz, was used as source of MT investigation. This band, particularly Schumann resonance frequencies (7.8, 14.2, 20.5 and 39 Hz), is convenient to pick up because of strong power of signals. The artificial electromagnetic source at very low frequency (VLF), 17.4 kHz generated for military purposes is also observed to estimate the resistivity of shallower layer.

Two kinds of electromagnetic field measurements were applied in this research. The first uses wide-band channel where all frequencies in the ELF-band are measured. The second uses narrow-band channel. In narrow-band outputs of magnetic and electric signals are amplified and the selected waves are band-passed to have peak responses at desired frequencies of Schumann resonance and in the certain VLF. The ELF-MT system is basically the same as that used by Handa et al. (1985), Mogi et al. (1986, 1988), Nishimura et al. (1986) and Katsura (1990). The ELF-MT meter is composed of induction coils for ELF and VLF bands, a pair of electrodes, and two amplifier units for magnetic and electric fields (Fig. 6).

2.3.2. Data acquisition of ELF-MT survey

In this study MT soundings were carried out at 41 sites around Sakurajima volcano as shown in Fig.7. Magnetic and electric signals were measured through wide-band and narrow-band channels. The field works were done in September 1985, March 1986 and March 1988. The observation sites are mostly along the shore or through a route where a road or a path is available. Unfortunately at the middle part or near the cones area is inaccessible because of very steep slope and eruption activities of volcano.

Two kinds of apparent resistivities of each frequency are taken out both through narrow-band and wide-band channels, ρ_{axy} and ρ_{ayx}. ρ_{axy} or ρ_{ayx} is an apparent resistivity where sensor of electric field in x or y

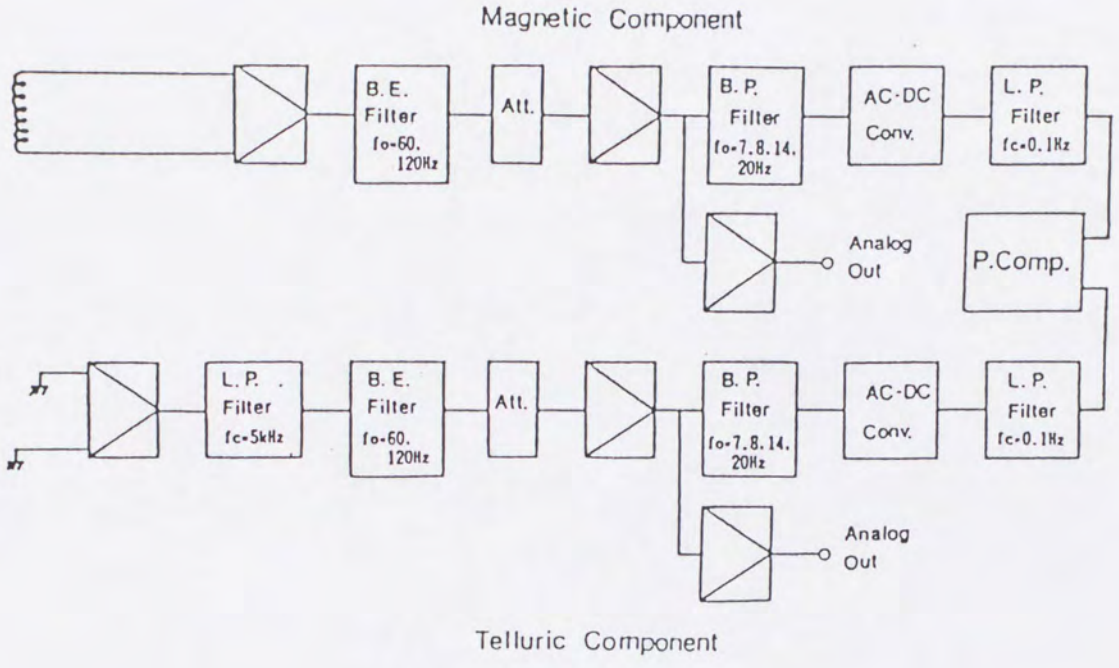

Fig.6. A block diagram of the ELF-MT meter system which is used to measure magnetic and telluric components in the field. f_o is the center frequency of the band-pass (B.P.) filter and band eliminate (B.E.) filter, and f_c is the cut off frequency of the low pass (L.P.) filter. All frequency ranging from 4 to 40 Hz were measured in wide-band channel (after Mogi et al., 1986).

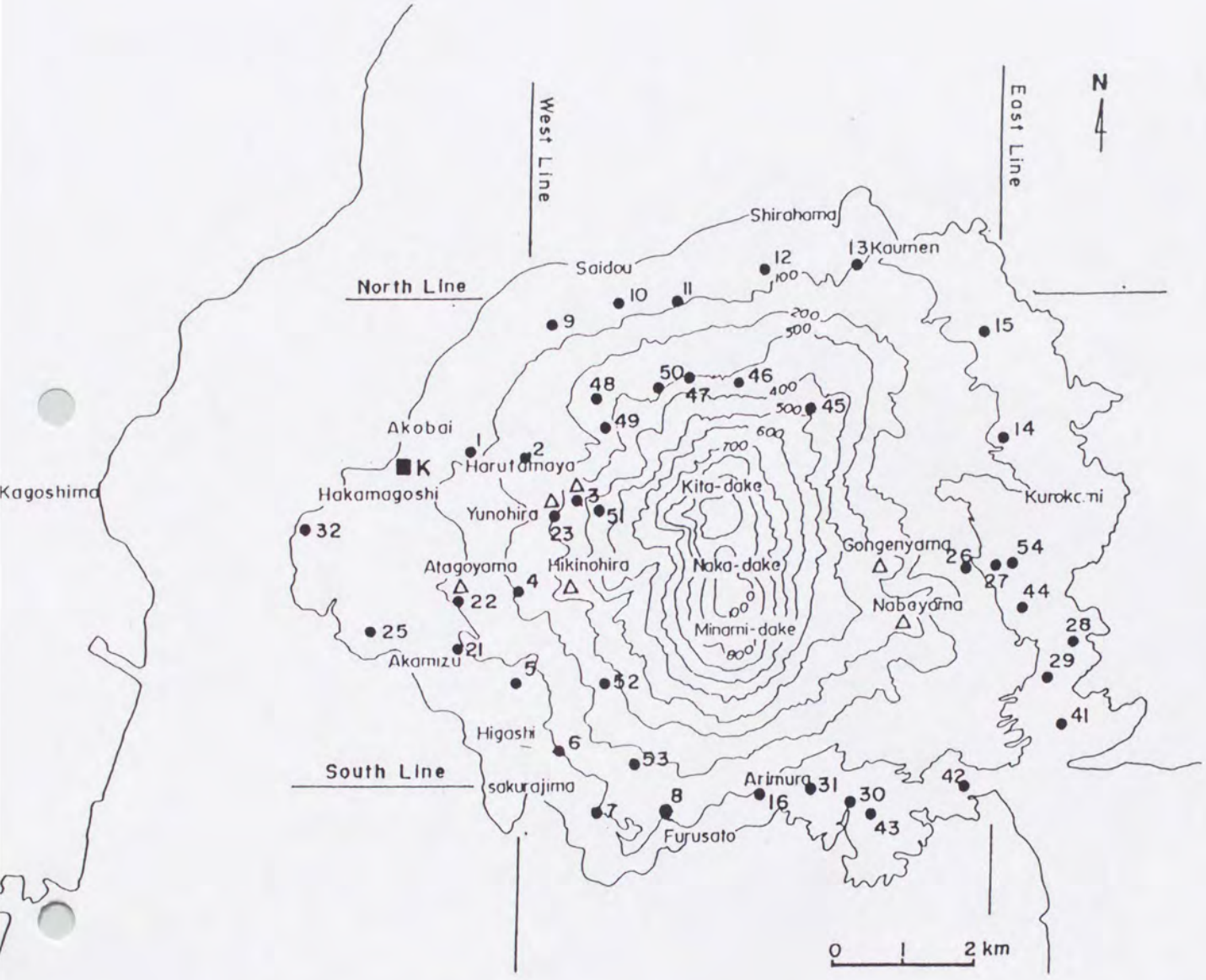

Fig.7. Location of the ELF-MT measurement sites (•) around Sakurajima volcano. **K** is the borehole site at Koike and Δ is parasitic cone.

direction and sensor magnetic field in y or x direction, respectively. x and y show directions of north-south and east-west. Illustration of the MT instrument set-up in the field is shown in Fig.8.

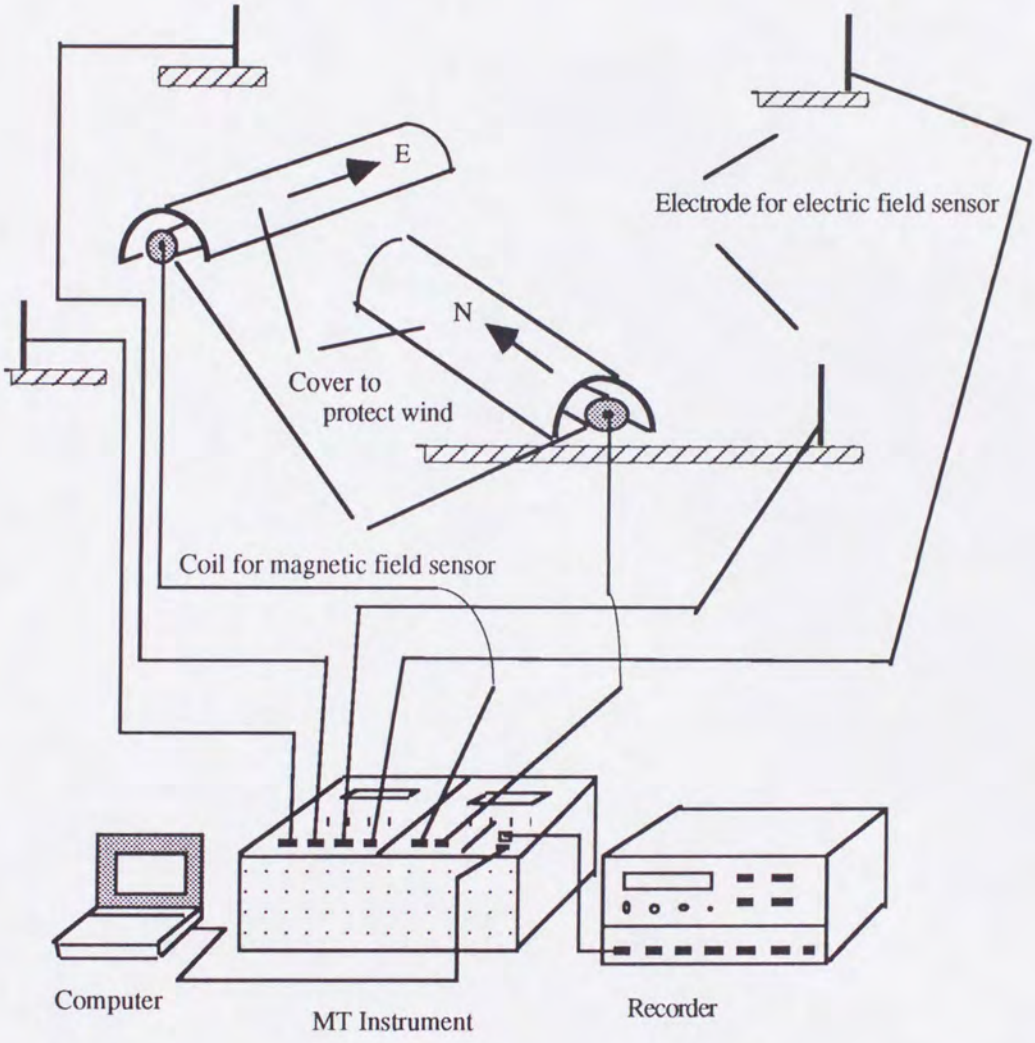

Fig.8. Field set-up of the ELF-MT survey at Sakurajima volcano, which measures magnetic and electric field components from natural electromagnetic wave.

2.3.3. ELF Signal analysis

Narrow-band system

Data analysis of the narrow-band system is implemented through a portable personal computer. After the test of ELF signals, which are often influenced and obscured by the power line, using an oscilloscope, the amplified and band-passed signals are introduced into a handhold computer through an AD converter. The apparent scalar resistivity is immediately calculated by Eq. (1). As the ELF signals are contaminated with random noises in general, the apparent resistivities of repeanted measurements (usually 30 times) for each frequency should make a log-normal distribution (Mogi et al., 1986). Mean apparent resistivity on log-scale for each frequency is calculated after statistical test by the way of Smirnov's rejection test. After the above procedures, we obtain four values of mean resistivities as function of frequency on log-scale and of log-standard deviations for a perpendicular set of magnetic and electric fields. This process was carried out during measurement in the field.

Wide-band system

The wide-band data analysis were carried out by a procedure proposed by Vozoff (1972). The digitized data were processed to yield estimates of the MT impedance tensor in the frequency domain. The data were then rotated into principal axis to calculate relevant apparent resistivity values. The rotation angle for the principal axis direction was

obtained by minimizing the diagonal elements of the impedance tensor. For two-dimensional situation, one axis, electric sensor, is parallel (TE mode) and the other perpendicular (TM mode) to the structural strike .

Flow chart of general procedure of wide-band data analysis is shown in Fig.9 with explanation as below:

(1). Analog to digital conversion.

The original data were recorded on a magnetic cassette tape, in analog form. Analog to digital conversion is done by using computer which has A/D converter module part. Analog to digital conversion is done with sampling frequency of 125 Hz, after overflow data are rejected. Then the data are saved on floppy disk.

(2). Fast Fourier Transform (FFT).

Before processing FFT, it is needed to make pre-processing that consists of some steps; (a) to select data which may be contaminated by extra high noise or data may be not continuous in one stacking, (b) to remove strong linear trend and (c) applying data window, cosine taper type, to reduce spectrum leakage.

After pre-processing, Fouriers coefficient are calculated for each component of magnetic and electric fields with 256 data length at sampling frequency 125 Hz.

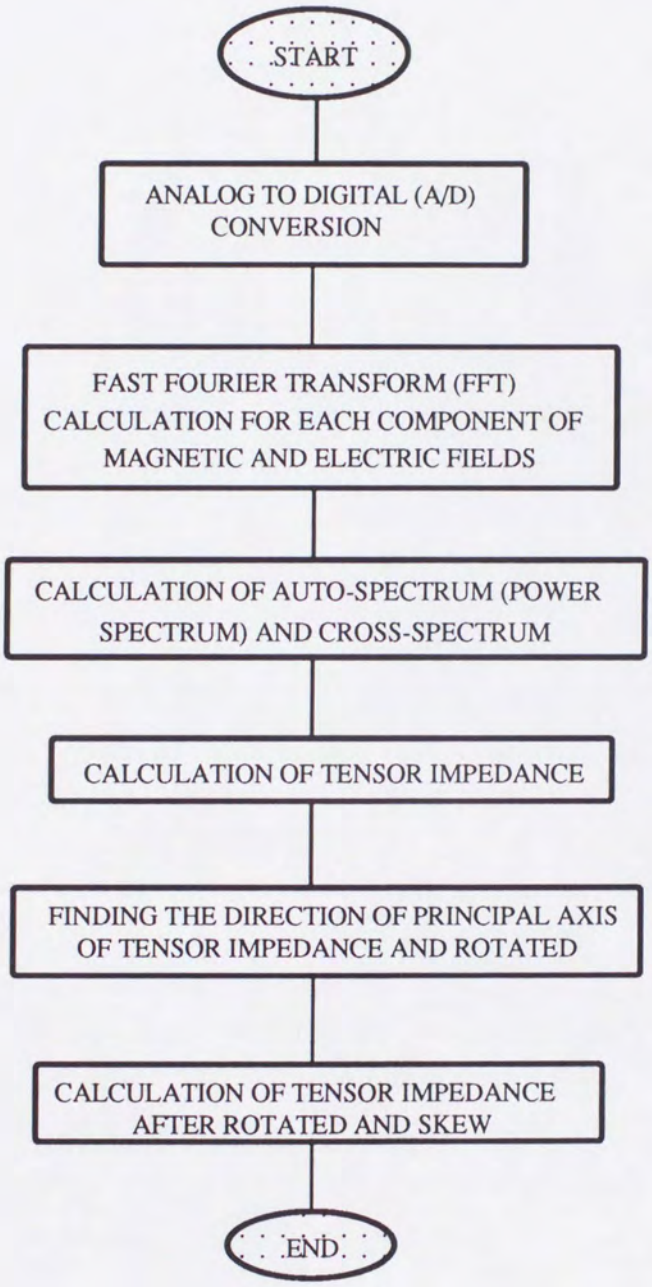

Fig.9. Flow chart of the ELF-MT wide-band analysis procedures.

(3). Auto-spectrum and cross-spectrum.

Calculations of auto-spectrum and cross-spectrum are used to observe coherency between each of magnetic and electric components. Auto-spectrum, cross-spectrum and coherency are calculated using Eqs. (5), (6), and (7). The coherency is calculated at every five stacking data.

(4). Tensor impedance elements.

The tensor impedance elements, Zxx, Zxy, Zyx, and Zyy before rotating are calculated by Eq.(8).

(5). Direction of principal axis of tensor impedance.

To find direction of principal axis of tensor impedance Eq.(10) is used.

(6). Tensor impedance elements after rotated and Skew.

The tensor impedance elements, Z'xx, Z'xy, Z'yx, and Z'yy, after rotation are calculated using Eq.(9). The apparent resistivity of principal axis and Skew are calculated using Eqs.(11) and (12).

For selecting data which are possibly contaminated by high noise, for statistical errors calculation and for checking quality data, some criteria are entered into the program analysis. Maximum value of magnetic and electric signals, upper and lower limit of power, lower limit of multiple coherence between one output E (Ex or Ey) and two inputs H (Hx,Hy), upper limit of coherence between Hx and Hy, are criteria conditions.

The multiple coherence function for 2-input and 1-output system is applied to examine the true linear relationship between multiple input and signal output (Bendat and Piersol, 1971). In the MT method, multiple inputs are Hx and Hy, and the output is Ex or Ey. The coherence between

Hx and Hy will be zero under the ideal condition when measuring natural electromagnetic waves which come from random orientations.

Fig.10 shows an example of power-spectrum calculated from the result of ELF-MT survey at site 10. In an ideal condition, free of noises, if there are peaks of magnetic spectrum (Hx or Hy) at certain frequencies, the peaks of electric spectrum (Ey or Ex) will appear at same frequencies with magnetic spectrum. However, almost at all MT sites, it is difficult to find such nearly ideal condition. After trial and error by inputtng various conditions, we found the optimum critical conditions as 0.5 for lower limit of multiple coherence between output E (Ex or Ey) and input H (Hx and Hy) and also 0.5 for upper limit of coherence between Hx and Hy.

The data will be rejected If we input relatively tight condition, for example 0.7 for lower limit of multiple coherence and 0.3 for upper limit of coherence between Hx and Hy. It is indicated that the natural electromagnetic sources in the ELF-band during measuring are contaminated by relatively high random noise or the source signals are too weak so that the ratio of signal to noise becomes low. The signal strengths are adequate if thunderstorm or lightning as source of ELF-band are relatively near (Goldstein and Strangway, 1975).

Two major noise sources of electric field are artificial noise and self potential voltages. Common sources of cultural telluric noise are electrical power lines, irrigation pumps, radio and telephone transmissions, and seismic vibration arising from automobile traffic near an electrode (Clarke et al.,1983). Noise from power lines is predominantly at 60 Hz at Sakurajima volcano. Mechanical instability of the coil set up, for example caused by the wind, could produce false

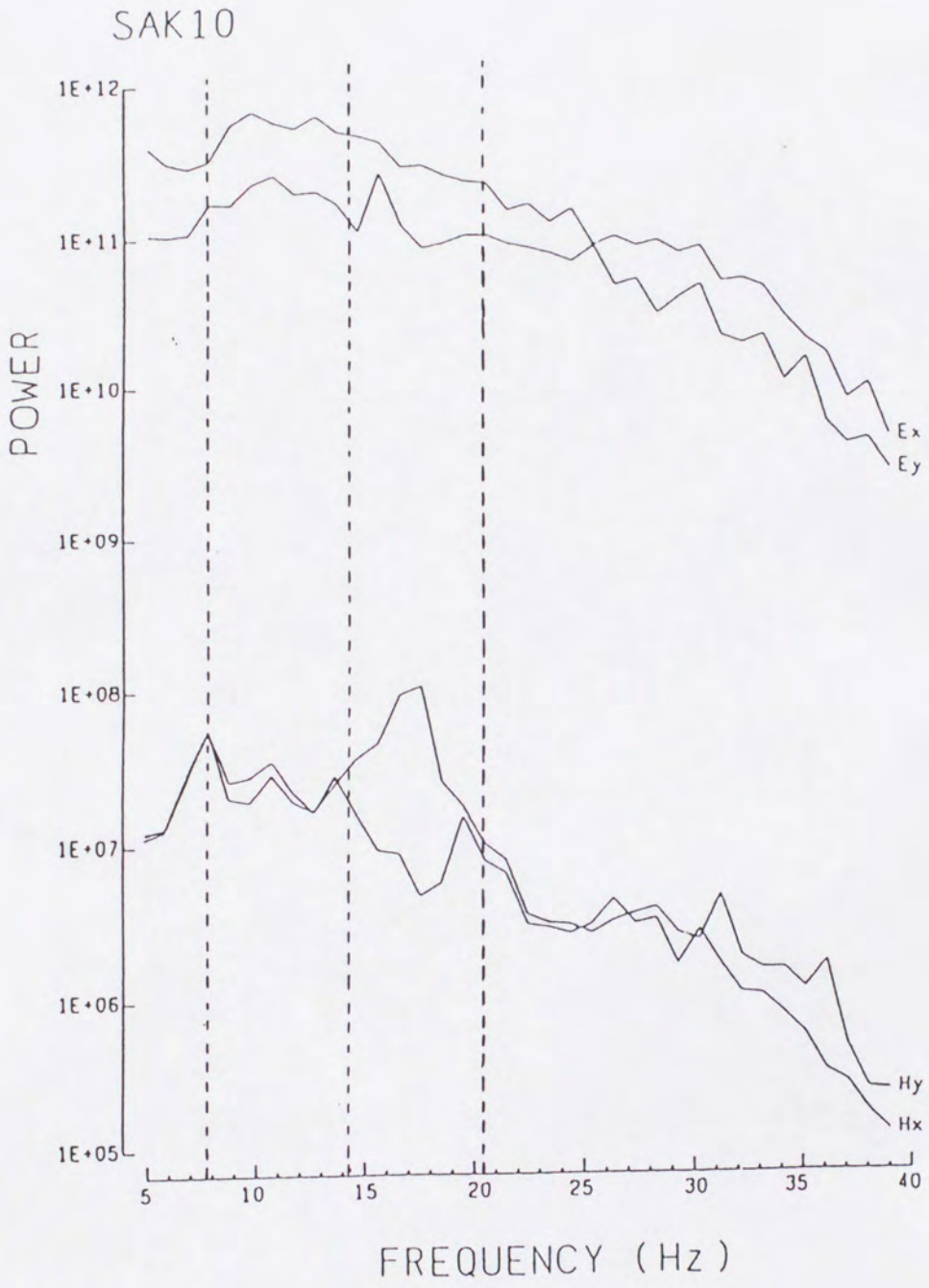

Fig.10. An example of the power spectrum of magnetic and electric field components calculated from the ELF-MT data at site 10.

signals or noise (Cantwell and Madden, 1960). In the field work we made an effort to minimized the above noises, such as using an oscilloscope to check the interference of power lines, carefully selecting locations, shortening the telluric line sensor to reduce self potential voltage, putting band eliminating filter at frequency 50 and 60 Hz in the instrument, and covering the magnetic sensor to protect from the wind disturbing. However, unpredictable noises were still leftovers. Electrical power line with frequency of 60 Hz became undesired signals because the source is located very closed to observation site. In Japan, there are many sources of artificial electromagnetic noise in the ELF range, but they still give reliable result (e.g., Handa and Sumitomo, 1985., Utada, 1990).

Although the signal coherence is not so excellent, in reconnaissance work it can be seen that these data are still sufficient and reliable to verify the existence of the conductive anomalies, measure their approximate value, and gain some idea of their distribution.

2.3.4. Tensor apparent resistivity and geologic structure

Pattern of the anisotropy of tensor apparent resistivity is shown in Fig.11. These values of skewness in Fig.11 are confined between 0.5 to 1 unit at some sites. These skew values are relatively large. If skew is large, structure at the site must appear to be three-dimensional in that frequency range (Vozoff, 1972., Ting and Hohmann, 1980). At Sakurajima volcano, the large skew values are indicating local three-dimensional structure

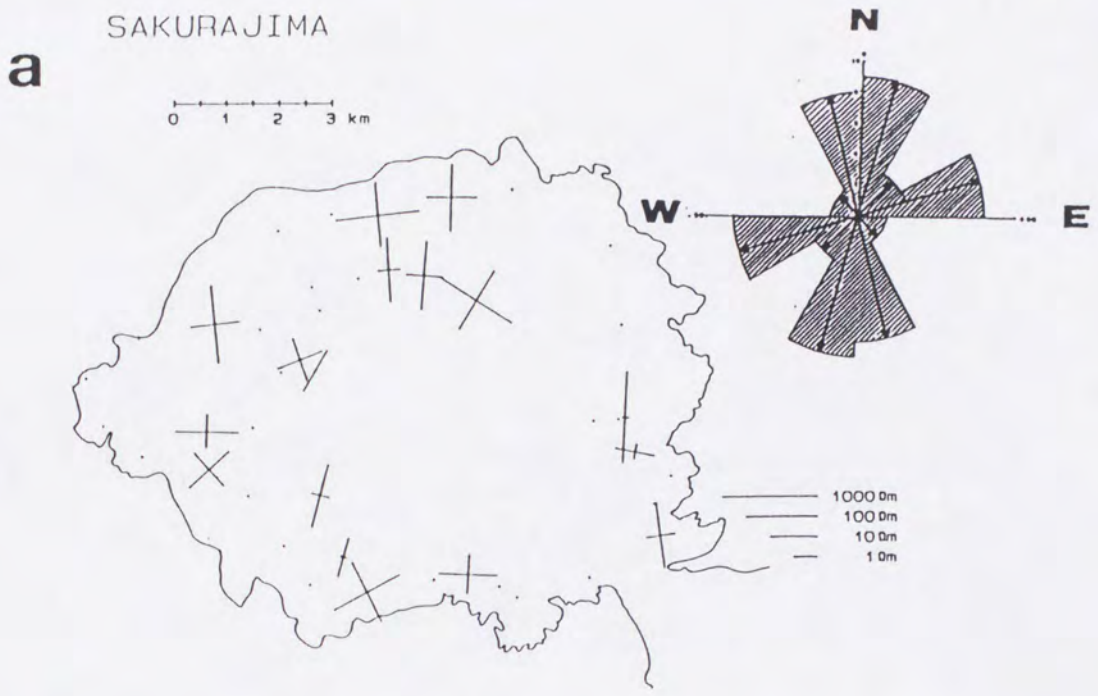

Fig.11. Anisotropy of tensor apparent resistivity and diagram of the major principal axis direction at each site for the related frequencies of variation. a) 7.8 Hz, b) 14.2 Hz, and c) 20.5 Hz. Length of the lines show the major and the minor of resistivity value. Points without line are the sites with no data which were rejected during the analysis. Hatched area of the rose diagram shows principal axis direction.

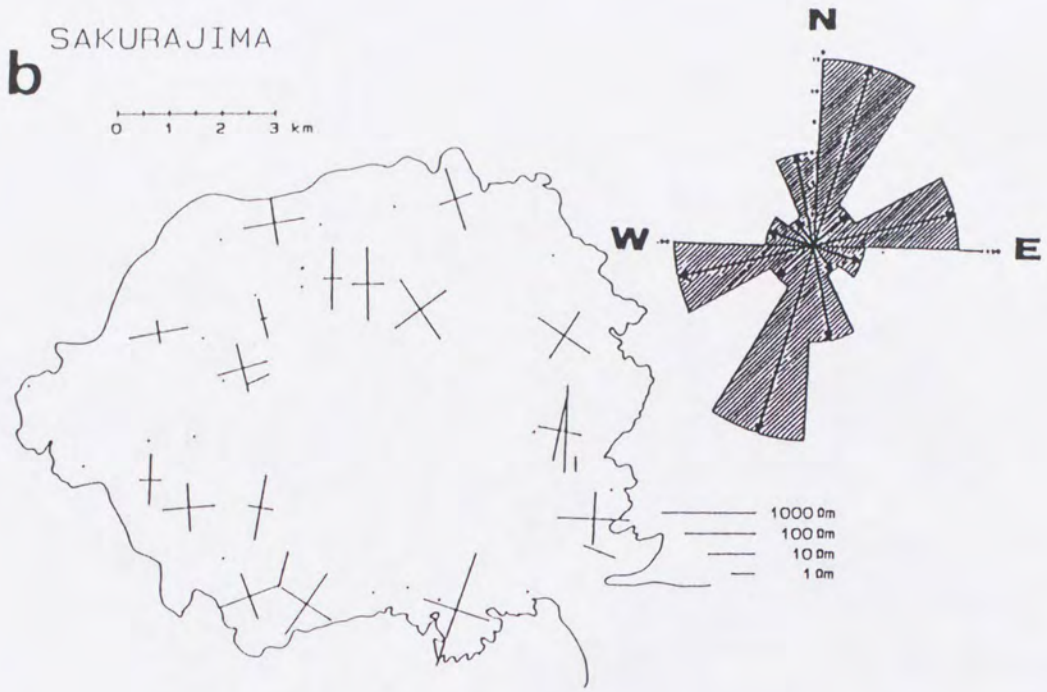
b
SAKURAJIMA
0 1 2 3 km
N
W
E
1000 0m
100 0m
10 0m
1 0m

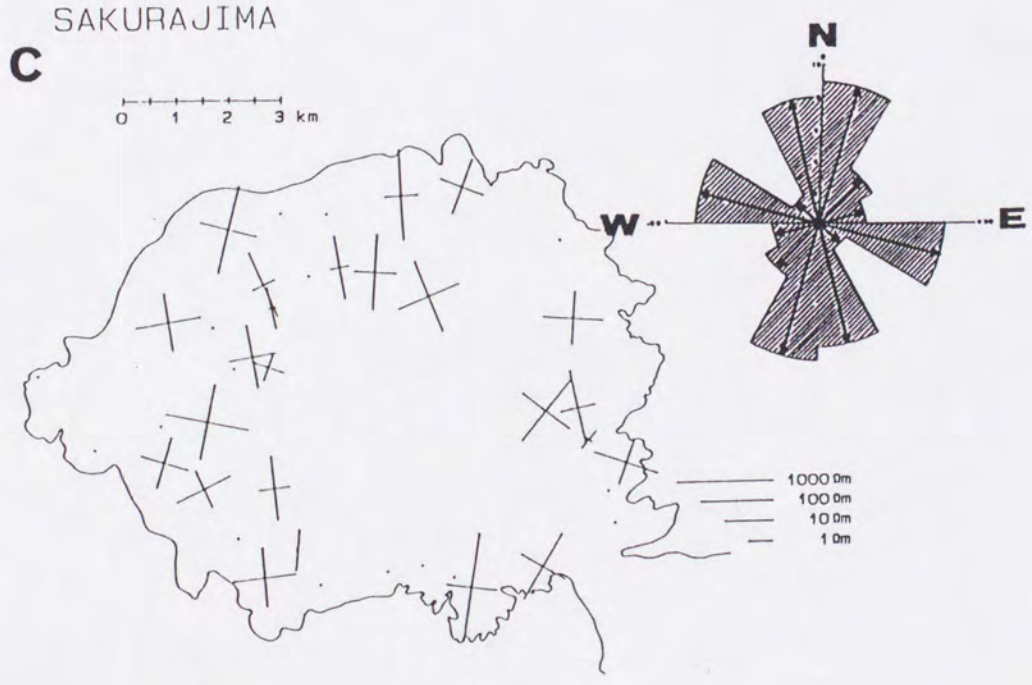
C
SAKURAJIMA
0 1 2 3 km
N
W
E
1000 0m
100 0m
10 0m
1 0m

which may be associated with sporadically distributed volcanic products.

The natural electromagnetic field as source of the ELF-MT method has random orientation when injected into the ground. This primary field will generate secondary magnetic and electric (telluric) fields which are measured by MT instrument. The orientation of the secondary field is dependent on the characters of the medium. The secondary field will show the same orientation with the primary field in homogeneous and isotropic medium. In fact, however, orientation of the secondary field will be polarized to follow direction of the conductivity structure of the medium, particularly of the electric field. The major principal axis of tensor apparent resistivity is defined as the orientation which is perpendicular to the conductivity structure. The lower frequency the deeper orientation of the conductivity structure can be recognized from the major principal axis of apparent resistivity.

The major principal axis of tensor apparent resistivity at Sakurajima volcano shows consistent trend in north-south and east-west directions for frequency 7.8, 14.2 and 20.5 Hz in the rose diagrams as shown in Fig.11. This direction seems generally to be associated with the direction of the conductive zone such as elongated-shape of Kagoshima Bay, the existence of caldera chain in the southern Kyushu and the boundary striking of southern rim of Aira Caldera. (Fig.1). This trend and low tensor apparent resistivities are coincident with the other measurements (Karaushi et al.,1989). It also seems to be consistent with the hypocentral distribution of A-type earthquakes (Nishi,1978).

Furthermore, the outward or concentric trend, shape of major axis particularly at frequencies of 14.2 and 20.5 Hz may be seen. This trend is probably caused by sea-water or hot rocks associated with the active magma vent. MT study applied in volcanic areas shows that direction vectors of the electrical and magnetic fields relate with regional and local structures. Direction vector of low frequencies reflects the volcanic alignment (deep structure) and high frequencies are oriented according to the direction of fractures (relatively shallow structure). Azimuth of the major or principal apparent resistivities is approximately parallel to the geological strike but that for the high frequencies are somewhat scattered (e.g., Ortiz et al.,1986, Ingham, 1991, Galanopoulos, 1991). These phenomena are also the case in Sakurajima volcano.

2.3.5.Resistivity structure beneath Sakurajima volcano inferred from ELF-MT survey

One-Dimensional analysis

One-dimensional (1-D) inversion method is adopted to solve true resistivity value of the layer and its thickness from the observed curve of apparent resistivity versus frequency. An example curve between apparent resistivity versus frequency is shown in Fig. 12. The basic principle of the inversion method is to match observed and calculated values of apparent resistivity based on the layer model. Calculated value is found by using mathematical approach for n-layer model under the

assumption of a plane-wave incident upon a layered half space and apparent resistivity as a function of layer resistivity and its thickness (Kaufmann and Keller, 1981). Fig. 13 is a model for n-layered earth and Eq.(13) is a mathematical formulation for calculating apparent resistivity as a function of layer resistivity and its thickness for n-layered earth model.

$$\rho_a = \rho_1 \,|\, [\coth\{k_1h_1+\coth^{-1}((\rho_1/\rho_2)^{1/2}\coth(k_2h_2+\coth^{-1}((\rho_3/\rho_2 \ldots\ldots$$
$$\ldots\coth^{-1}\{(\rho_{n-1}/\rho_{n-2})^{1/2}\coth(k_{n-1}h_{n-1}+\coth^{-1}(\rho_n/\rho_{n-1})^{1/2})\}\ldots\}|^2 \qquad (13)$$

Where k is wave number = $(i\,\mu 2\pi f/\rho)^{1/2}$, i, μ and f are imaginary unit, magnetic permeability and frequency.

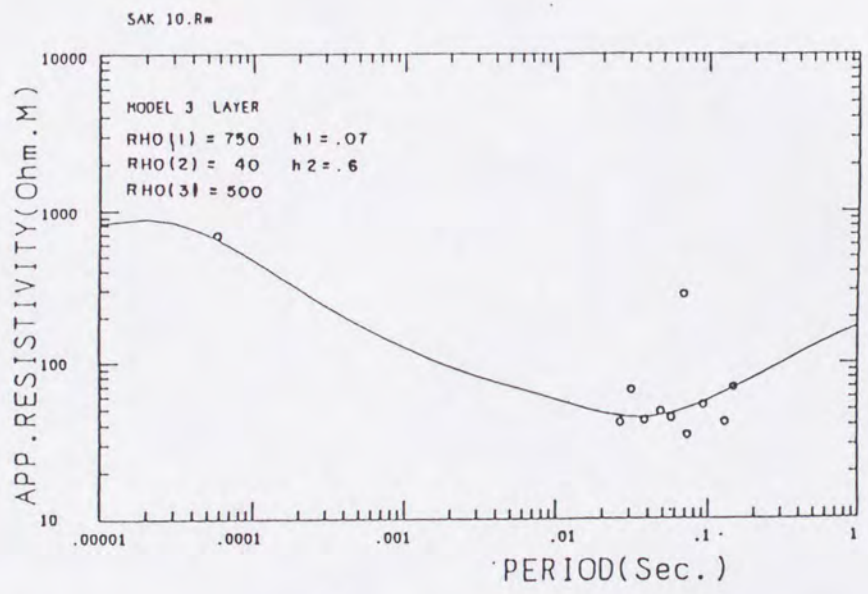

Fig.12. An example of 1-D analysis result of the ELF-MT survey at site 10. The open circles are observed data and solid line is calculated value. Mean resistivity (Rho) value in ohm-m and thickness (h) in km.

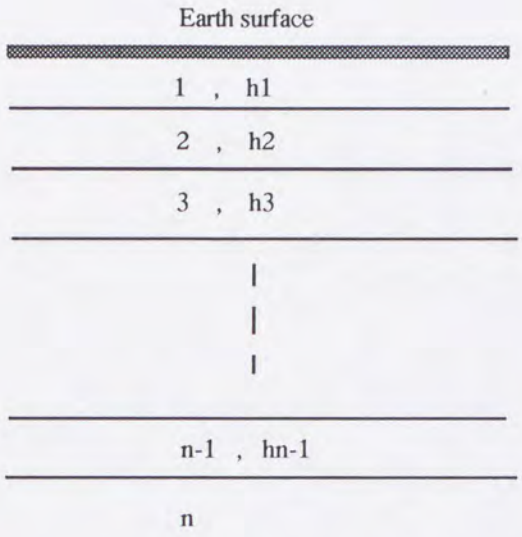

Fig.13. Model of n-layered earth, ϱ_i is resistivity and h_i is thickness of the i-th layer.

In order to find the best fitting between observed value and calculated value derived from the model, the least-square method and iteration procedures are combined or mathematically expressed as:

$$\phi = \Sigma_i (\varrho_{ci} - \varrho_{oi})^2 = \text{a minimum} ,$$

where ϱ_{ci} and ϱ_{oi} are calculated and observed apparent resistivities at certain frequency f.

Initial parameter values of the model such as numbers of layers, resistivity and thickness of each layer, are assumed based on the shape of observed curve. If the initial parameter is not fit yet, the parameter values are changed then next iteration is continued, and so on. The iterations are finished after obtaining the residual minimum. The apparent resistivity inputs (observed values) of several frequencies are geometric

mean values which are derived from the tensor apparent resistivity by using a formula:

$$\varrho_{mean} = \{ (\varrho_{xy}) \cdot (\varrho_{yx}) \}^{1/2} \qquad (14)$$

where ϱ_{mean} is geometric mean value of resistivity, ϱ_{xy} and ϱ_{yx} are resistivities in x, y direction and in y, x direction.

Fig.14 shows resistivity structure derived from 1-D analysis with respect to the site array as north, east, south and west lines. The site numbered above 41 (observed at March, 1988) are not solved by 1-D method, because the VLF was not measured.

Two-dimensional analysis

Two-dimensional (2-D) resistivity structure model is made from 1-D section as a preliminary bases. A numerical method for calculating electromagnetic fields from a given 2-D model used Reddy and Rankin's (1975) approach. This method has a great potential in handling problems involving irregular discontinuities, surface effects and boundaries, especially in the case of volcanoes. A finite element method (FEM) was attempted by using quadrilateral elements to discretize the equation where the FEM consists of 1652 triangular elements and 853 nodes. 1652 triangular elements give sufficient pattern for constructing 2-D structure. Finite element form which used for construction and calculation of 2-D model as shown in Fig.15. The program calculates apparent resistivity depending on the model section for TM (transfer magnetic), TE (transfer electric) modes and mean. The model is modified to fit the

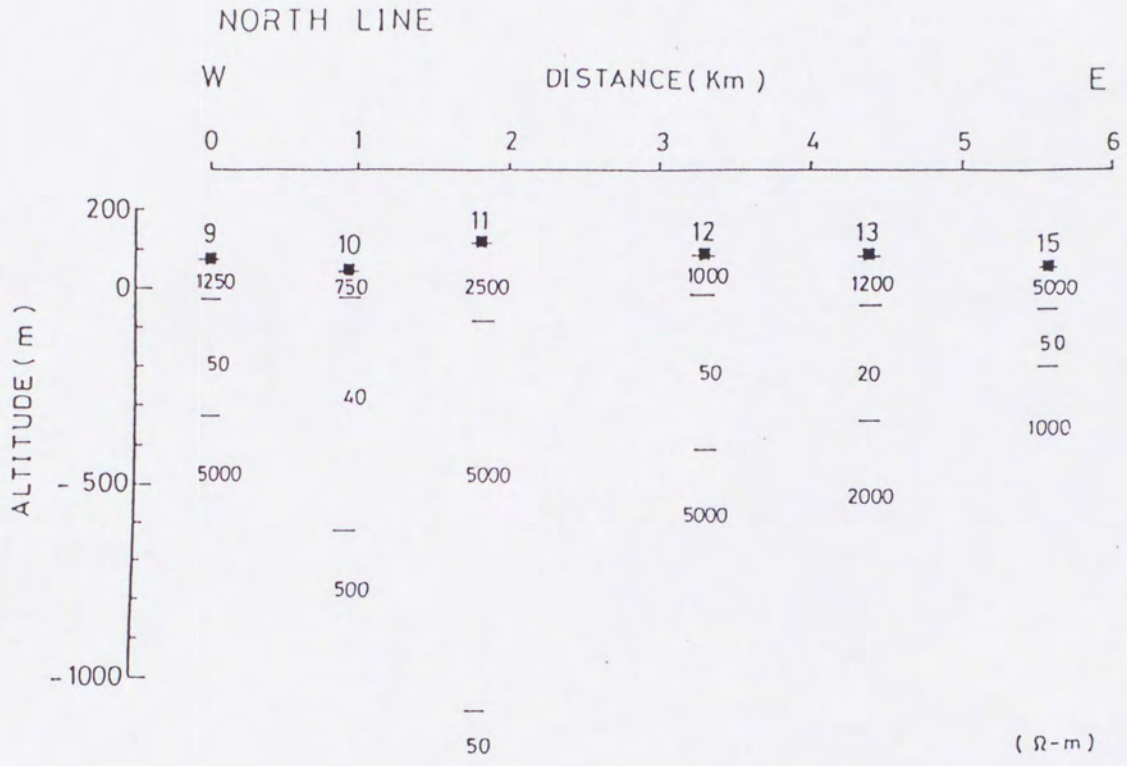

a

Fig.14. Resistivity structure of Sakurajima volcano inferred from ELF-MT 1-D inversion. a) north line, b) east line, c) south line, and d) west line.

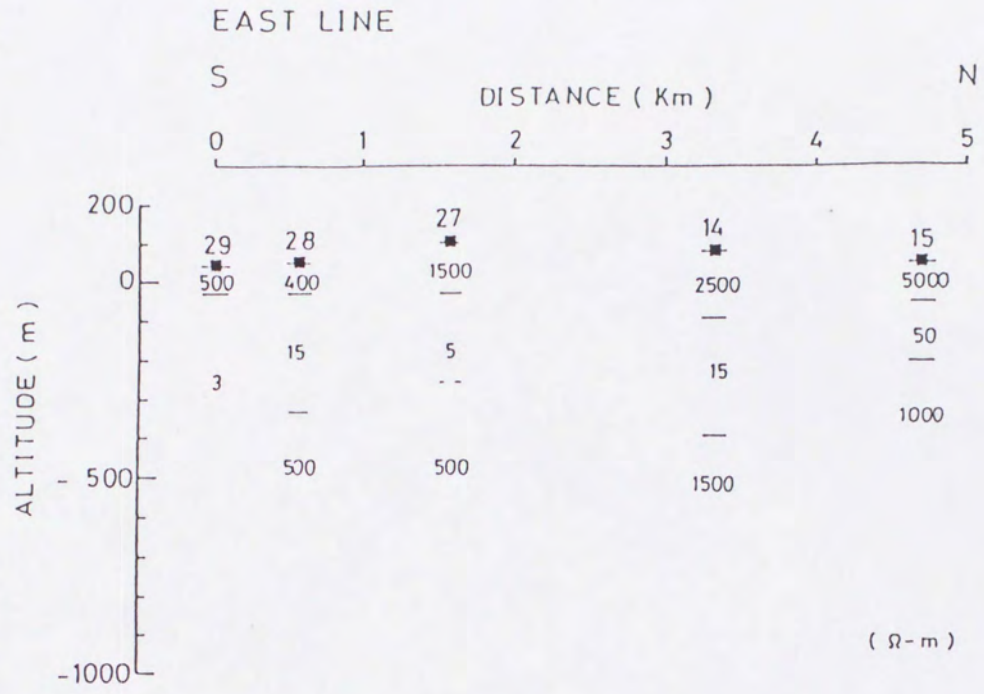
EAST LINE
S
N
DISTANCE (Km)
0
1
2
3
4
5
200
0
- 500
-1000
ALTITUDE (m)
29
28
27
14
15
500
400
1500
2500
5000
15
5
50
3
15
1000
500
500
1500
(Ω-m)

b

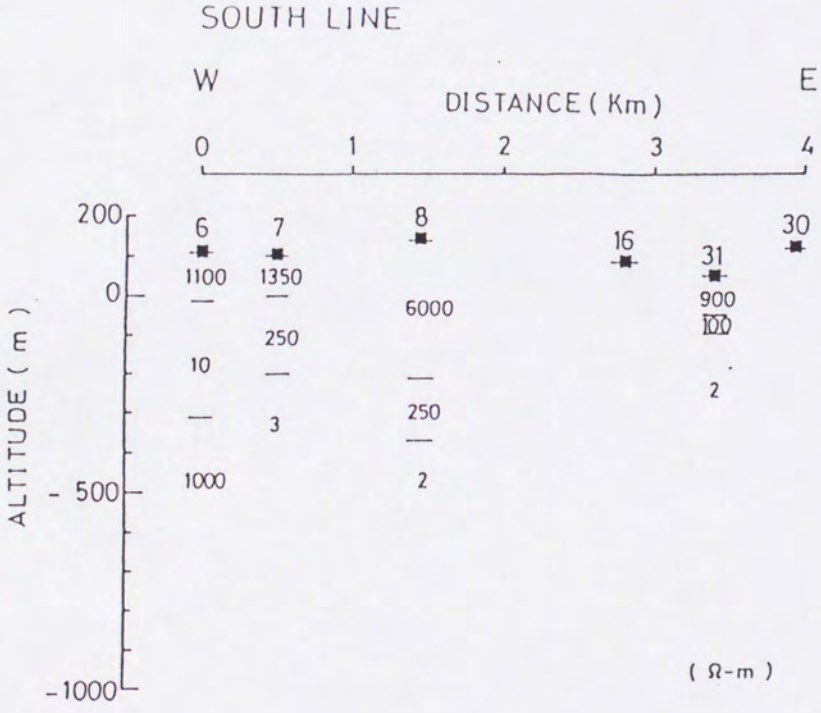
SOUTH LINE
W
E
DISTANCE (Km)
0
1
2
3
4
200
0
- 500
-1000
ALTITUDE (m)
6
7
8
16
31
30
1100
1350
6000
900
100
250
10
2
3
250
1000
2
(Ω-m)

c

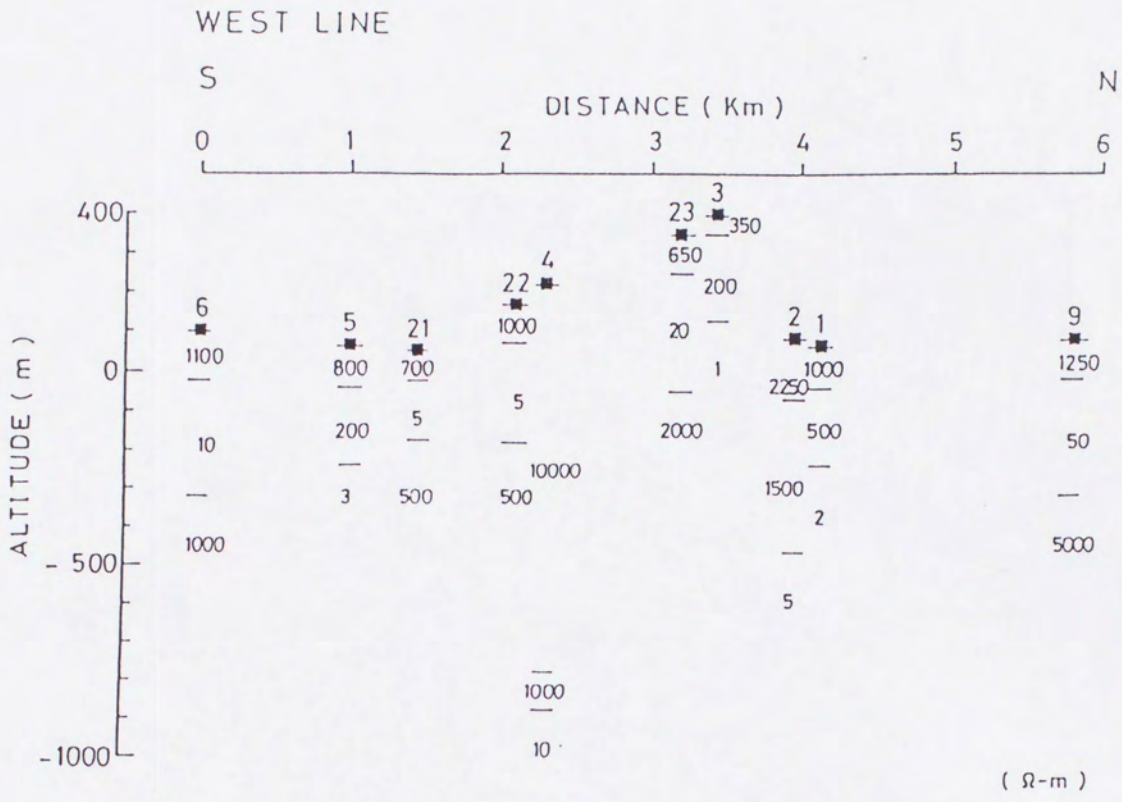

d

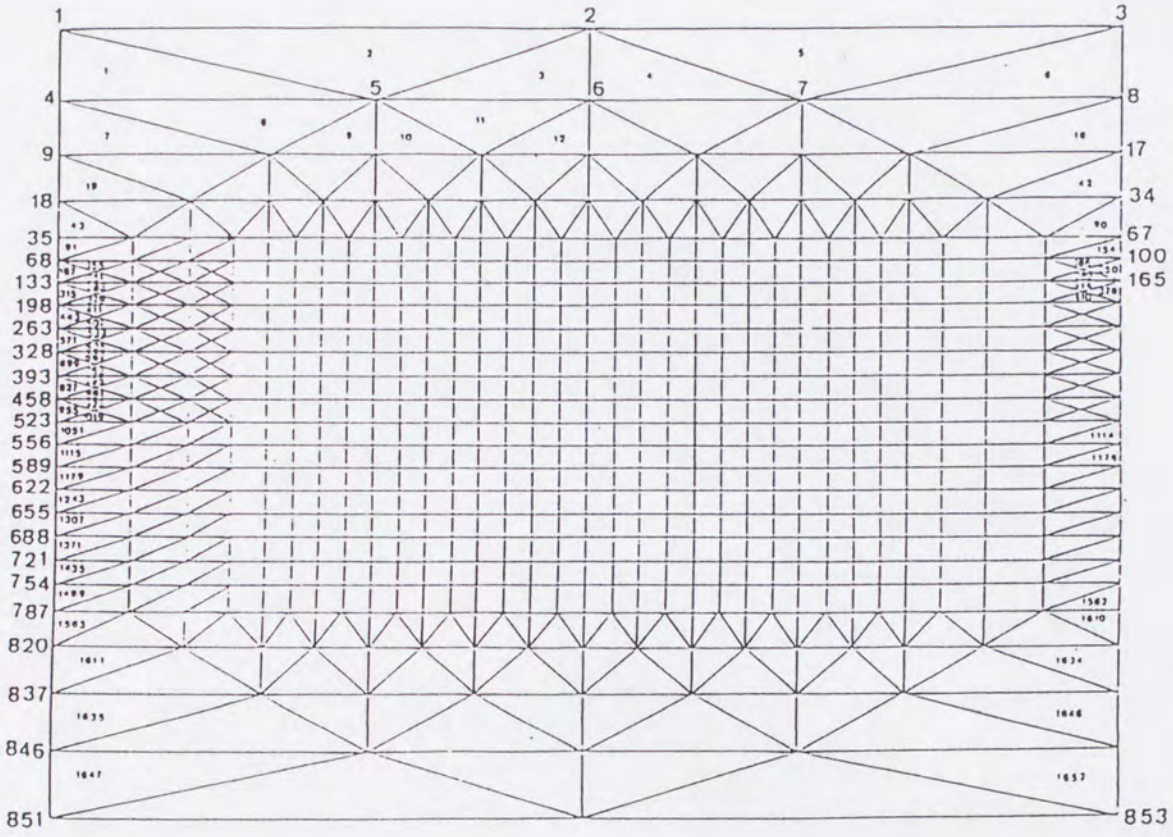

Fig.15. Finite element form which is used for construction and calculation of 2-D model. Form consists of 32 columns, 24 rows, 853 nodes, and 1652 elements.

calculated apparent resistivity with the observed data by trial and error until the least-square error attains minimum value.

The boundary conditions used in 2-D model are as follows: the bottom of boundary is assumed as several times of the skin depth below the air-earth interface and all the components of E and H are set to equal be to zero. At the lateral boundaries, which is kept several times of the skin depth away from the closest lateral contact, the normal derivatives of E and H are set to be equal to zero. At the top layer of the air, a constant E or H is specified for the case of H or E polarization, respectively. The air layer is thick enough to reduce the secondary fields induced by the lateral inhomogeneities of the earth. The sea water layer is assumed to be 0.5 ohm-m.

From the available MT data, three frequencies in ELF and one in VLF, the subsurface structure is assumed to be a simple-layer structure model.

Resistivity structure beneath Sakurajima volcano

The results of 2-D resistivity structure for north, east, south and west lines are shown in Fig.16. The sections of the north, east, south and west lines are located about 500 m or more away from the coastal line of the island. The horizontal length of each line is approximately 5.5, 4.7 and 4.2 km, respectively. The topography is relatively flat with altitude variations from 50 to 125 m above sea-level, except for the west line

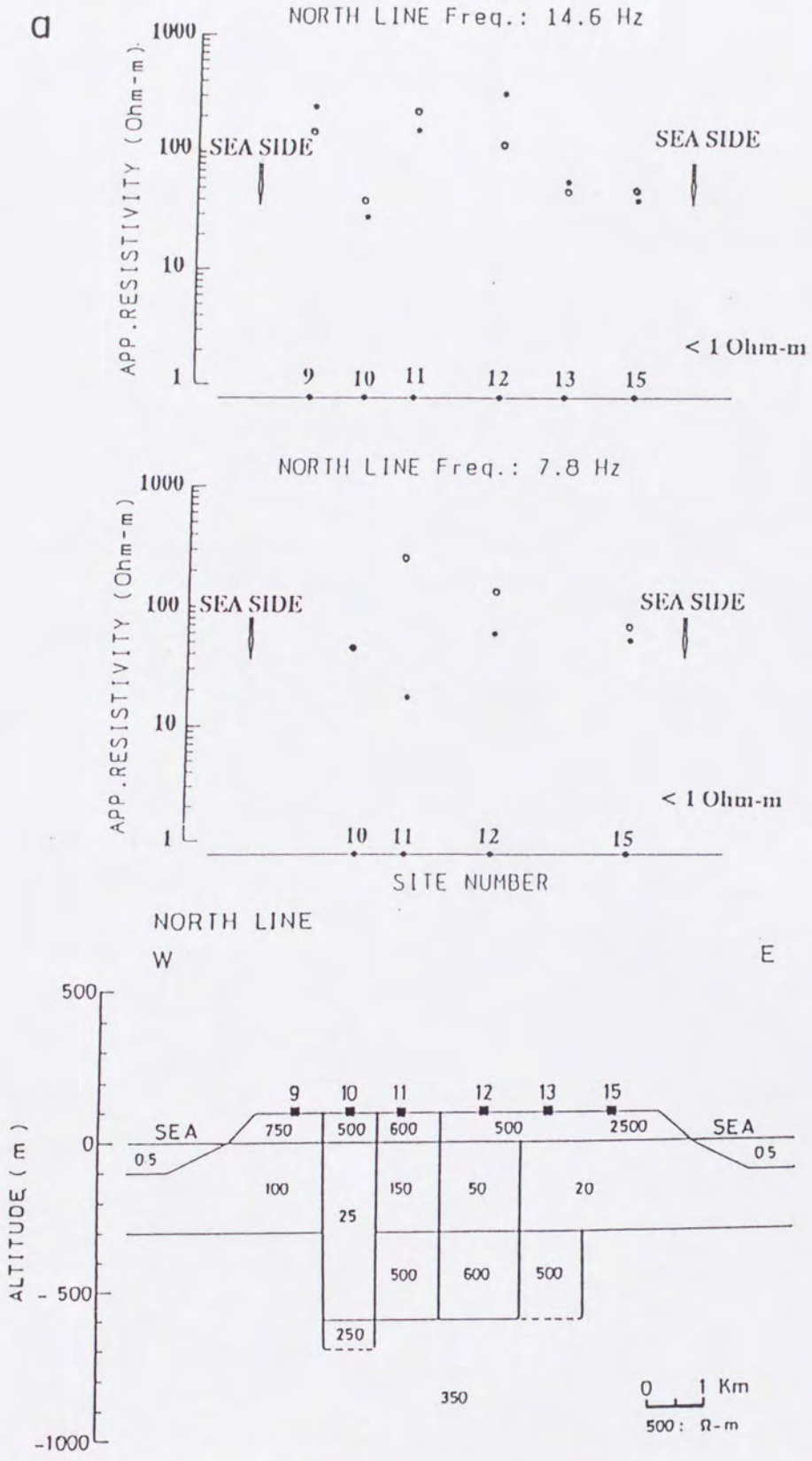

Fig.16. Resistivity structure of Sakurajima volcano inferred from ELF-MT 2-D model. a) north line, b) east line, c) south line, and c) west line. The solid circles are observed data, and open circles are calculated data.

b

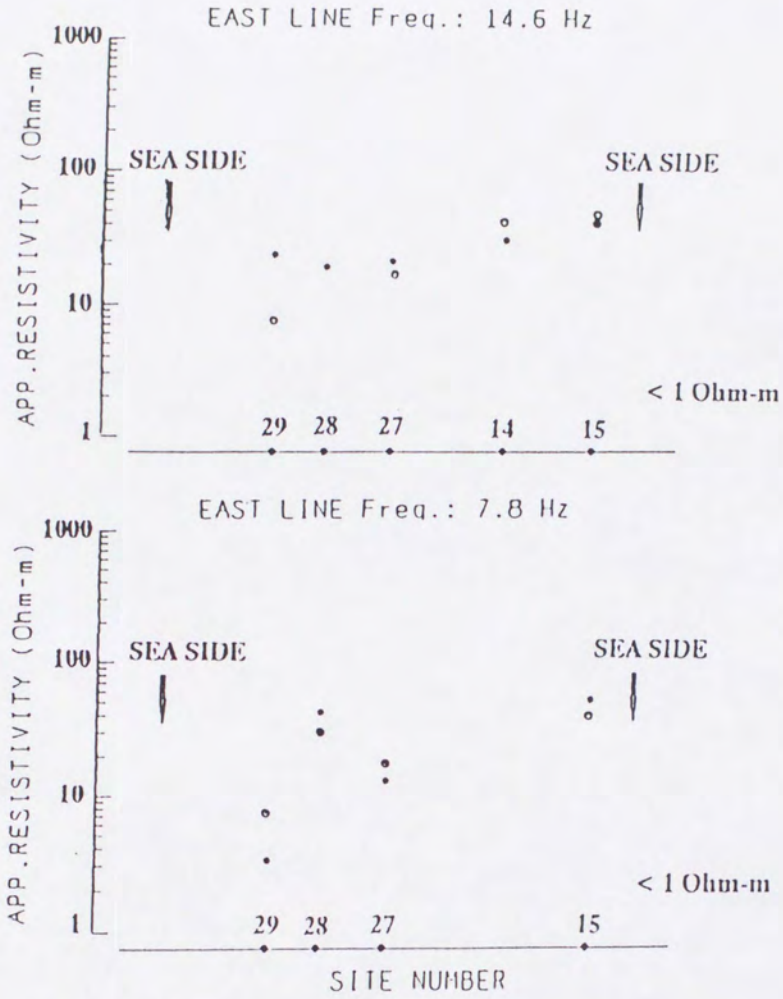
EAST LINE Freq.: 14.6 Hz
APP.RESISTIVITY (Ohm-m)
1000
100
10
1
SEA SIDE
SEA SIDE
< 1 Ohm-m
29 28 27 14 15
EAST LINE Freq.: 7.8 Hz
APP.RESISTIVITY (Ohm-m)
1000
100
10
1
SEA SIDE
SEA SIDE
< 1 Ohm-m
29 28 27 15
SITE NUMBER

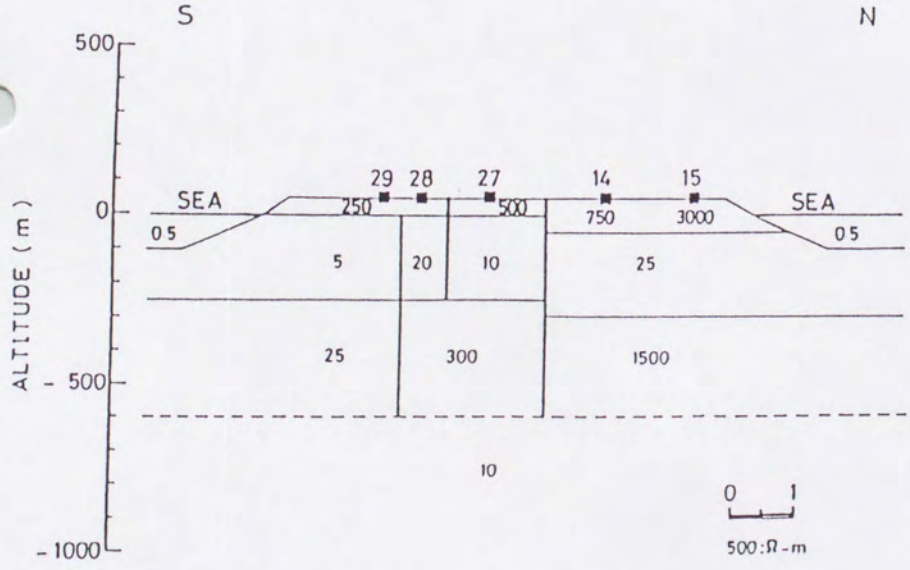
EAST LINE
S
N
ALTITUDE (m)
500
0
- 500
- 1000
29 28 27 14 15
SEA
250
500
750
3000
SEA
0 5
0 5
5
20
10
25
25
300
1500
10
0 1
500:Ω-m

C

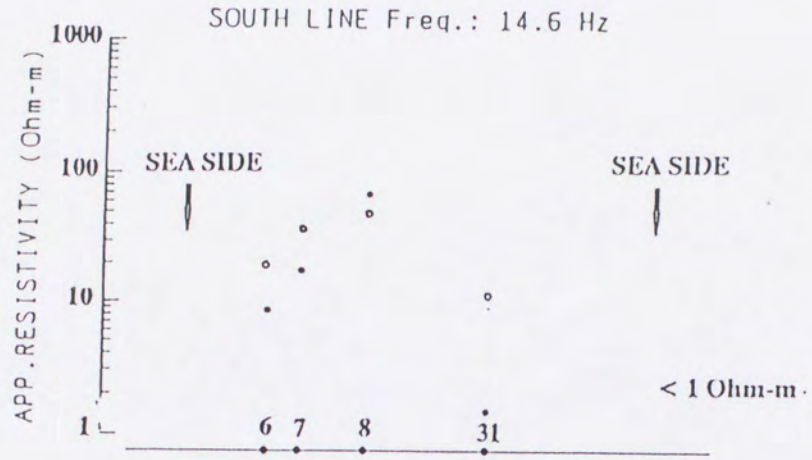
SOUTH LINE Freq.: 14.6 Hz
APP.RESISTIVITY (Ohm-m)
1000
100
10
1
SEA SIDE
SEA SIDE
< 1 Ohm-m
6 7 8 31

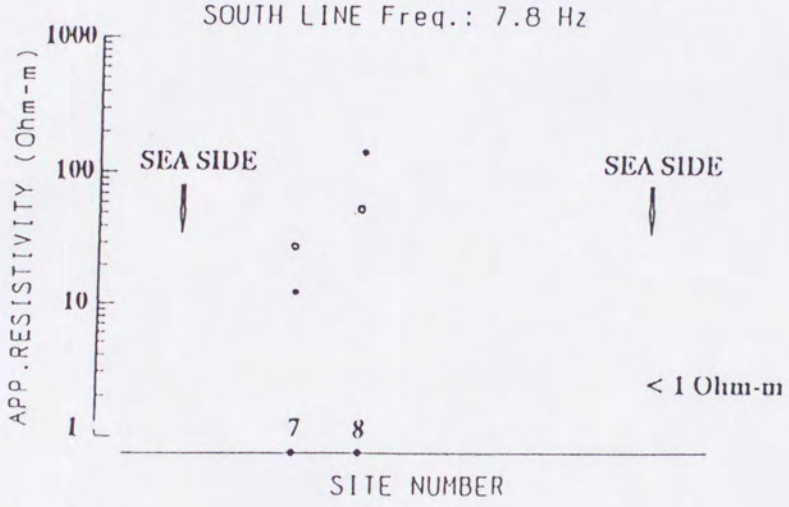
SOUTH LINE Freq.: 7.8 Hz
APP.RESISTIVITY (Ohm-m)
1000
100
10
1
SEA SIDE
SEA SIDE
< 1 Ohm-m
7 8
SITE NUMBER

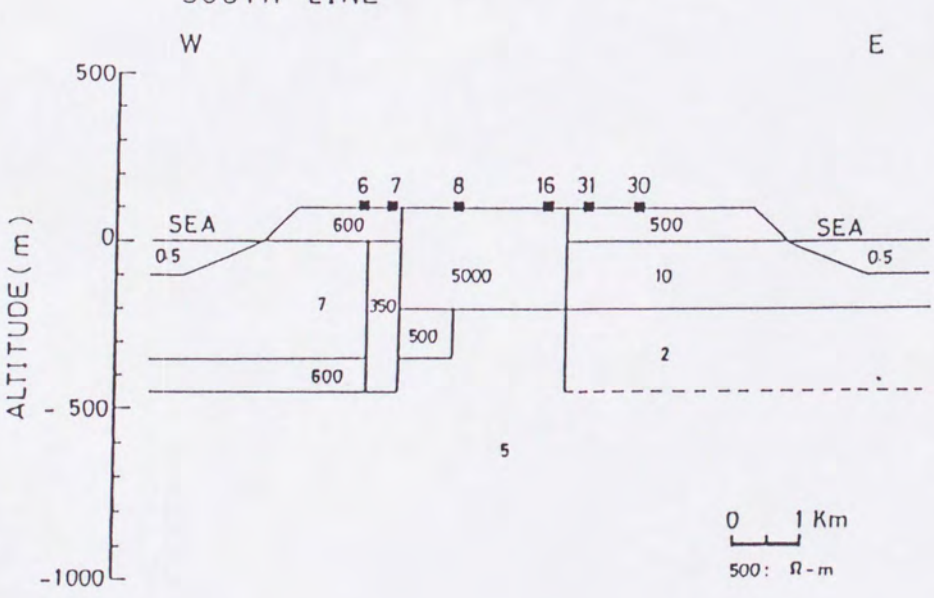
SOUTH LINE
W
E
ALTITUDE(m)
500
0
- 500
-1000
6 7 8 16 31 30
SEA
SEA
600
500
0.5
0.5
5000
10
7
350
500
2
600
5
0 1 Km
500: Ω-m

d

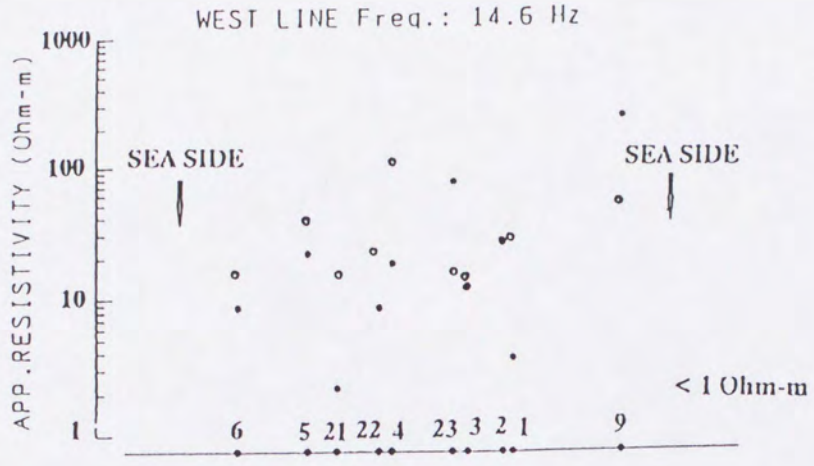
WEST LINE Freq.: 14.6 Hz
APP.RESISTIVITY (Ohm-m)
1000
100
10
1
SEA SIDE
SEA SIDE
< 1 Ohm-m
6 5 21 22 4 23 3 2 1 9

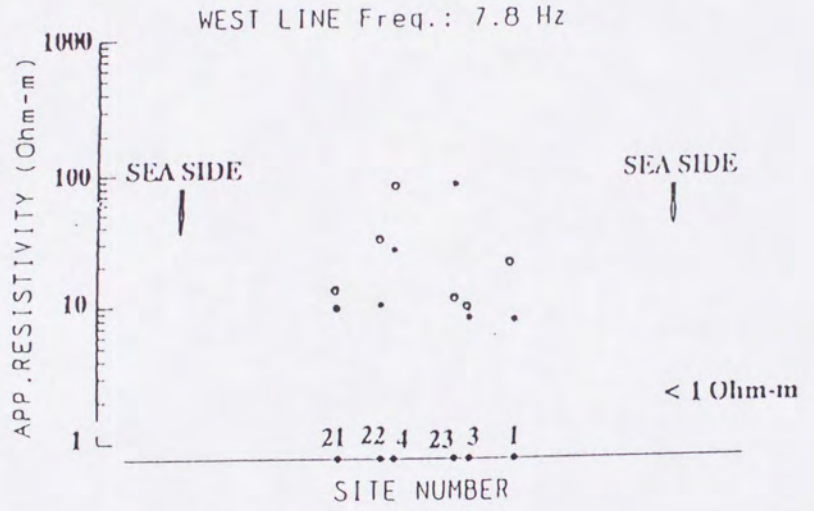
WEST LINE Freq.: 7.8 Hz
APP.RESISTIVITY (Ohm-m)
1000
100
10
1
SEA SIDE
SEA SIDE
< 1 Ohm-m
21 22 4 23 3 1
SITE NUMBER

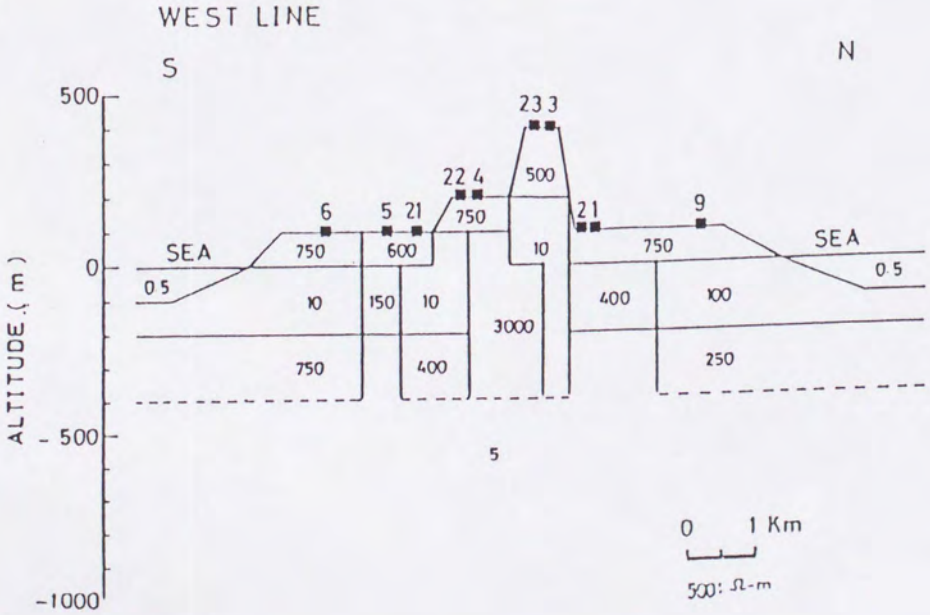
WEST LINE
S
N
ALTITUDE.(m)
500
0
- 500
-1000
SEA
SEA
0.5
0.5
6
5 21
22 4
23 3
21
9
750
600
750
10
750
10
150
10
400
100
3000
750
400
250
0 1 Km
500: Ω-m

which crosses the mountainous body, as cone and dome, with the lowest altitude approximately 60 m at site 1 and the highest about 400 m at site 3. The resistivity structures of 2-D analysis are characterized by disappearence of high resistivity contrast between successive layers and the thickness of each layer smoother than 1-D model. These conditions are reasonable and may give information about resistivity structure.

The geological evidence along the north line shows that this area is mainly covered by historically old lava flows and is overlain by fan-deposits, sand, mud and gravel (Fukuyama, 1978). The Koike borehole data shows that the welded tuff layer and the pumiceous tuff layer exist from a few meters above sea-level successively to tuffaceous and aqueous deposits which are correlated to the Kekura Formation lower than 194 m deep below sea-level (Aramaki, 1977). The lava flows underlying the east line, and beginning from the northern part of Sakurajima volcano are the An'ei, Bunmei, Showa and Taisho lava (Fig.2). Along the south line, the An'ei lava flow exists around site 16. The west line passes through the old lava and the parasitic cones (Harutayama and Yunohira) and domes (Hikinohira), except the middle segment of the line which runs through the Taisho lava flow area.

The top layer of resistivity structure for all the lines with the thickness of about 50 to 100 m has resistivity from 250 to 3,000 ohm-m. The resistivity values at depths less than 100 m inferred from the Schlumberger method also ranges from 680 to 2,500 ohm-m (Yukutake et al., 1980). The top layer is interpreted as lava flows, ash and pumice deposits. The resistivity of old lava flows is about 500 to 750 ohm-m. Generally, the resistivities of the old lava flows are about 250~500 ohm-

m, and are higher than those of young lava flows. In the northeastern part of the volcano around the sites 14, 15 and 27 (Fig.16.b), the estimated thicknesses are consistent with the thicknesses of lava flows, about 100 m evaluated from topographical features (Ishihara et al., 1981).

The second layers have resistivity values mainly in the range from 50 to 150 ohm-m. The depth of these layers are 200 to 300 m below sea-level. It is suggested that the pyroclastic flows and falls will have relatively low resistivity value, especially of secondary flow deposits or non-welded parts. The second layers, therefore, are interpreted as the pyroclastic layer emitted from the Aira caldera. The resistivity values of second layer are slightly smaller in the southern parts of volcano than in the northern parts.

The third layers are interpreted as the Kekura Formation with resistivity values about 300 to 1,500 ohm-m. The Koike borehole data, however, supports the existence of the Kekura Formation (Aramaki, 1977). The boundary depth between the second and third layers also supports this interpretation. The Kekura Formation is made up of marine deposits, as tuffaceous silt and sand, and distributed from Kagoshima City area to the western end of Sakurajima (Hayasaka and Oki, 1971; Aramaki, 1984), with increasing thickness towards the latter area. Those resistivity value is higher than that of the upper pyroclastic layers.

The basement complex (Shimanto Group), which are expected to have high resistivity value, do not appear at the bottom layer of each resistivity structure. This is in good agreement with the Koike borehole data in that even at 800 m depth of drilling they have not reached the basement (Aramaki, 1977). The bottom layer shows very low resistivity

values except for the north line. It is interpreted to be identical with the third layer, i.e. the Kekura Formation. However, the influence of heat originated from magmatic activities suggests to make lowering resistivity values.

The anomalous resistivity structure of each line is described as follows. In the north line, there is a thick second layer of 25 ohm-m at site 10. The lower resistivity values of second layers are obvious in the eastern part of north line. Along the east line, the low resistivity values, less than 25 ohm-m, of the second layer are remarkable. The low resistivity of the third layer under the site 29 suggests the effect of sea-water impregnation, because this area is a new land (formed after the 1914 eruption) connecting the Sakurajima island to the Osumi Peninsula. Along the south line, the lower resistivity of second layers are extended except for the segment between sites 7 and 16. The eastern parts under the sites 30 and 31 have also very low resistivities in the third layer. In this part, the Taisho lava flows widely extend into the sea. The south line also gives a thick and high-resistivity top layer around the sites 8 and 16 at Furusato and Arimura. The An'ei lava flow and the old lava flows are thick formations (Fig.2). Along the west line, the low-resistivity of the second layers are remarkable under the sites 3, 6, 21, 22 and 23. The 3,000 ohm-m layer below the sites 4 and 23 is also a very singularity structure. These sites are located on the Taisho lava flows among the parasitic domes and cones (Atagoyama, Hikinohira, Harutayama and Yunohira).

2.4. CSAMT and TDEM surveys

2.4.1. CSAMT and TDEM methods and Instrumentation

CSAMT

Two kinds of electromagnetic fields are used as energy source in the magnetotelluric survey. The first one is a natural fluctuation of electromagnetic field in a broad range of frequencies between 0.001 Hz to about 100 Hz, this technique is known as Magnetotelluric (MT) method. The second one is an artificial electromagnetic field which is generated through a long grounded wire. Both ends of the wire connect to the earth and to the electrical power generator (transmitter). The technique is commonly called Controlled Source Magnetotelluric (CSMT) method. This technique was improved by Goldstein (1971), and Goldstein and Strangway (1975). Furthermore, the frequency range which is used in the technique can be added to the name of both MT and CSMT methods. CSAMT is abbreviation from Controlled Source Audio-frequency (10 Hz to 10 kHz) Magnetotelluric method.

The advantages of the controlled source method over those employing natural source are;

1. The polarization of the fields can be chosen by the orientation of the transmitting wire source and the signal strengths do not depend on the time of day or season.

2.Signals are stronger, therefore the receiving equipment does not need to be as sensitive as for natural MT.

To avoid near-field effect, the receiver must be placed at some distance where the transmitted electromagnetic field satisfies a plane wave assumption. The far-field distance, L_f, is approximately given by the following equation (Goldstein and Strangway, 1975));

$$L_f >= 3 \text{ X skin-depth} = 1{,}509 \, (\rho/f)^{1/2} \qquad (15)$$

where L_f is in meter, ρ is resistivity of the homogeneous earth in ohm-meter and f is frequency in Hz. Cagniard (1953) equation is valid if L_f satisfied the above equation.

CSMT survey may be categorized as scalar, vector, and tensor, depending on the number of source used. The scalar CSMT measures only two components, Ex and Hy or Ey and Hx, using a single source polarization. The vector CSMT measures four or five components, Ex, Ey, Hx, Hy, and optional Hz, using also a single source polarization. While the tensor CSMT measures four or five components, Ex, Ey, Hx, Hy, and optional Hz (vertical), but using two distinct source polarization. In the CSMT method, x and y are defined as an orientation of the sensor which is parallel to and perpendicular to transmitter orientation.

CSAMT instrument, transmitter and receiver, is designed for measuring several frequencies in audio-frequency band. The transmitter is designed to produce certain frequencies which are synchronous with the receiver system. The transmitter system transmits a maximum current 10 Ampere with maximum power and voltage outputs of 6 kW and 1000

Volt. Fig.17 shows an example of circuit diagram of receiver system developed by Mogi et al. (1990). The system has processor that can calculate the Fourier sine wave transform at each channel. To define a sounding curve, twelve selected frequencies are used. These frequencies are spaced roughly logarithmically i.e. 4.2, 8.5, 17, 34, 68, 136, 272, 545, 1000, 2100, 4300, and 8700 Hz. Also frequency 17.4 kHz emited from the military VLF transmitter in central Japan is added in the receiver to estimate the shallow resistivity layer. Narrow-band active filters are used to remove 50 and 60 Hz power line signals which are very strong when work is done in near electrical power line. The sensor of electric and magnetic fields are almost same with the sensor of ELF-MT method, an induction coil for magnetic field and two copper electrodes for electric field.

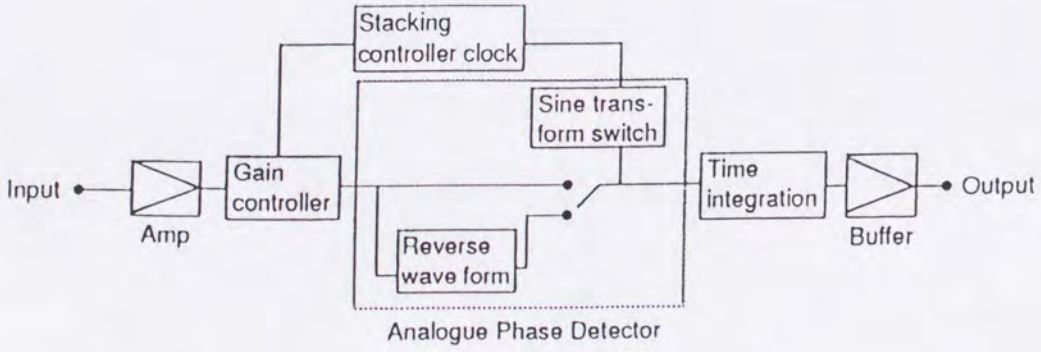

Fig.17. A block diagram of the CSAMT receiver system (after Mogi et al., 1990).

TDEM

Time Domain Electromagnetic (TDEM) method is a mean to study resistivity structure by measuring the transient of secondary magnetic field. In TDEM method, a strong direct current (dc) is usually passed through a grounded line wire. At time t=0 the current is abruptly interrupted. The secondary magnetic field due to the induced current in the ground is measured with suitable receiver in the absence of the primary field (Widarto, 1994). Illustration of TDEM measurements is shown in Fig.18.

TDEM method is different from CSMT method, because it measures only the magnetic components (Hx, Hy, and Hz). The advantage of the TDEM method is in depth penetration, therefore it is useful for estimating the deep layered earth. However, the static shift of the apparent resistivity caused by topographic features and shallow lateral changes in resistivity is a significant problem in TDEM method (Zonge and Hughes, 1991).

Fluxgate magnetometer is used as the sensor of secondary magnetic field in this survey. The sensor has high sensitivity up to 1 mV/pT and high frequency characteristics that work up to 100 Hz. A schematic block diagram of fluxgate magnetometer circuit installed in TDEM receiver system is shown in Fig.19. The transmitter used in the field work is a square-wave generator to output current of 100 Ampere at period from 1 sec to 128 sec. A crystal clock controlling the transmitter can be synchronized with an identical clock in the receiver unit to provide a cut-off time reference at twhich measurement is started.

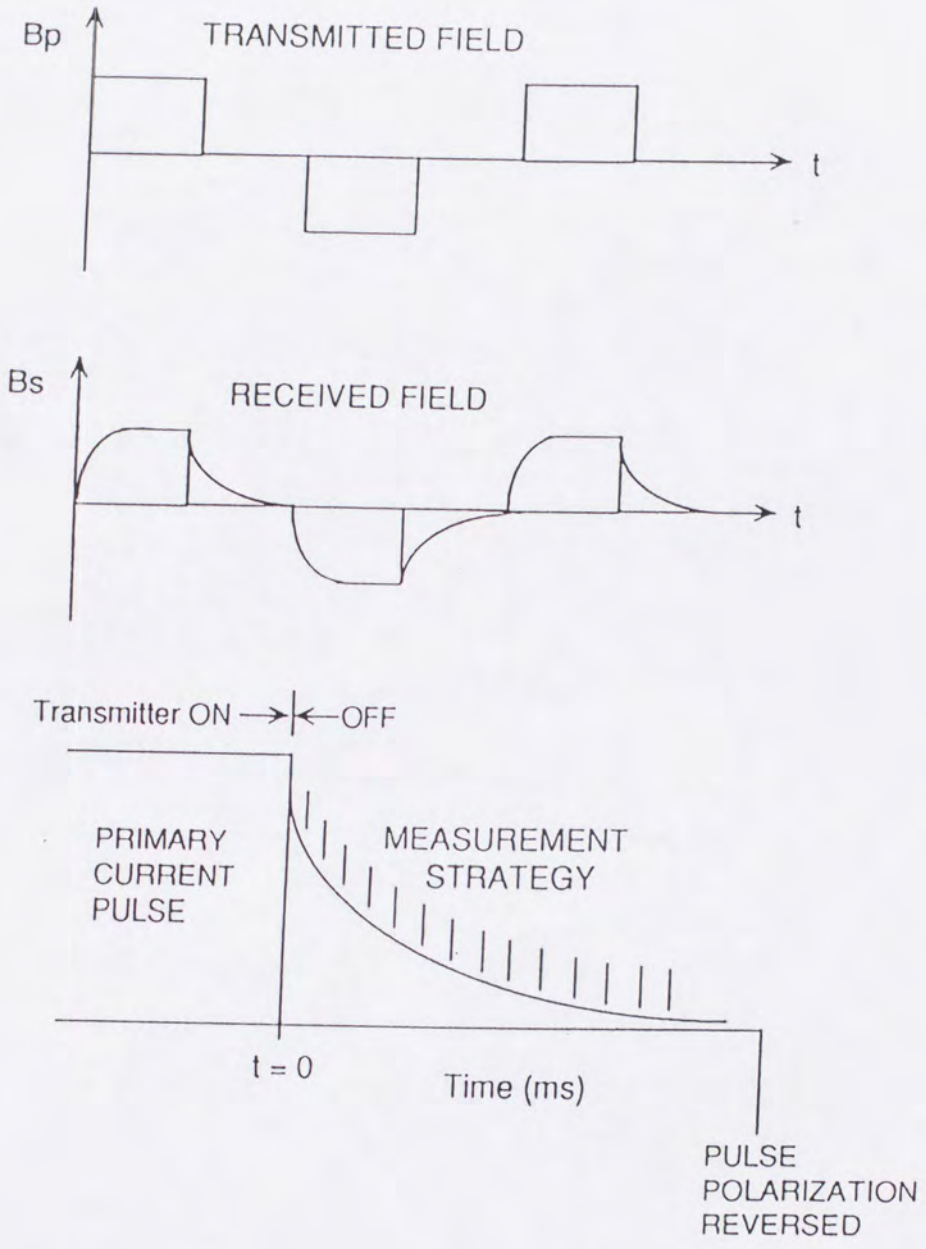

Fig.18. Measurement proceduse of the TDEM method. The secondary magnetic field due to induced currents in the ground can be measured in the absence of the primary field. Bp and Bs are primary and secondary magnetic fields, respectively (after Widarto, 1994).

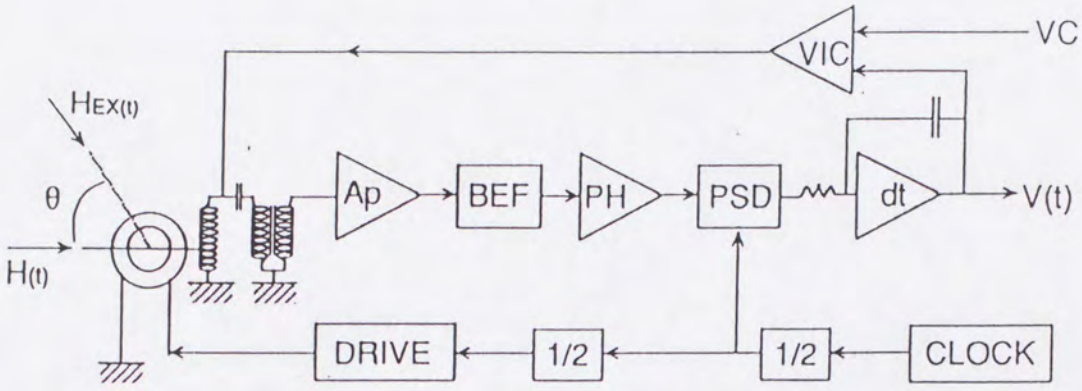

HEX (t)	: Steady (natural) geomagnetic field overlies with source field
H (t)	: External field component along fluxgate as projection form of HEX (t)
Ap	: Pre-Amplifier
BEF	: Band Eliminate Filter (12.5, 37.5 KHz)
PH	: Phase detector circuit
PSD	: Synchronized tuning
dt	: Integrator circuit
VIC	: Steady current circuit
VC	: Cancelling external main field
V (t)	: Output voltage which is proportional to external field H (t)
CLOCK	: 50 KHz output quartz oscillator circuit

Fig.19. A block diagram of the Fluxgate magnetometer which is installed in the TDEM receiver system (after Shimoizumi et al., 1991).

2.4.2. Data Acquisition of CSAMT and TDEM surveys

CSAMT

To deal with the weakness of unstable electromagnetic source and lack of measured frequencies in the ELF-MT method, CSAMT method has been carried out at Sakurajima volcano. The electric currents are injected into ground at various frequencies through the grounded bipole which are separated about 1.5 to 2.5 Km. Illustration of CSAMT survey lay-out in the field is shown in Fig.20. A scalar CSAMT measurement was carried out along the north, south and west sides of Sakurajima volcano by placing two bipole sources during March 1987. Current wire line I is the source of CSAMT measurement at sites along south side, and current line II is the source of CSAMT measurement at sites along west and north sides of Sakurajima volcano (Fig.21). Apparent resistivity values of ten frequencies, 7.8, 20, 40, 80, 160, 320, 640, 2560, 5120 Hz in audio frequency and 17.4 kHz in Very Low Frequency (VLF) were measured at each site.

In December 1989 a new design of CSAMT instrument which has twelve frequencies, 4.2, 8.5, 17, 34, 68, 136, 272, 545, 1000, 2100, 4300, 8700 Hz, was applied to complete CSAMT measurement along east side of Sakurajima volcano. For a given operating frequency and recording period, the outputs of the narrow band filter are rectified, stacked, integrated and then introduced into personal computer through an A/D converter.

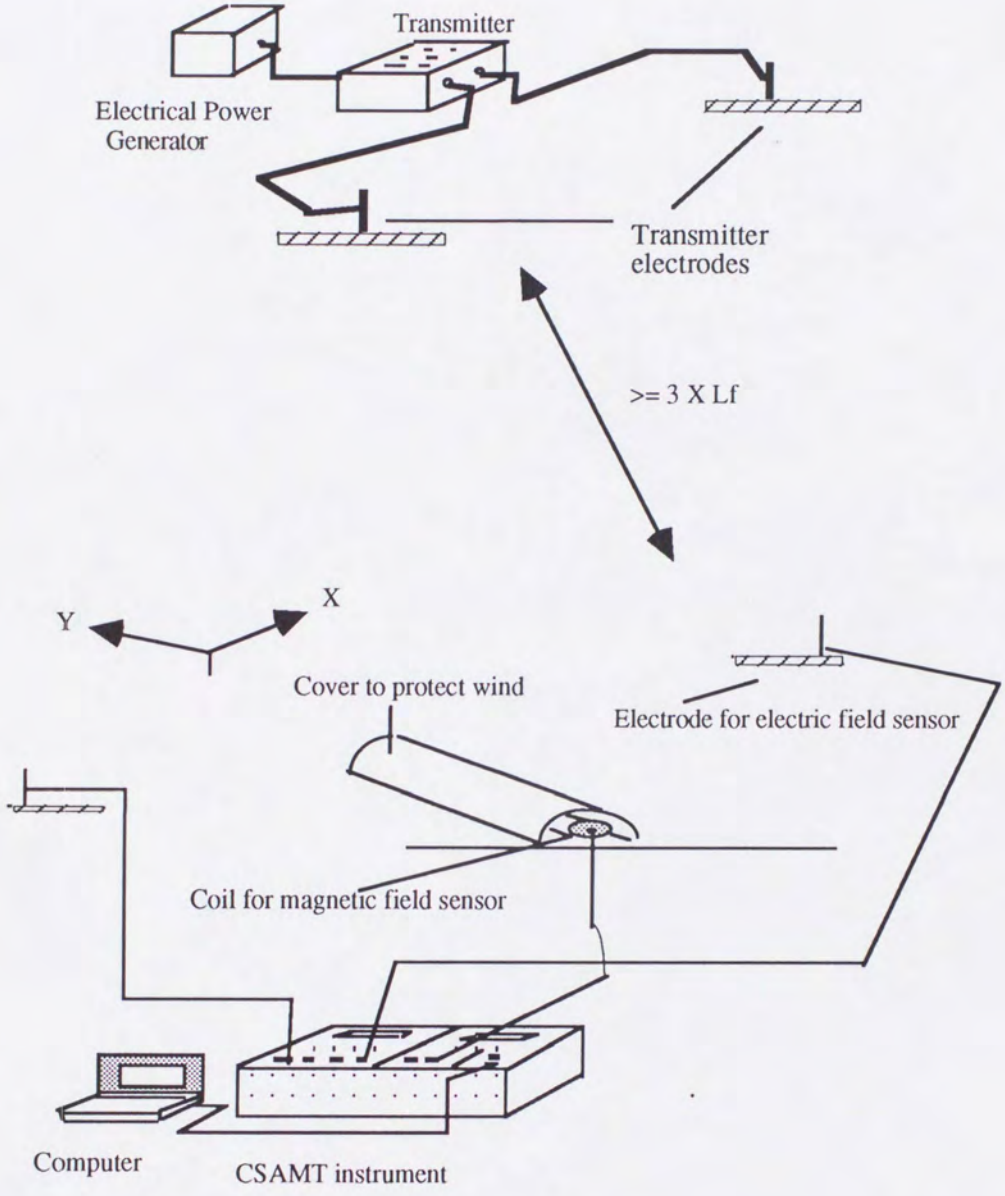

Fig.20. Field set-up of the CSAMT survey at Sakurajima volcano, which measures magnetic and electric field components from a finite grounded dipole source.

The total of CSAMT measurement sites at Sakurajima volcano are 49 sites. Some of the CSAMT sites are coincident or located very close to the previous natural MT as shown in Fig.21.

Two steps of magnetic and electric fields measurement were done for each frequency. The first step is to measure only natural magnetic noise; in this case the source was turned off. The second step is to measure magnetic signal that is composed of natural magnetic noise and source signal; in this case the source was turn-on.

TDEM

TDEM method was applied at Sakurajima volcano in order to overcome the depth penetration problems. The depth resolved resistivity structure using natural MT or CSAMT methods is limited in depth especially in low resistivity zones like Sakurajima volcano. The secondary magnetic field is generated by injecting step voltage direct-current through a grounded wire-line which is separated 1.5 to 2.5 km. Transmitter with maximum output capacity 100 Amperes at period from 1 sec to 128 sec was used. In this survey, the current was 30 A to 26 A for per 16 seconds automatically turn-on and off every 16 seconds. Field set-up of the TDEM survey is shown in Fig.22.

The Fluxgate magnetometer as sensor of secondary magnetic field records an external steady geomagnetic field $Hex_{(t)}$ which is overlain with earth induced source field $H_{(t)}$. By canceling the steady (natural) geomagnetic field, the remaining magnetic field is proportional to the

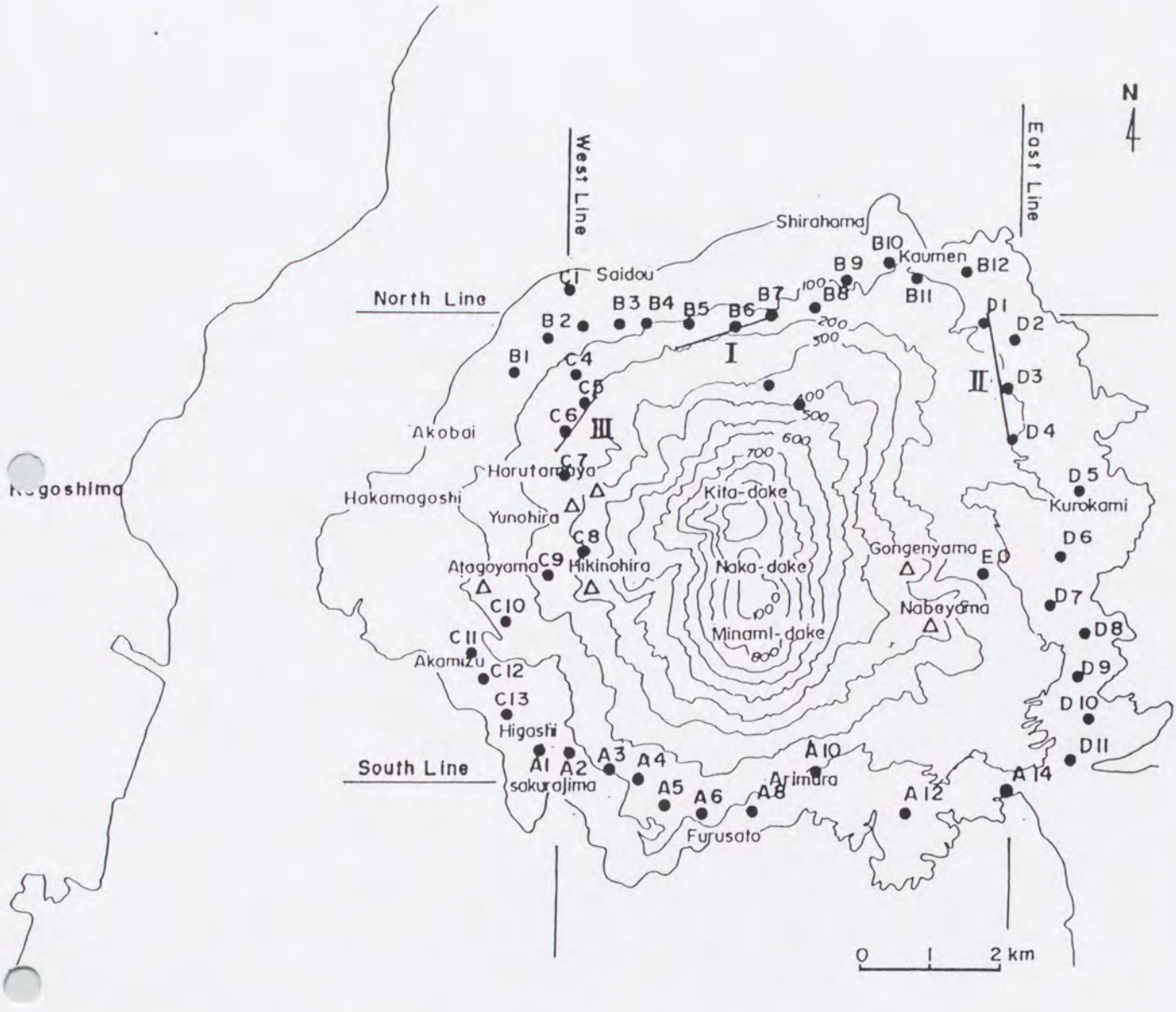

Fig.21. Location of the CSAMT measurement sites (•) around Sakurajima volcano. I, II, III are the electric current sources to generate the electromagnetic field. I is as source of the south line, II is as source of the west and the north lines, and III is as source of the east line. Δ is parasitic cone.

output voltage $V_{(t)}$. This output voltage then transformed by an A/D converter and stored digitally in a personal computer. After the current is shut-off, the Fluxgate magnetometer sensor measures the transient responses of the magnetic field of the earth. The decay of the magnetic field is proportional to voltage response as time function. Sampling at the rate from 0.4 to 1 ms of transient electromagnetic responses was done during this survey.

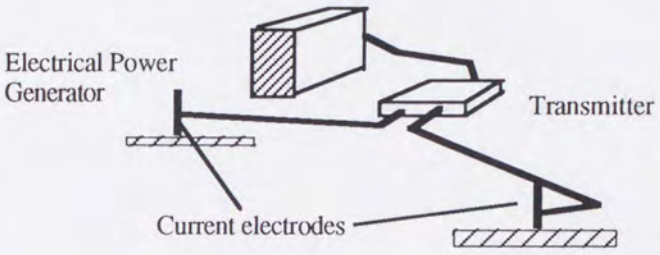

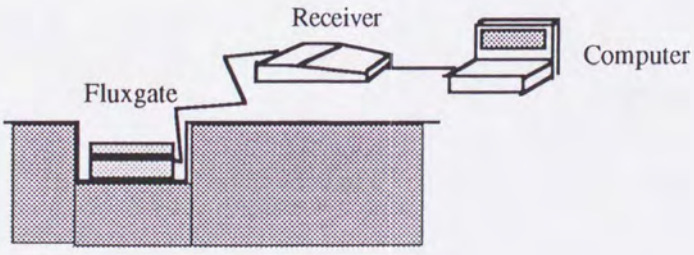

Fig.22. Field set-up of the TDEM survey at Sakurajima volcano, which measures all magnetic field components from a finite grounded dipole source.

The TDEM survey along north, west and south sides of Sakurajima volcano have been conducted using source I and source II in 1990. Source III was used as source for TDEM survey along east side of Sakurajima volcano in October 1993. Transmitter positions and 36 TDEM observation sites around Sakurajima is shown in Fig.23.

2.4.3. Data analysis of CSAMT and TDEM surveys

CSAMT

The analysis of CSAMT data is relatively simple because measured apparent resistivity values are in scalar value. First step in analysis is to extract the source signal from the signal which is contaminated with natural electromagnetic noise. We defined formulation:

$$S = \{ (NS)^2 - (N)^2 \}^{1/2} \qquad (15)$$

Where S is source signal, NS is natural noise plus source signal and N is natural noise.

Ratio of source signal to natural noise (S/N) is used as criterion to select data. The data is only accepted if it has S/N ratio equal or more than 1. An example of CSAMT sounding curve is shown in Fig.24. The next steps of the CSAMT data analysis are 1-D and 2-D resistivity modeling in order to know resistivity structure. The procedures are the same as in the ELF-MT analysis. Fig.25 is the result of 1-D analysis.

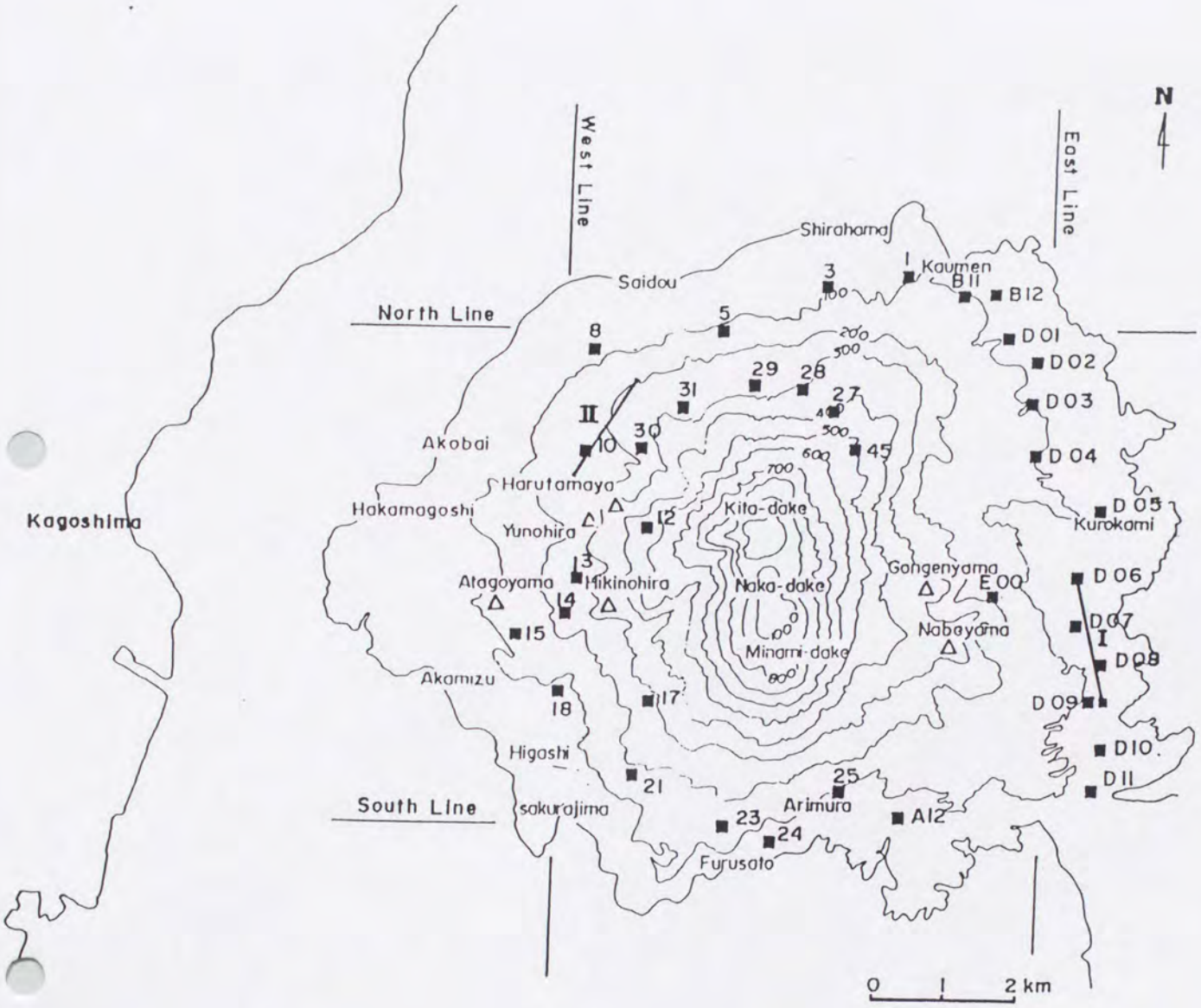

Fig.23. Location of the TDEM measurement sites (■) around Sakurajima volcano. I and II are the electric current sources to generate the magnetic field. I is as source of the west, south and north lines, II is as source of the east line. Δ is parasitic cone.

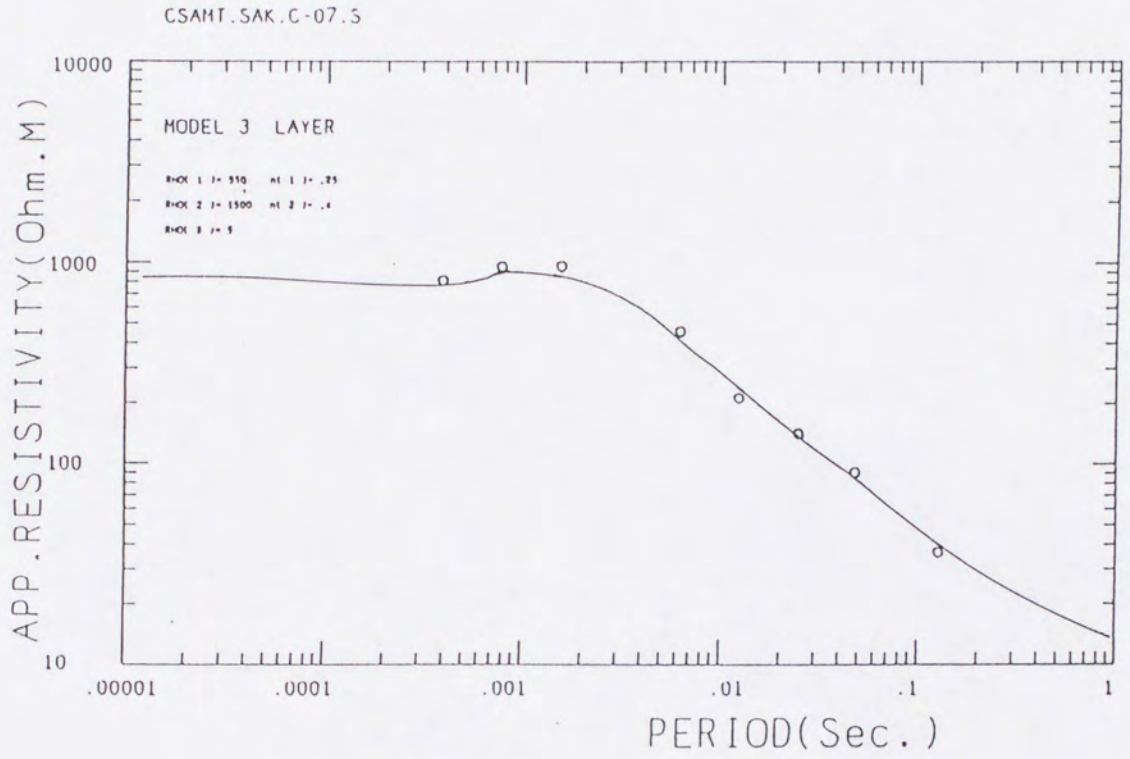

Fig.24. An example of 1-D analysis result of the CSAMT survey at site C-07. The open circles are observed data and solid line is calculated value. Resistivity (Rho) value in ohm-m and thickness (h) in km.

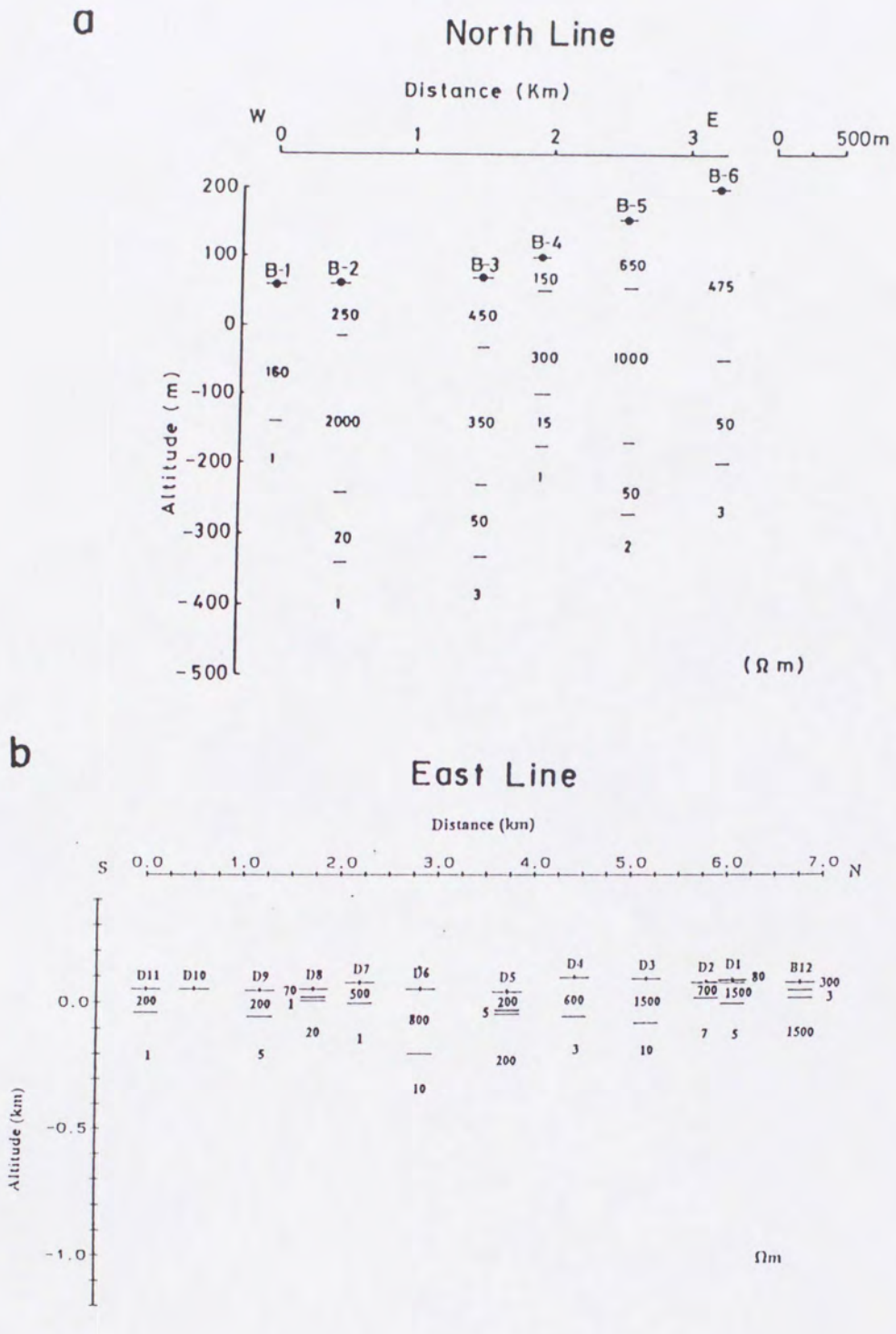

Fig.25. Resistivity structure of Sakurajima volcano inferred from CSAMT 1-D model. a) north line, b) east line, c) south line, and d) west line.

c

South Line

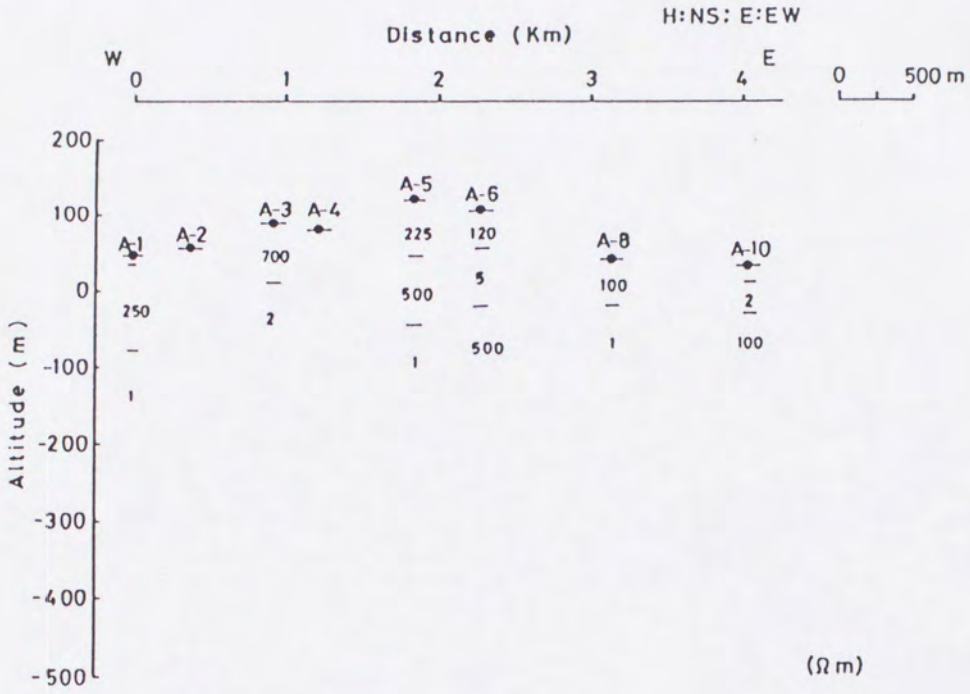

d

West Line

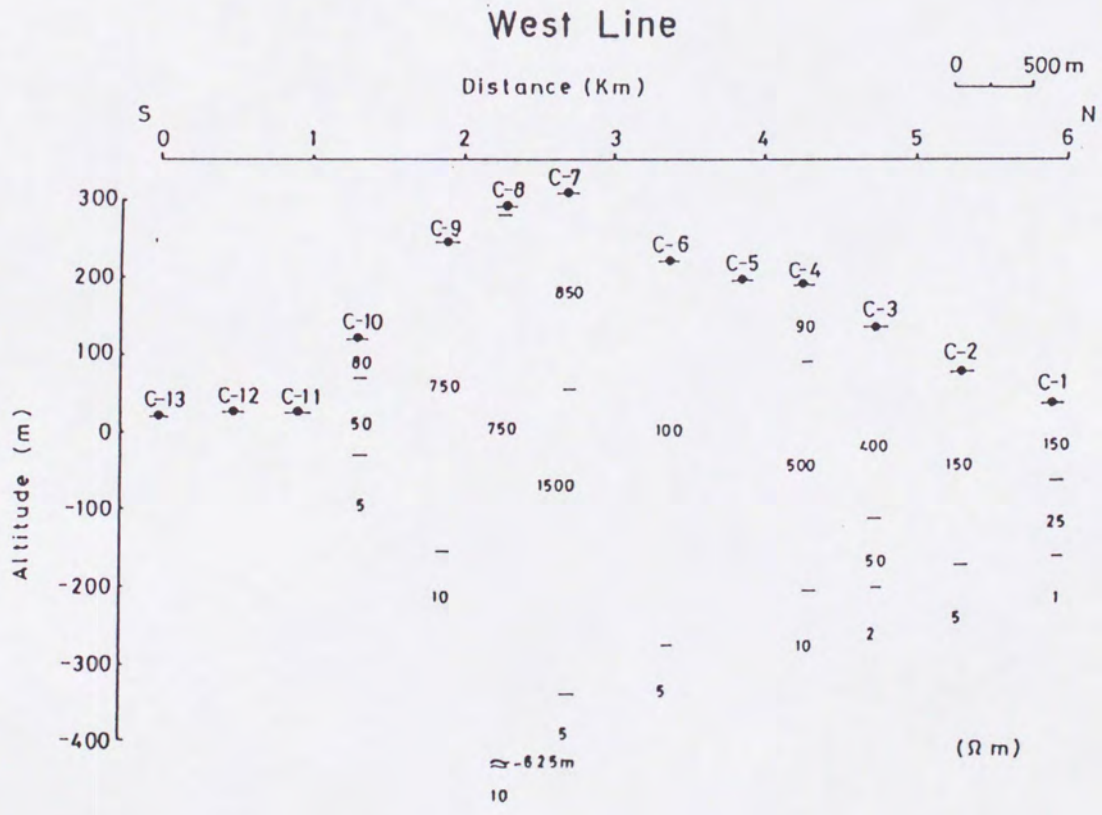

TDEM

Data processing and analyses of TDEM data are;

(1). Cumulative stacking of a set of recorded field data for every site.

During data acquisition in the field, the signals were recorded for every 5 up to 20 stacks, depending on the signal strength or noise situation. It was done repeatedly to obtain an average of about 100 stacks in a measurement at a sounding site. A single primary level of magnetic field is found by doing cumulatively continuous stacking at laboratory. The result of a cumulative stacking at site D.03 is shown in Fig.26.

(2). Static shift correction

Static correction was applied due to the fact that the initial strength of recorded signals in the field are sometimes lower than their theoretical value of primary field. It was caused by lateral changes in conductivity, Instrumental error, topographic and artificial electromagnetic noise.

$$Bz_{(t)\,cor.} = Bz_{(t)} + \delta_{(t)} \qquad (16)$$

Where $Bz_{(t)\,cor.}$ is the discretely primary vertical magnetic field intensity as time function after corrected, Bz(t) is the discrete primary vertical magnetic field intensity as time function before correction, and $\delta(t)$ is static shift correction.

$$\delta_{(t)} = (Bz_{p.cal} - Bz_{p.obs}) \times \{(Bz_{(t)} - Bz_{(t).min})/Bz_{p.obs}\} \qquad (17)$$

Where $Bz_{p.cal}$ is theoretical value of primary vertical magnetic field

a

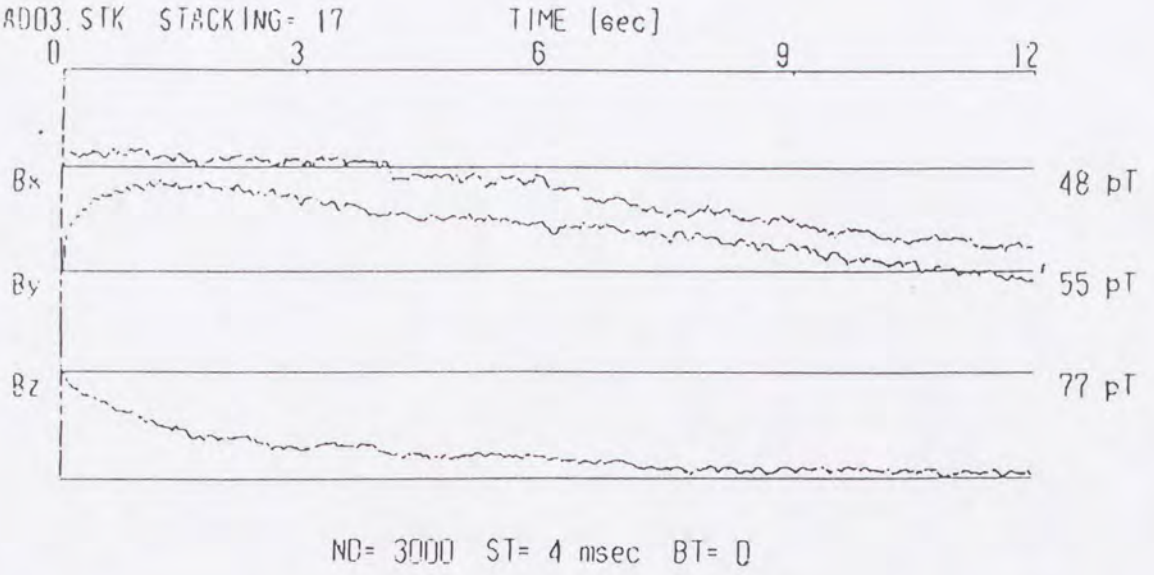

b

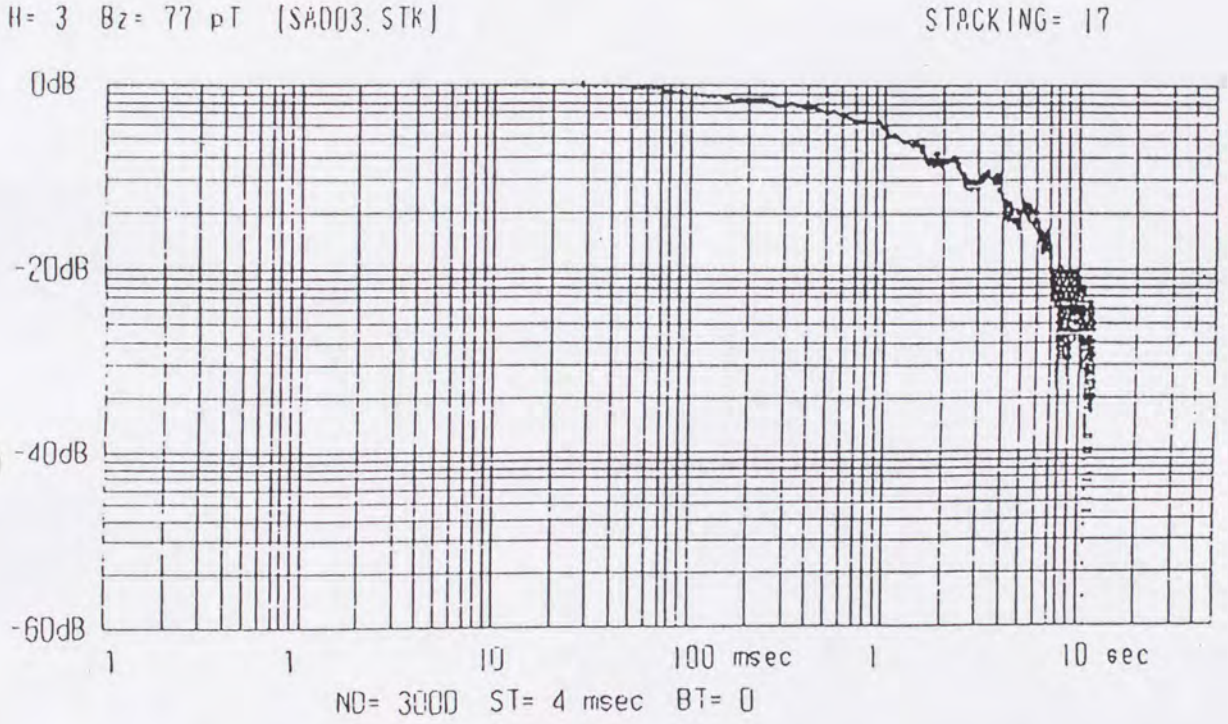

Fig.26. An example of step transient response curve of the TDEM survey at site D.03. Decreasing of the magnetic field intensities for all components (Bx, By, Bz) are given in linear scale (a), and in log-log scale only for vertical component, Bz (b).

intensity and $Bz_{p.obs}$ is an observed value of primary vertical magnetic field intensity.

$$Bz_{p.cal} = \mu_o \, i \, dl \sin\theta / 4\pi r^2 \qquad (18)$$

Where r is source-receiver distance in meters, i is current source in Amperes, dl is a finite length of the source, and θ is the orientation angle between source and receiver.

(3). Instrumental correction

The objective of instrumental correction is to extract the response of the earth from the received signal. It was done by deconvolution process in the frequency domain.

(4). Calculation of apparent resistivity and depth

To calculate apparent resistivity and depth, Hasegawa (1985) and Nekut (1987) proposed direct interpretation technique to perform 1-D resistivity structure using formulations :

$$\rho_a = \mu_o r^2 \, g \, [B_z(t)] / 4t \qquad (19)$$

$$\delta = \{ 2 \, t \, \rho_a / \mu_o \}^{1/2} \qquad (20)$$

Where g is the function of the transient response Bz(t), the diffusion depth, δ, is equivalent to the usual skin-depth formula.

Joint inversion of CSAMT and TDEM data analysis

The CSAMT method has good accuracy and resolution for estimating shallow resistivity structure, but is weak in penetration. The TDEM gives information for deep resistivity structure but has low resolution for shallow resistivity structure. Therefore joint inversion of CSAMT and TDEM data analysis to construct 1-D resistivity structure is a better way for study resistivity structure to overcome resolution and penetration.

A 1-D CSAMT-TDEM joint inversion was evaluated using the simplex method (Nelder and Mead, 1965). The initial resistivity structure for shallow layers was fixed from CSAMT data and for deeper part was taken from TDEM data. A Fortran program was created to compute resistivity and thickness of each layer iteratively (Mogi, 1992; personal comm.). The program will be terminated automatically at n-th iteration when the minimum error between calculated and observed data has been reached or the calculation approximates the convergence limit. The location and the result of joint inversion of CSAMT and TDEM data analysis are shown in Fig.27 and Fig.28.

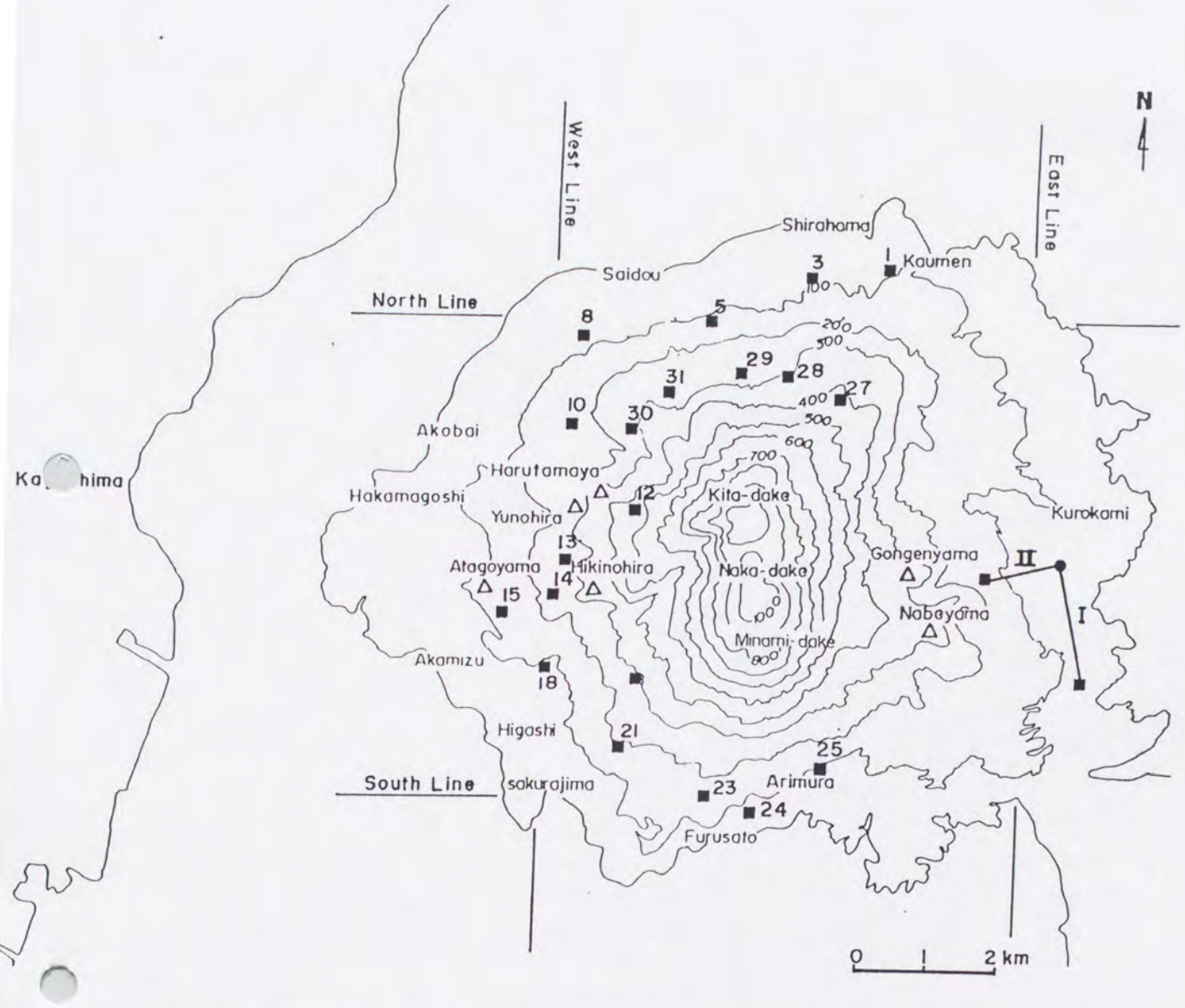

Fig.27. Location of the CSAMT and TDEM joint measurement sites (■) around Sakurajima volcano. I and II are the electric current sources to generate the magnetic field. I is as source of the west and the south lines, and II is as source of the north line. Δ is parasitic cone.

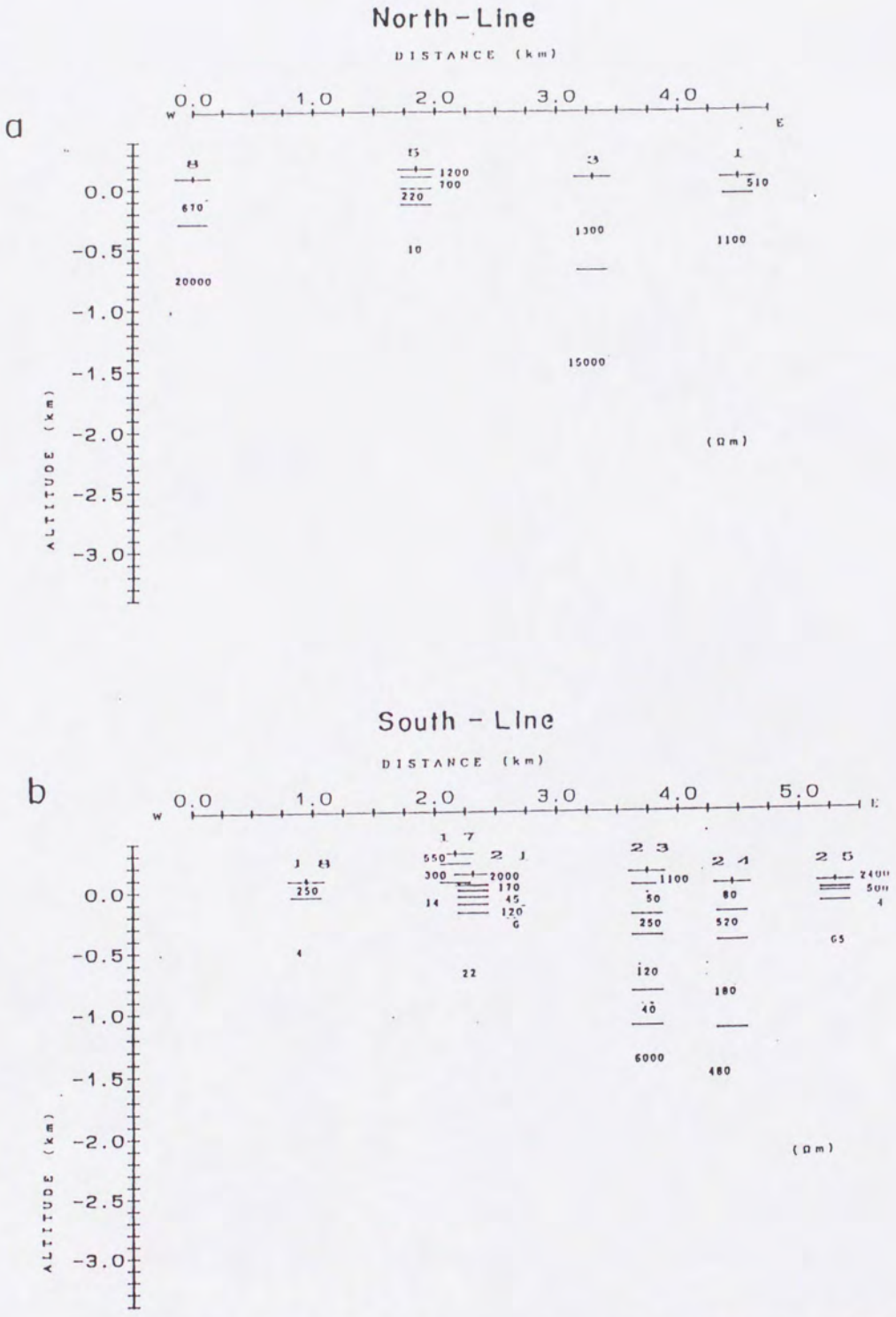

Fig.28. Resistivity structure of Sakurajima volcano inferred from CSAMT and TDEM joint 1-D analysis. a) north line, b) south line, and c) west line.

C

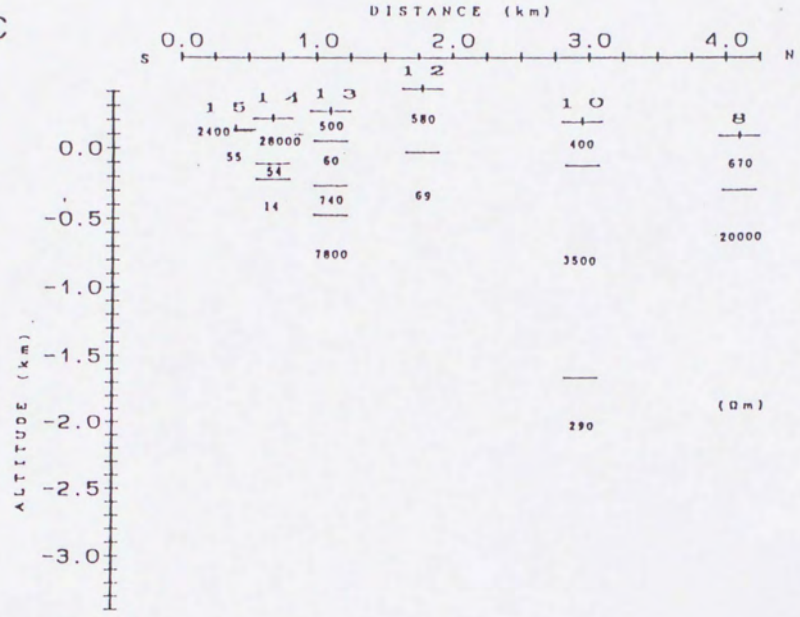
West – Line
DISTANCE (km)
0.0
1.0
2.0
3.0
4.0
S
N
ALTITUDE (km)
0.0
-0.5
-1.0
-1.5
-2.0
-2.5
-3.0
15
14
13
12
10
8
2400
28000
500
580
400
670
55
54
60
69
14
140
20000
7800
3500
290
(Ωm)

2.4.4. Resistivity structure beneath Sakurajima volcano Inferred from CSAMT and TDEM surveys

Fig.29 shows 2-D model analysis resulted from CSAMT survey for north, south and west lines. These results show good correlation with the ELF-MT results in case of resistivity structure pattern such as;

1) The top layer has high resistivity values.
2) Resistivity of north side is relatively higher than other sides.
3) Highly conductive layer (1 ohm-m) is found at south line beneath sea level, but beneath site of A6 has resistivity ten times higher where this site is coincided with site 8 of ELF- MT.
4) Contrast resistivity caused by parasitic cones, lava dome also clearly appears, see site C-7, C-8, C-9 and C-10 of west line.
5) The basement is a highly conductive layer.

Numerical value of each layer and detailed resistivity structure are different between ELF-MT and CSAMT methods. Resistivity values have great variation from time to time because they have been related to earthquake signals (Mazzella and Morrison, 1974; Sumitomo and Noritomi, 1986), salinity and temperature (Honkura et al., 1976), groundwater level and ground temperature (Xu, 1986) and drastic rainfall changes (Padilha et al., 1992). At Sakurajima volcano, as an active volcano, changes of resistivity values suggest a closely relation with magma activity. It will be described in discussion.

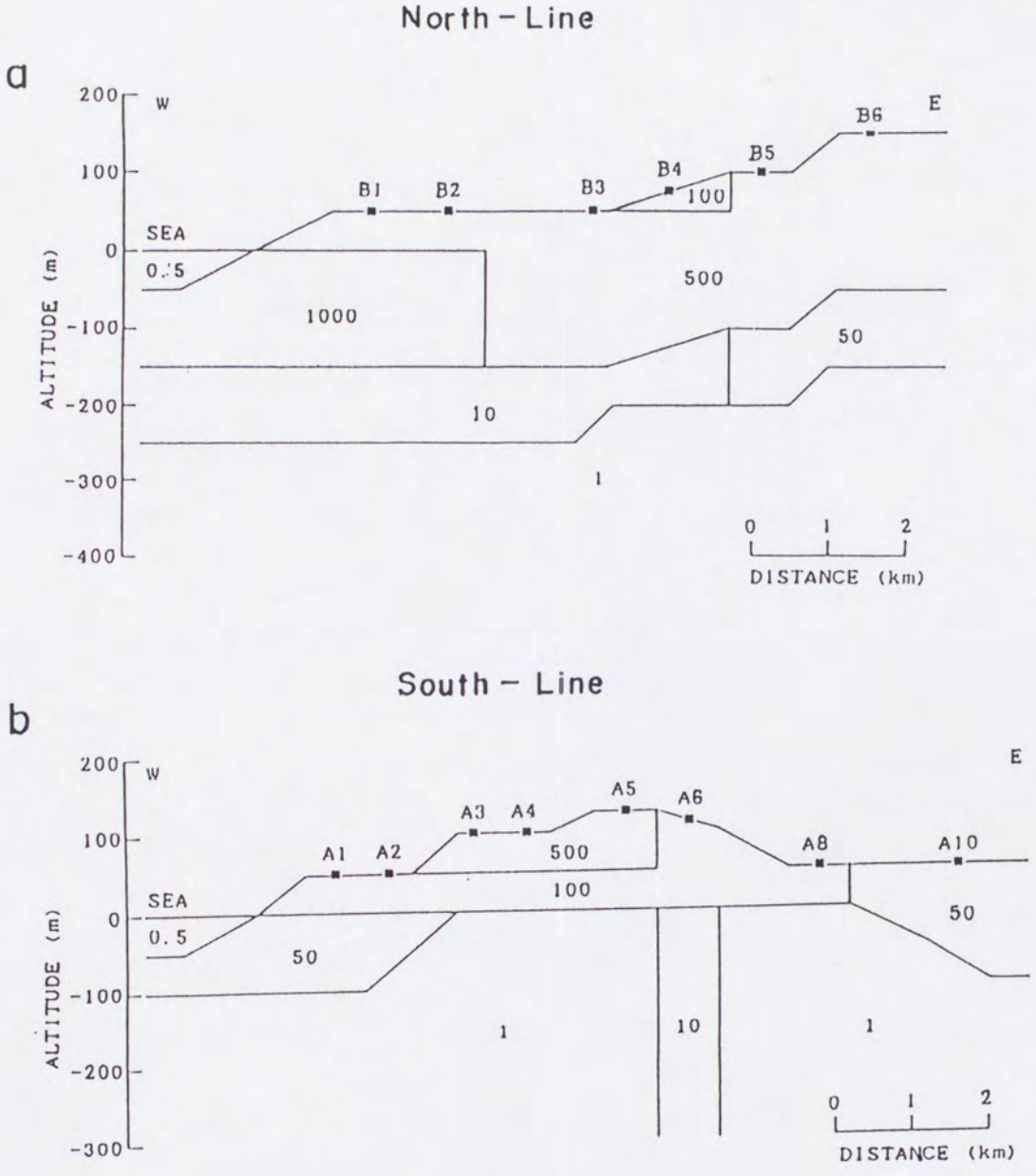

Fig.29. Resistivity structure of Sakurajima volcano inferred from CSAMT 2-D model. a) north line, b) south line, and c) west line. Numerals denote resistivity in ohm-m.

C

West – Line

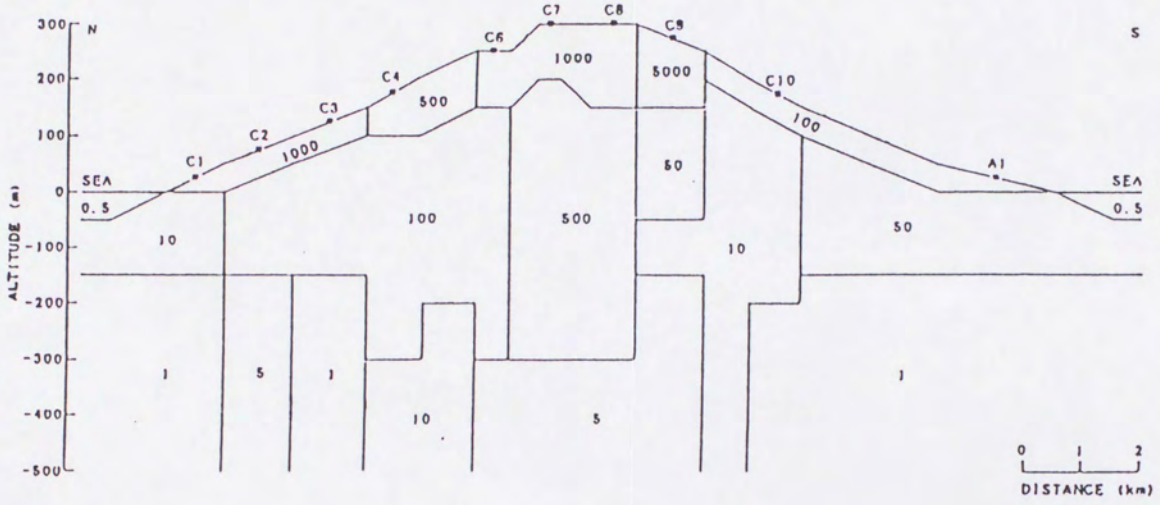
N
S
C1
C2
C3
C4
C6
C7
C8
C9
C10
A1
SEA
SEA
0.5
0.5
1000
500
1000
5000
100
50
10
100
500
10
50
1
5
1
10
5
1
ALTITUDE (m)
300
200
100
0
-100
-200
-300
-400
-500
0
1
2
DISTANCE (km)

Fig.28 shows results of a joint inversion of 1-D analysis of CSAMT and TDEM method for north, south, and west lines. The deep resistivity structure inferred from TDEM method is almost the same as previous method in that resistivity structure beneath Sakurajima volcano is characterized by low resistivity values. The resistivity of north line shows higher than other sides particularly at site 8 and 3. Low resistivity values of the north line are found at site 5. At south line with conducting layers are observed from almost sea level and the high resistivity anomaly is seen beneath site 23 and site 24. These sites are same locations with the past surveys. The resistivity values of the northern part of the west line has high resistivity values.

2.4.5. Presence of high conductive body beneath Sakurajima volcano estimated by TDEM method

The vertical component of magnetic induction field which measured by Fluxgate magnetometer in TDEM method, shows different transient pattern depending on the resistivity of medium between transmitter and receiver. The presence of a very conductive body or low resistivity value of medium between transmitter and receiver will yield a slow transient pattern of vertical component of magnetic induction field. An example of this phenomenon at the site 12 appears as shown in Fig.30. Using source I, the transient pattern decreases slowly because the magnetic field passed the conductive body. However, using source II,

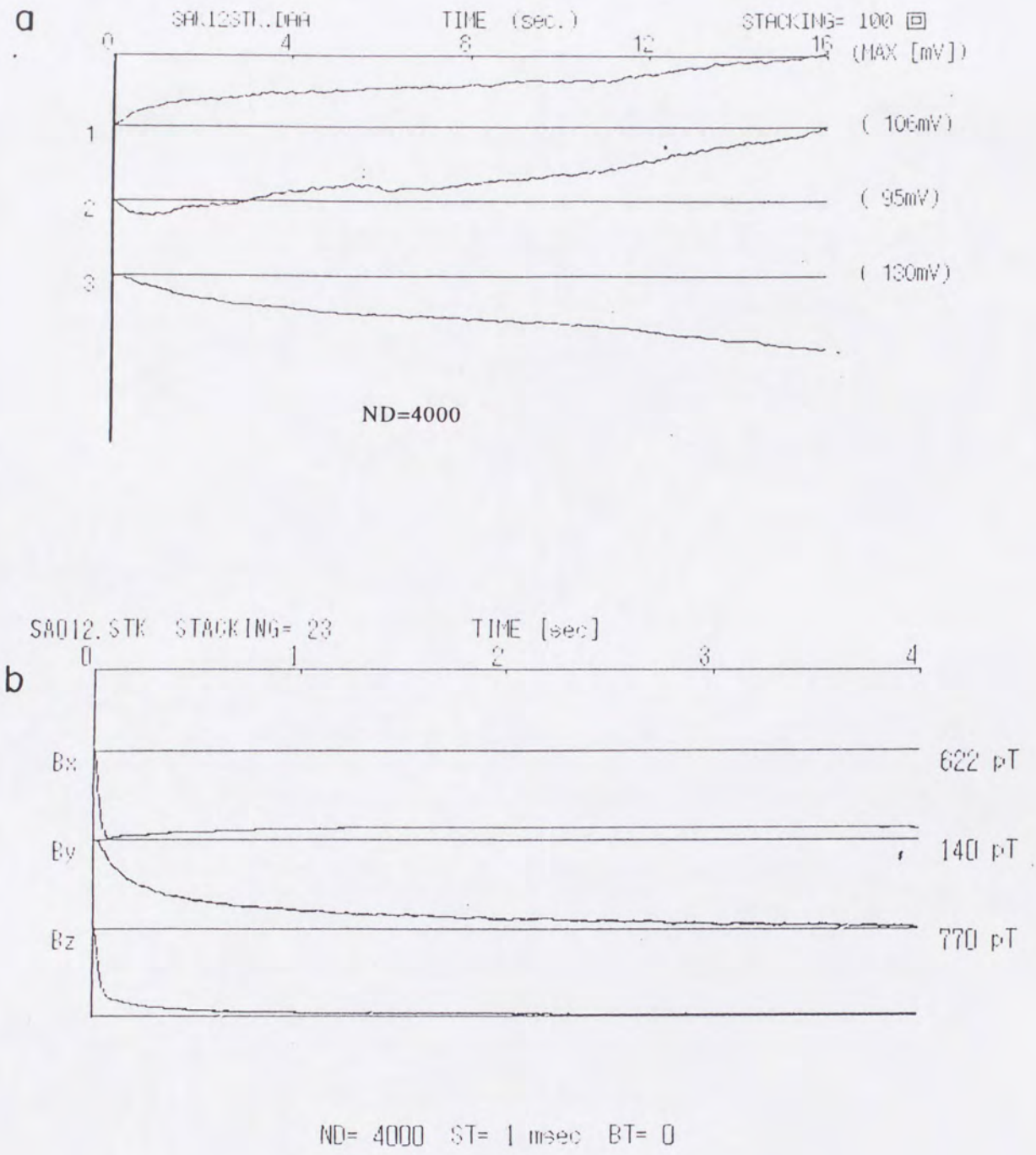

Fig.30. An example of the different transient pattern of vertical component of magnetic induction field at site 12. a) Slow transient pattern using source I and b) Fast transient pattern using source II.

the transient pattern decreases quickly.

TDEM method which were measured in 1990 and 1993 gives evidence of the presence of very conductive body beneath Sakurajima volcano. The measurement results from site 21 to site 31 which were measured in 1990 by using source I, yield slow transient pattern of vertical component of magnetic induction field after the electric source was cut-off. The same patterns appear from site D06 to site A12 of the TDEM results measured in 1993 by using source II. By drawing the line from each the source to the each slow transient site, the "shadow" area was found as shown in Fig.31. This shadow area represents a conductive zone which may be high temperature rocks associated with magma reservoir, however, the depth of shadow area is not known yet.

The existence of high temperature rocks or magma reservoir beneath Sakurajima volcano has been recognized by Ono et al. (1978) and Kamo et al. (1977, 1980) based on seismic survey. They found out that a large attenuation of seismic wave occurred under Sakurajima volcano and Aira caldera.

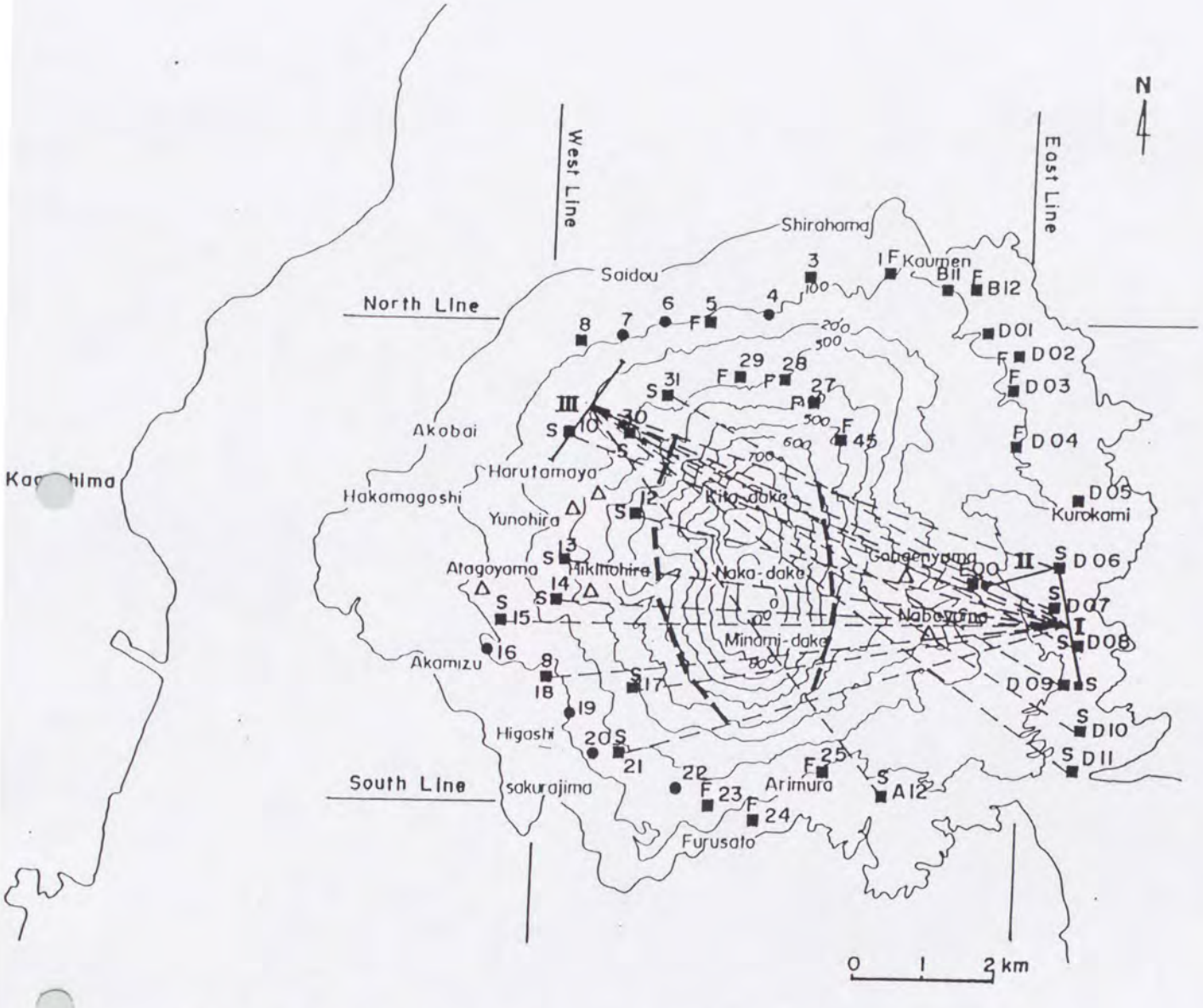

Fig.31. Distribution of slow-transient anomalies as a result of TDEM survey around Sakurajima volcano. I and II are the transmitters. S and F are the sign of the site for slow-transient and fast-transient decreasing secondary magnetic field. Thin dash lines connect between the slow-transient sites and the source. Thick dash line is the estimated the boundary of an area ("shadow area") which exhibits slow-transient of TDEM result. ç and Δ are TDEM measurement site and parasitic cone.

2.5 Discussion

Based on a line of evidence of geomagnetic anomaly (Blank et al., 1966, Matsuzaki and Utashiro, 1966), distribution of epicenters and hypocenters of volcanic earthquakes (Nishi, 1978), the observation of large attenuation of S-seismic wave (Ono et al., 1978, Kamo et al., 1977, 1980), distribution of heat flow and Curie point (Ehara, 1992) and TDEM results, it is suggested that the low resistivity value of the lowest layer model beneath Sakurajima volcano reflects that of high temperature rocks associated with magma activity. The resistivity value of the south line is more conductive than the north line, conforming with distribution of epicenters and hypocenters of volcanic earthquakes (Nishi, 1978) that magma activity comes from the southern part of volcano. Comparison between geological and resistivity cross section is presented in the appendix of Sakurajima volcano.

The resistivity value in a volcano mainly depends on the rocks type, porosity fraction, concentration of clay and hydrothermal minerals. The low resistivity layer may reflect either water bearing rocks or high temperature. Generally, fresh igneous rocks have resistivity values higher than sedimentary rocks. Relation between porosity factor and formation factor (rock resistivity and water resistivity) for volcanic and sedimentary rocks have been reported by Keller and Rapolla (1974). Formation factor of sedimentary rocks having 0.20 porosity factor is about 0.35 times the formation factor of those having 0.10 porosity factor. The resistivity value of the sedimentary rocks decreases with increasing porosity.

Based on the Koike borehole data to depths of 800 m (Aramaki, 1977), the formation of the fourth layer as the bottom layer of the third and the basement layers in the resistivity structure corresponds to the Kekura Formation. Kekura Formation consist of marine deposits, composed of tuffaceous silt and sand. The third and the basement layers, however, show high contrast resistivity values. The third layer has about 300 to 1,500 ohm-m resistivity and the basement layer has less than 10 ohm-m resistivity. Porosity factor of the general sedimentary rocks has ranges from 0.07 to 0.40 (Keller and Frischknecht, 1966, Keller and Rapolla, 1974). Naturally, the lower part of the sediment piles should here a slightly higher density than the upper part in the same formation, unless if the materials sedimented is different. Assuming that the lower part and the upper part of the Kekura Formation have porosity factor of 0.20 and 0.10, the difference in porosity factor is not enough to lower resistivity value to that of the basement layer. Therefore, the high contrast of resistivity values between the lower and upper parts of the Kekura Formation is difficult to explain based on the concept of different porosity factor.

Concentration of the electrolyte conductivity in water bearing rocks is a significant factor in lowering resistivity. At temperature 20°C, the resistivity of sodium chloride solutions having salinity 1.0 gram/liter is 0.10 times of the same solutions having salinity 0.10 gram/liter. The influence of sea water on resistivity structure may occur at the southern part of the east line and at the eastern part of the south line with resistivity less than 10 ohm-m. In this part, the Taisho lava flows extend far into the sea. The sea water has high salinity about 10 - 100 gram/liter. The pore-

water resistivity of rhyolitic tuff from the Oak Springs Formation, southern Nevada was determined by Keller (1974). He found pore-water resistivity to be about 1.04 to 2.13 ohm-m. However, the high resistivity value of the third layer beneath Sakurajima volcano is evidence that the sea water does not seep intensively into volcanic system. Thus, the influence of the electrolyte conductivity coming from the sea water intrusion into the basement layer of Sakurajima volcano is almost excluded.

Fig.32-1 shows relation between resistivity of water saturated rock samples and temperature. The resistivity values of granite, gabbro, andesite, sandstone and quartz sand at temperature 200 °C are about 0.15 to 0.10 times of the resistivity value at temperature 27 °C (Yokoyama, 1983). The resistivity of almost all volcanic rocks decreases sharply at temperature about 500 to 700 °C (Parkhomenko 1967, Keller and Frischknecht, 1966). Changes of resistivity value as function of temperature can be seen from the direct measurement of molten rocks. The molten basaltic lava with temperature about 1000 to 1200 °C measured in the lava lake of Kilauea-Iki crater by a two-loop frequency-domain electromagnetic technique has resistivity value about 2.5 ohm-m. This value is about 0.025 times the resistivity of a sample of the same rock immediately below the melting point, and many hundreds of times lower than the resistivity of a basaltic lava flow as normally found at the surface of the volcano (Keller and Rapola, 1974).

In many cases, the results measured in the laboratory or on the surface in the normal pressure and temperature conditions do not always reflect the true condition of the natural subsurface condition. However, the results are useful in predicting unknown conditions. The basement layer

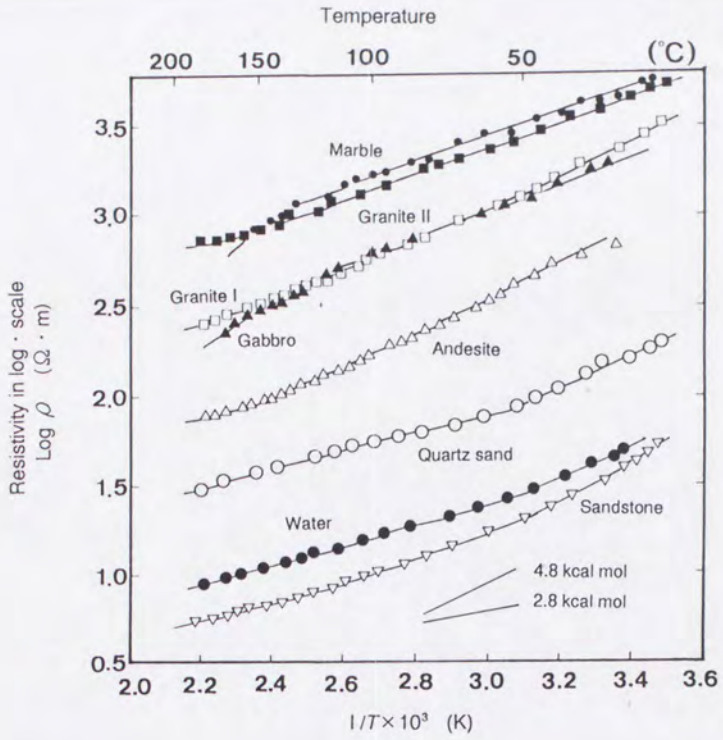

Fig.32-1. Resistivity values of water saturated rock samples in the ranges temperature 27°C and 277°C (Yokoyama, et al., 1983).

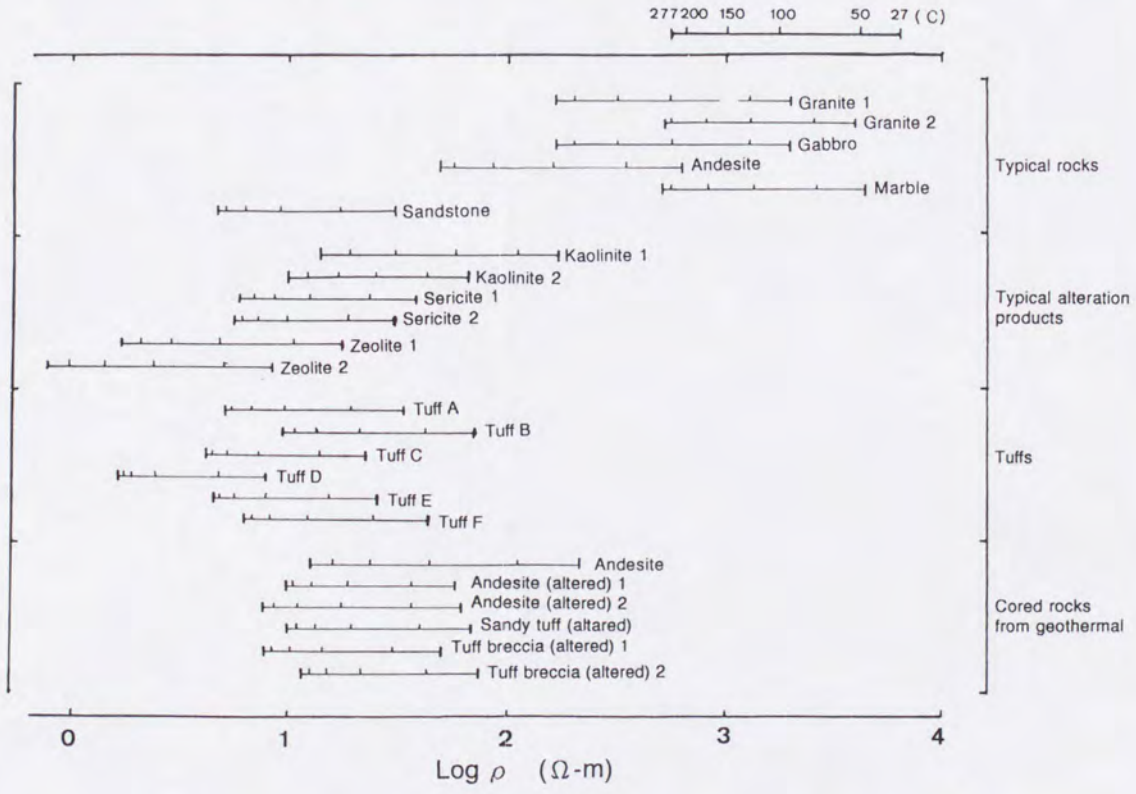

Fig.32-2. Resistivity values of water saturated rock samples in the range of temperature 27°C and 277°C (Yokoyama, et al., 1983).

beneath Sakurajima is not in molten condition, but it should at least have high temperature or another conditions.. The dependence of resistivity on temperature for either an electrolyte or a rock saturated with an electrolyte is given by the equation (Keller and Frischknecht, 1966) :

$$\varrho_t = \frac{\varrho_{18^o}}{1 + \alpha_t (t - 18^o)} \qquad (21)$$

where ϱ_t is the resistivity at temperature t°C, ϱ_{18^o} is the resistivity measured at a reference temperature of 18°C, t is the ambient temperature and α_t is the temperature coefficient of resistivity, which has a value of about 0.025 per degree centigrade for most electrolytes. Temperatures within the first few km of the earth's crust rise gradually with depth at a rate of about 0.5°C per 30 m in sedimentary rocks and about 0.2°C per 30 m in igneous rocks. Temperature at depth of 2400 m in sedimentary rocks will be about 40°C higher than the temperature at the surface, and this difference in temperatures means the rock at depth of 2400 m has a resistivity of half value of the same rock would have at the surface.

If temperature gradient of 0.5°C per 30 m is applied to estimate the temperature at the boundary between the third and the fourth layer which has depth of 400-600 m, the temperature would be 26.6-30°C, assuming 20°C for ground temperature. Temperature gradient around Sakurajima volcano is about more than 10°C /100 m (Okubo, 1993). The temperature at the boundary between the third and the lowest layer would be 50-80°C applying the temperature gradient , and with assuming 20°C for ground

temperature. Both estimated temperatures seem to be low for 400-600 m depth beneath Sakurajima volcano. The temperature is about 578 to 778 ^{o}C at the boundary the third and the lowest layers calculated using Eq.(21). The estimated temperature is calculated assuming that resistivity at reference temperature of 18^{o}C is in the ranges from 150 to 200 ohm-m and resistivity at the boundary layer is about 10 ohm-m.

Another possibility for lowering resistivity related to thermal activity beneath Sakurajima volcano is the presence of clay minerals. Hydrothermal interactions with the surrounding rocks produces alteration clay minerals. It may be kaolinite, halloysite, montmorilonite, illite, sericite, zeolite etc. depending on the source rock. Yokoyama et al. (1983) reported that the low resistivity values were obtained for typical alteration products and tuffs in the range of temprerature 27 °C and 277 °C, as shown in Fig. 32-2. Even in room temperatures the resistivity of rocks containing clay minerals is low. The decrease in resistivity at low salinities is more pronounced in fine-grained rocks.

From deep structure analysis it is difficult to figure out the exact magma chamber dimension beneath Sakurajima volcano, since the heat coming from the magma chamber is transmitted to the surrounding rocks. The high temperature rock will make low resistivity zones around the magma chamber and reduce the capability of penetration of electromagnetic energy. Similar cases have been observed in the active volcanic areas at Western United States. Almost all electromagnetic methods (Direct current resistivity, Magnetotelluric Soundings, Controlled Source electromagnetic Soundings and Transient electromagnetic soundings) have been applied to study Mt. Konocti. The conductor

appears to be associated with hot fractured rock saturated with water, but a magma chamber was not successfully mapped. Perhaps the shallow conductor masked any signature which may be produced by a deeper magma chamber. Magma chamber is either too small or too deep for detection by electromagnetic method (Skokan, 1993). The presence of shallow conductor will generate current channeling so that the response from a deep structure is subdued (Newman et al., 1985).

2.6. Summary

The resistivity structure of Sakurajima volcano has highly inhomogeneous and anisotropic characteristics. The major principal axis of tensor impedance, seems to be related with the elongated-shape of Kagoshima Bay, the caldera chain in the southern Kyushu, the hypocentral distribution of volcanic earthquakes, and the boundary striking along the southern rim of Aira caldera. The outward or concentric directions of major axis at frequency 20.5 Hz is probably caused by sea water.

Some important notes in the resistivity structure beneath Sakurajima volcano can be summarized as below;

1. The resistivity structure beneath Sakurajima volcano inferred from 2-D model analysis consists of 4 layers.
2. Resistivity in the northern part of Sakurajima volcano relatively higher than in the southern part of Sakurajima volcano.

3. The surface layer represents lava-flows of Sakurajima volcano characterized by high resistivity value from 250 to 3,000 ohm-m to depths of 50-100 m.
4. The second layers have mainly resistivity of 100-150 ohm-m and 200-300 m thickness. It is interpreted as non-welded pyroclastic deposits emitted from Aira caldera. The boundary between the surface and the second layers almost coincides with the sea-level.
5. The third layers have 300-1,500 ohm-m resistivity and 200-300 m in thickness. This layer represents the Kekura Formation.
6. The basement layer has resistivity of 5-10 ohm-m except for the northern part of volcano which has 350 ohm-m.
7. The Shimanto Group cannot be detected by this survey.

The basement layer is also a part of Kekura Formation, as confirmed by the Koike borehole data . However, the resistivity is very low. It suggests the influence of heat originated from magma activity and the presence of clay minerals may be responsible for decreasing resistivity.

Appendix of Sakurajima volcano

Aramaki (1984) shows a schematic east-west cross section of the southern part of the Aira caldera passing through the Sakurajima volcano in Fig.app.-1. The basement complex of this sction is Shimanto Group composed of highly deformed melange-type sediments of shale, sandstone, conglomerate and pillow lava. The Shimanto Group is broken by step faulting in the western part and is overlain by welded pyroclastic flow deposits, Kekura Formation which is mainly composed of volcanic materials. In the western part, the Kekura Formation is overlain by Tsumaya pyroclastic and Ito pyroclastic flows. Beneath Sakurajima volcano is located on caldera.

In order to compare with the geological and the resistivity cross sections, the east-west resistivity cross section passing through the Sakurajima summit is the best one. Unfortunately, there is no MT data in the summit area because its morphology and volcanic activity. North or south lines should be good lines because the same east-west cross section. However, the location of the lines are too close to the shore. The west line has been chosen because the line is crossing the mountain body with the lowest altitude about 60 m at site 1 and the highest about 400 m at site 3 (Fig.app.-2). The west line may represent suitable for correlation between geologic and resistivity cross sections.

Geologically, the MT sites of the west line cross the Bunmei lava flow, old historitical lava flow, Taisho lava flow and some parasitic cones (Fig.app.-3). The top layer of the resistivity model with resistivity varies from 500 to 750 ohm-m represent the lava flow with different eras and present volcanic products such as tuff, scoria, sand etc. The influenced of sea water in the southern part of the cross-section may be occurred which is characterized by 10 ohm-m resistivity beneath site 6. The site 23 and site 3 are located around

Yunohira and Harutayama parasitic cones. The 10 ohm-m continuous resistivity beneath these sites is interpreted as the vent of the Taisho lava flow. The old intrusive volcanic body may correspond with the high resistivity, 3000 ohm-m, beneath site 4 and site 23. The third layer of the resistivity model shows different value between south and north parts. Based on the Koike borehole data, the southern part represents Kekura Formation with resistivity about 750 ohm-m. In the northern part, 250 ohm-m resistivity, is interpreted as "Shirasu" which is composed of white color unconsolidated pyroclastic materials.

Schematic east-west cross section passing through the Sakurajima volcano proposed by Aramaki (1984) does not show geological structure beneath Sakurajima volcano completely such as the vent of volcano. It does not yet clear about caldera fill material beneath Sakurajima volcano. Based on resistivity model of the west line, the Kekura Formation is still continuously beneath the Sakurajima volcano. The presence of the caldera fill material beneath Sakurajima volcano is not observed.

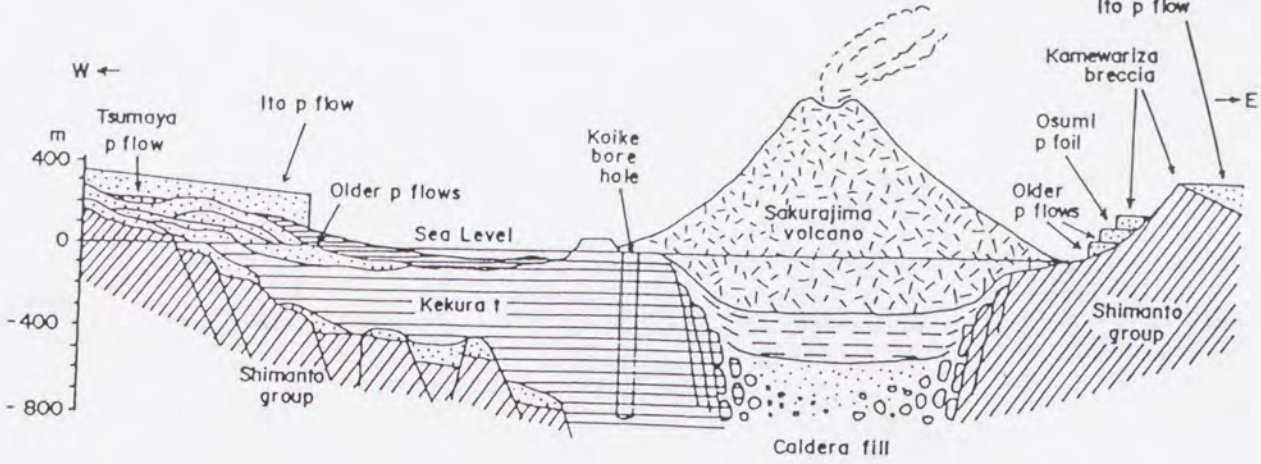

Fig.app.-1. Schematic east-west cross section of the southern part of the Aira caldera passing through the Sakurajima volcano (Aramaki, 1984).

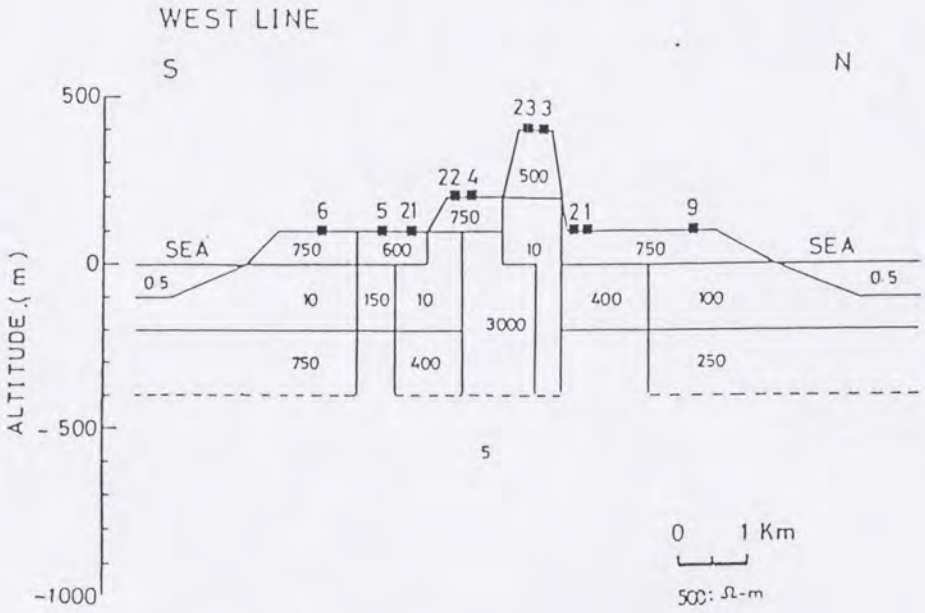

Fig.app.-2. Resistivity structural model of west line inferred from ELF-MT survey.

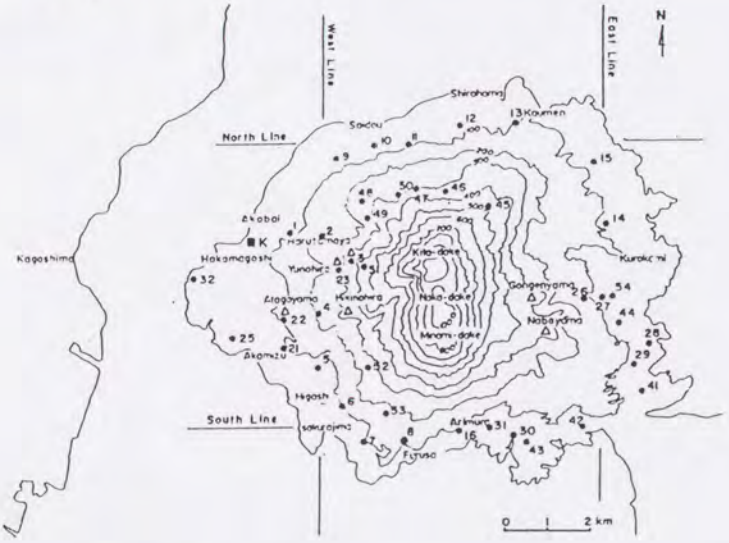

Fig.app.-3. Location of the ELF-MT measurement sites (●) around Sakurajima volcano. K is the borehole site at Koike and Δ is parasitic cone.

3. RESISTIVITY STRUCTURE BENEATH MERAPI VOLCANO

3.1. Introduction

The Indonesian archipelago is one of the active volcanic belts in the world, where about 129 active volcanoes are located. Merapi volcano in Central Java is one of the most active volcano in Indonesia. It is surrounded by densely populated area such as Yogyakarta, Klaten, Boyolali and Magelang cities (Fig.33). Merapi is a strato volcano with altitude 2,986 meters above sea level, located at 7°32' south-latitude and 110°26' east-longitude. The craters of the volcano are not open but plugged by a lava dome. Eruptions have occurred very frequently. The period of eruption ranges between 1 to 7 years, while the period of apparent dormancy is 1 to 12 years. Based on its short interval of eruption, duration of its activity, the product and its distribution, and also the number of population in the surrounding area, the Merapi volcano is classified as a very dangerous volcano in Indonesia (Siswowidjoyo, 1989). The continuous volcanic activity of Merapi serves as good field laboratory for volcanologists and earth-scientists to investigate the volcano and to install various kind of equipment for experiment and research purposes. At present, the Volcanological Survey of Indonesia (VSI) is continuously monitoring the activity by applying various kind techniques known in the volcanological field (Merapi Volcano Observatory, 1990).

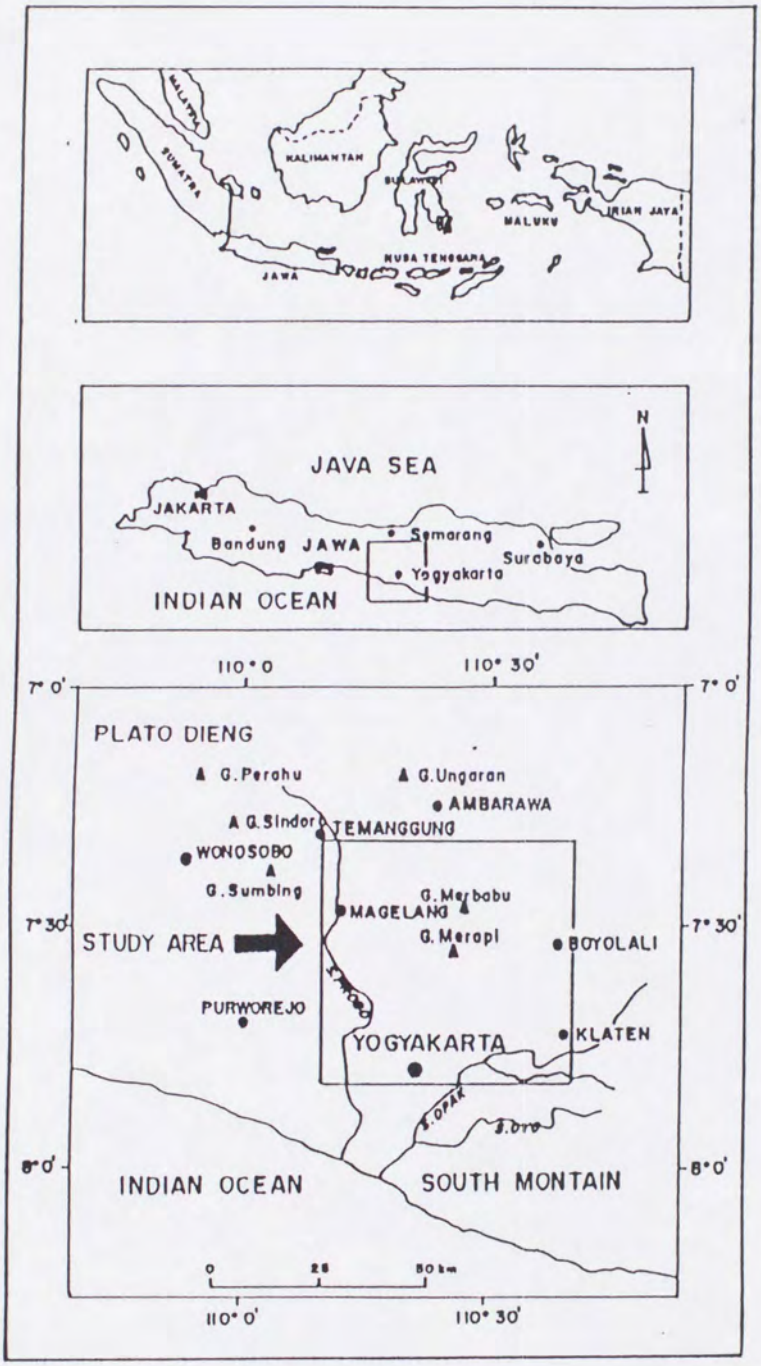

Fig.33. Location of the study area.

The analysis of volcanic seismicity indicates that Merapi volcano has two magma reservoirs; a shallow-reservoir with depth about 2-3 km, and a deep-reservoir with depth about 7-8 km. These magma reservoirs are vertically distributed beneath the summit (Ratdomopurbo, 1991). Based on the volcanic tremor analysis, there are two distinct groups of tremor source locations which can be connected to the volcanic activities of Merapi. The shallow one is about 0.5 km underneath the lava dome and the deep one is about 2.0 Km below the lava dome (Kirbani, 1991). Regional gravity traverse crossing the Merapi volcano made by Yokoyama (1974) shows that the regional trend increases from the north (Java sea) to the south (Indian ocean) but sharply decreases around Merapi zone. The gravity anomaly of Merapi volcano is characterized by bird's eye, concentric low gravity anomaly at the summit area. Magnetic anomaly pattern shows that Merapi was magnetized as a dipole in north-south direction with both the old and young Merapi products contributing to the magnetic anomaly pattern (Arsadi et al., 1991).

The subsurface structure beneath Merapi volcano, especially resistivity structure, has not yet been studied. MT survey was carried out to study resistivity structure around Merapi volcano and its adjacent area in 1989, 1990, 1991, 1992 and 1993. Resistivity structure beneath Merapi volcano will be presented based on 2-D analysis. After the first MT survey, Merapi volcano erupted in February, 1992. MT re-measurement was carried out to examine the resistivity change during the active stage. The change of resistivity values between inactive and the active stages is presented and discussed.

3.2. Geological setting and volcanic activity

According to Van Bemmelen (1949) Merapi volcano is situated on the intersection of two faults i.e., a north-south (transverse) fault which forms the boundary between East and Central Java and a east-west (longitudinal) fault. Along the fault, the Ungaran, Telomoyo, Merbabu, and the Merapi volcanoes are distributed from the north to south. The four volcanoes are closely related in origin (Fig.34). The development of volcanism along the transverse fault started in the north with the oldest or proto-Ungaran in the Early Pleistocene. During the Middle to Late Pleistocene, proto-Ungaran had grown and in the same age, Telomoyo, Merbabu and old Merapi volcanoes were developed. The activity of young Merapi began in 10th century and has continued until the present time .

Merapi is an andesitic-strato volcano and built upon a basement of plastic marine sediments. Geologically, the volcano is composed of young and old Merapi products. Old Merapi products were produced before the catastrophic eruption in 1006. These products dominate the north, east and southeastern slopes of the volcano. The young products which have been continuously erupted until present are mainly distributed in the southwest of the volcano (Wirakusumah et al., 1989). The boundary between old Merapi and the young one can be determined from the morphological features such as concave plane on the summit (Furuya, 1989). Fluvial, weakly to strongly consolidated clay, tuff and breccia which are reworked deposit of young and old Merapi are distributed around Merapi below altitude 400-300 m above sea level

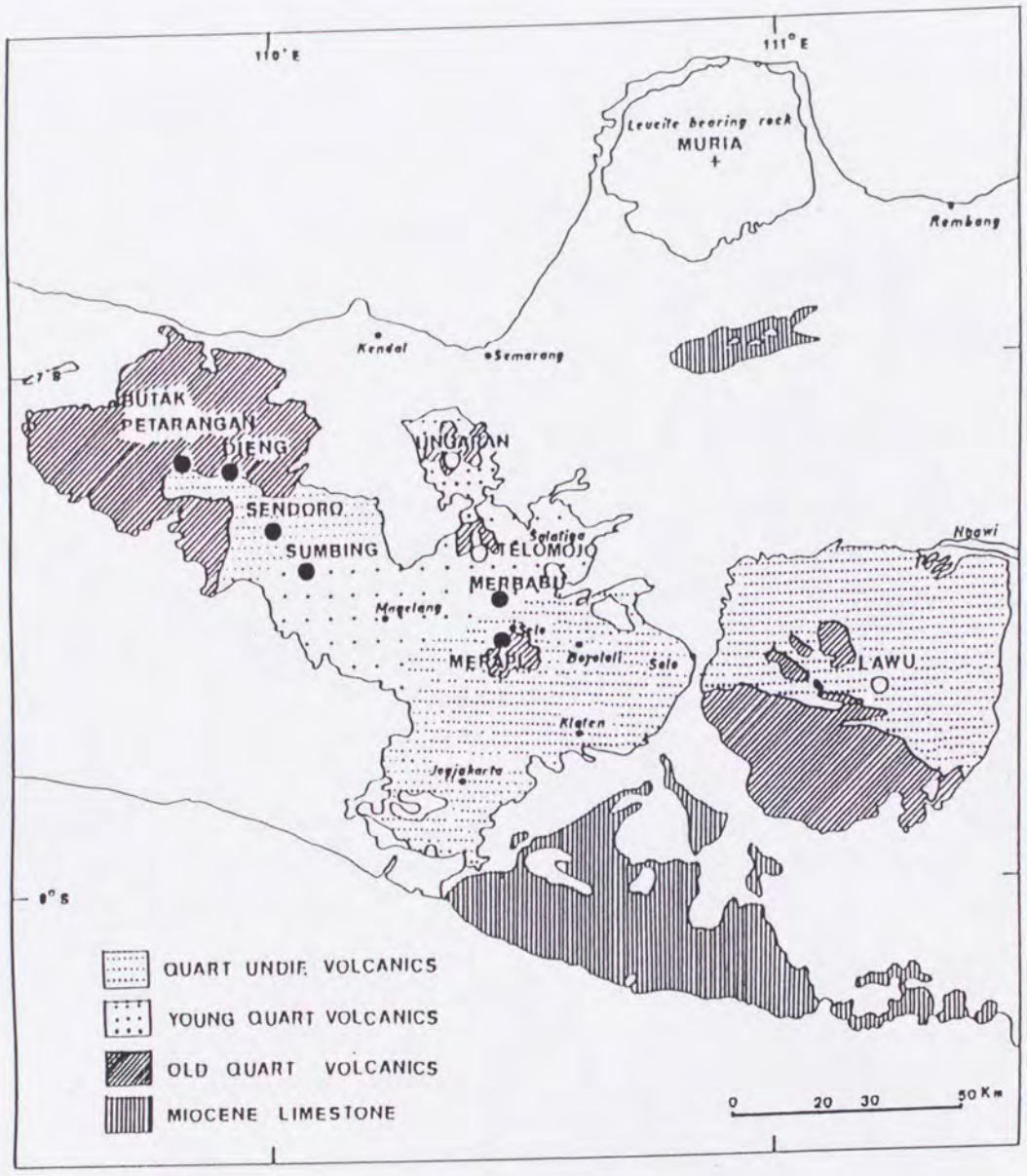

Fig.34. Geological sketch map of Central Java according to the Geological survey of Indonesia. (●) volcanoes, (○) Ungaran, Telomojo and Lawu are in fumarolic stage, no eruption known. For the other, magmatic and phreatic eruption observed (Yokoyama, 1974).

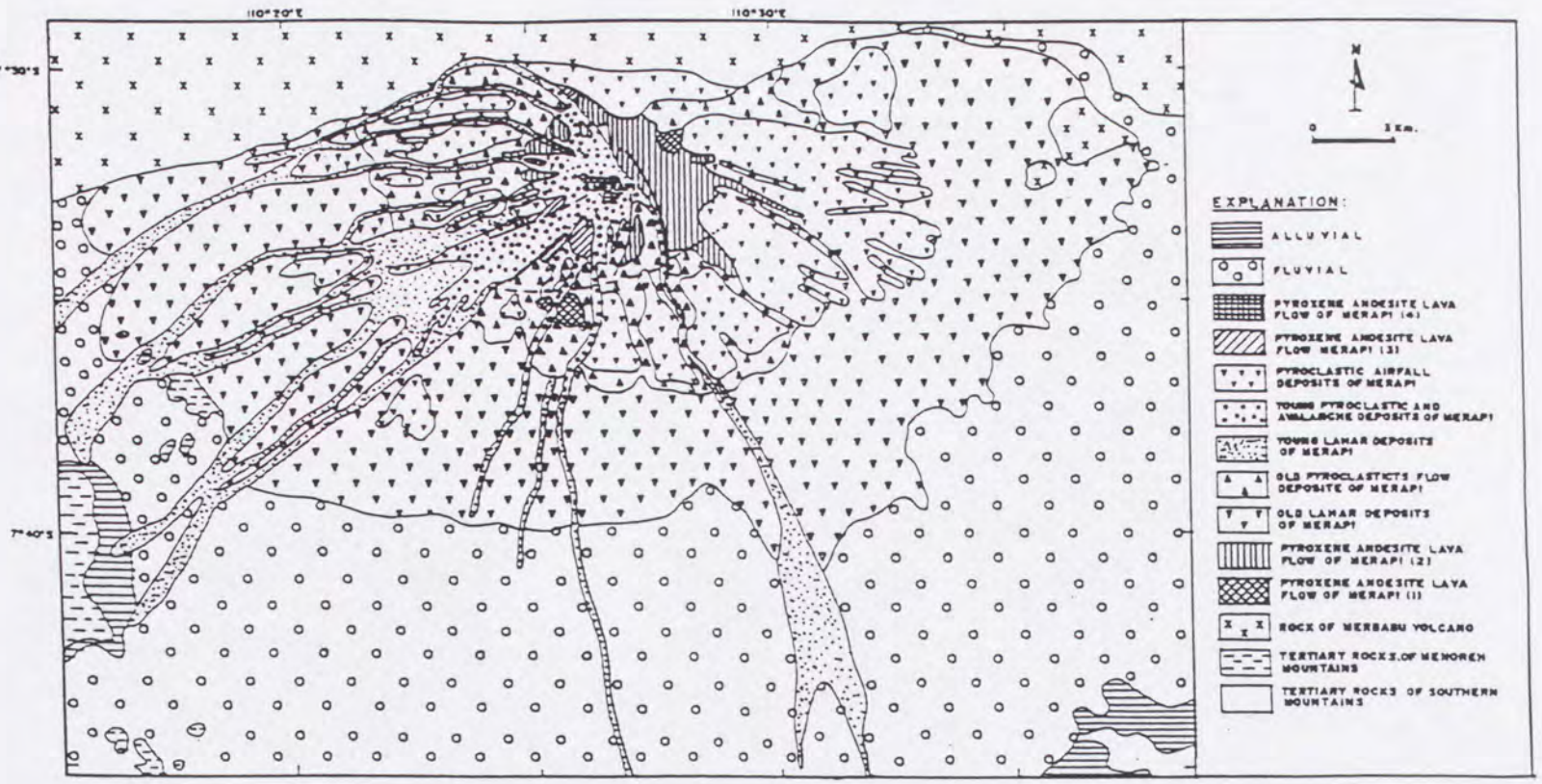

Fig.35. Simplified geological map of Merapi volcano, Central Java (after Wirahadikusuma et al., 1989).

(Fig.35).

In "Geology of Indonesia" by Van Bemmelen (1949), Merapi eruptions are classified into four classes based on the previous eruptions. Class **A** is characterized by magma poor in gas, milder eruption, and development mainly of lava dome. Class **B** is characterized by magma somewhat richer in gas, eruption destroying part of the summit, explosion accompanied by nuee ardante d'avalance as well as nuee ardante d'explosion volcannien, and terminated by the viscous lava flow forming dome or lava tongue. Class **C**, is characterized by magma moderately rich in gas, blowing up or destruction of dome followed by direct gas escape, and terminated by the outflow of lava tongue or dome. Class **D** is characterized by gas magma charge, no initial lava flows, strong gas phase eruption, destruction of the upper part of volcano, collapse, and lava flows or lava dome terminating the eruptions. Collapses of lava dome or parts of it then accompanied by the glowing cloud or nuee ardante of sliding during lava dome development is known as "Merapi type eruption".

Some Merapi activities in the central crater, are normal explosion, lava dome forming, lava flow, glowing avalanche, mudflow and hot cloud (Merapi volcano observatory, 1990). Sometimes gas outbursts in short duration and in other occasions viscous lava are extruded from the vent during successive months or years, without any significant explosive activity. The growth of new lava dome occurred in October 1986 and the most recent eruption took place on February 1992 (Tjetjep et al., 1993). Until the July 1993, Merapi volcano is in the active stage, intermittently ejecting incandescent lava. The chemical composition of the lava,

however, varies only very slightly in this historical period from about 50.74 wt. % to 55.45.% of SiO_2 (Merapi volcano observatory, 1990).

3.3. Seismic, gravity and magnetic surveys

At present, the integrated geophysical method is indispensable for general study of volcanic structure and for the methods used to predict eruption. The Research and Development Centre for Geotechnology, Indonesian Institute of Sciences (RDCG-LIPI) has taken part on gravimetric, magnetic and magnetotelluric (MT) measurement (Arsadi et al., 1991) where the members of Gajah Mada University have taken part on continuous monitoring of volcanic activities by using seismic method.

The aim of these investigation are mainly to obtain better understanding of the dynamic processes inside the volcano. The other is to understand correlation between volcanic activity, tectonic setting and internal subsurface structure.

In this section, preliminary analysis of integrated geophysical measurement crossing Merapi volcano and seismic data will be presented.

Seismic monitoring

A seismic network consisting of three stations (KLT, LBH and KKN) at the volcano and the fourth station (MTK) located about 50 km south of Merapi have been installed by Gajah Mada University (Kirbani, 1990). The fourth station allows comparison with signals of non-volcanic

(Merapi) origin.

Each station consists of a 1 Hz vertical seismometer. Radio telemetry (FM) is used for data transmission to the Geophysical Laboratory of Gajah Mada University in Yogyakarta. The data acquisition system using magnetic tape recording has a dynamic range of about 50 db and a frequency bandwidth of 1 to 100 Hz.

Analysis in space, time, and frequency domain have been carried out the seismic and tremor volcanic data recorded from November 1985 - December 1988. The tremor source locations have been calculated using the average amplitude ratios of average amplitudes recorded at the three stations (KLT, LBH, and KKN). There are two distinct clusters in the diagram. The first cluster is located in the upper left side of the diagram, and the second is found in the central right part of the diagram. The two clusters correspond to location of the tremor source at depth of (500 + 100) meters and (2800 + 300) meters.

Gravity survey

Previous gravity and magnetic measurement around Merapi have been done by Yokoyama et al. (1974), Untung and Sato (1978), and Gunawan (1985). All of the traverses survey were done mainly along the road relatively far from the volcano. Eight traverses of gravimetric, geomagnetic and Magnetotelluric (MT) surveys were carried out on the body of Merapi volcano by RDCG-LIPI team in 1988 and 1990. Gravimetric, geomagnetic and MT surveys were in the same traverse. The interval of point observations are 250 meters for gravity and geomagnetic, and 500 meters for MT as shown in Fig.36.

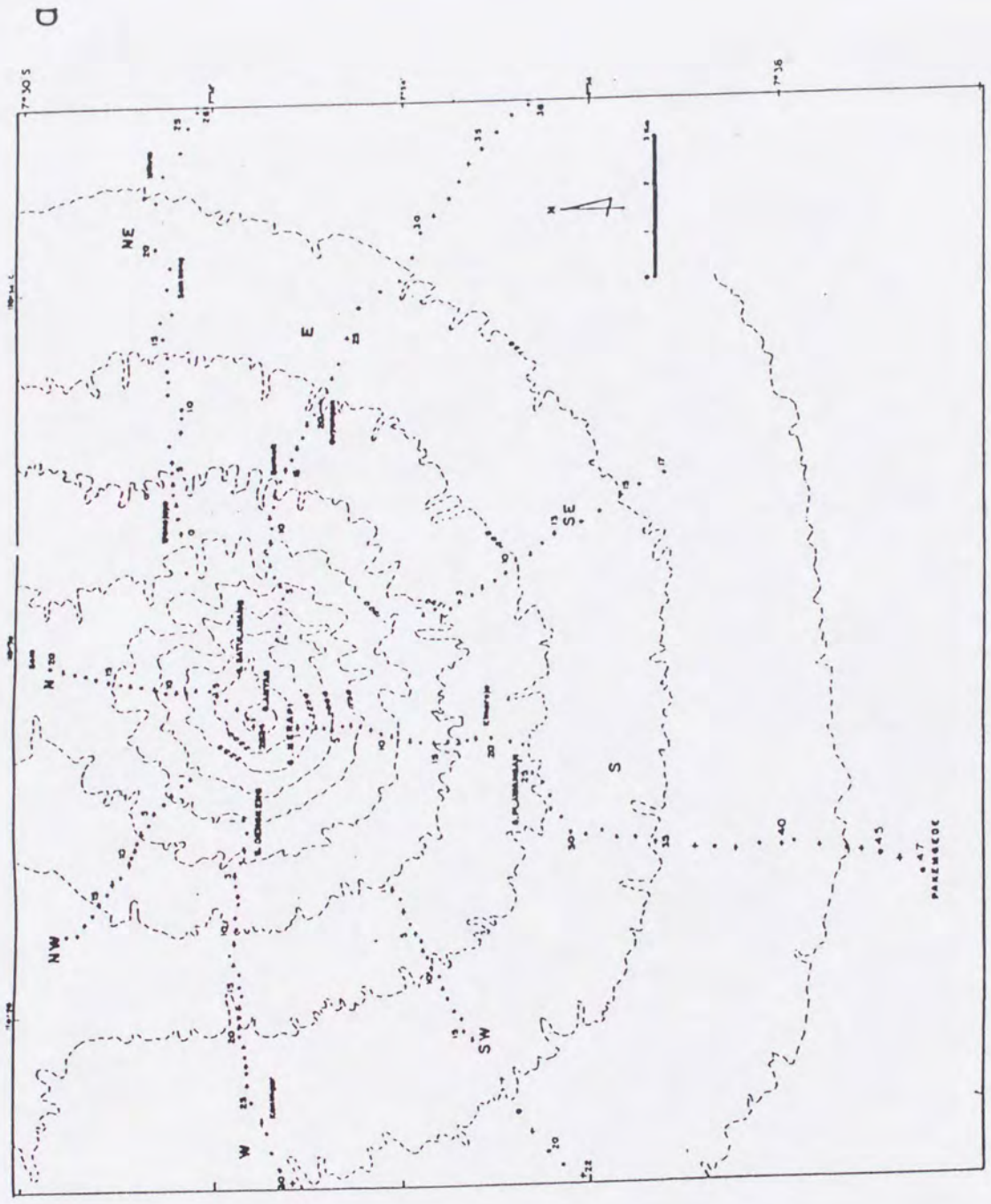

Fig.36. Location of ELF-MT, gravity and magnetic measurement sites. Solid circle is the coincided ELF-MT, gravity, and magnetic measurement site. Cross sign is the site without ELF-MT measurement. a) On the body of Merapi volcano, b) West and east sides of Merapi volcano.

b

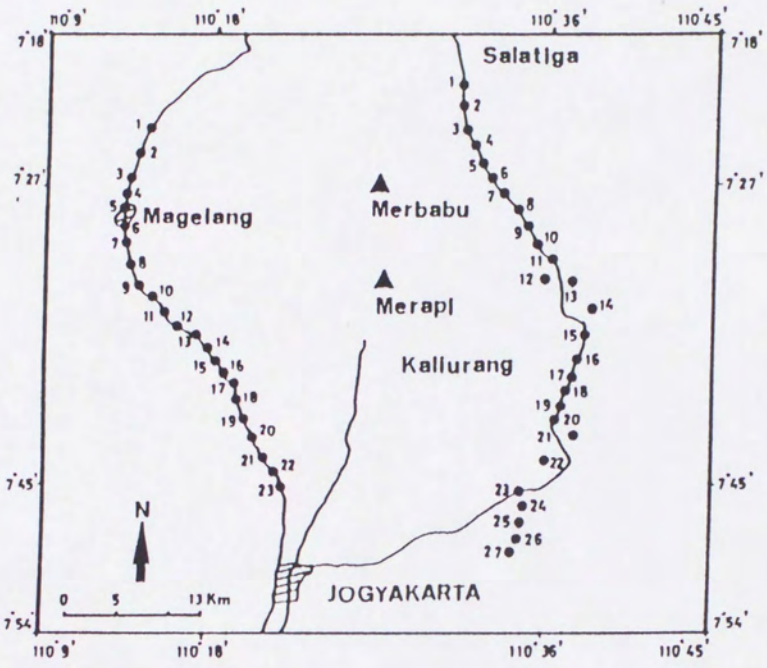
110° 9'
110° 18'
110° 36'
110° 45'
7° 18'
7° 27'
7° 45'
7° 54'
Salatiga
Magelang
Merbabu
Merapi
Kalurang
JOGYAKARTA
N
0 5 13 Km

A Lacoste & Romberg gravity meter of model G-804 was used to measure the relative earth's gravity field. Compass and rope-measure and an altimeter Pauline for altitude measurement with accuracy 0.5 meter using loop method were used to position each station. The measurement of positions was started from a point already known on the map. The gravity measurement was carried out by the loop method where the observed value of gravity at each station was determined by referring to the gravity values at the Base Station at Kaliurang, Yogyakarta and Boyolali.

The calculation of Bouguer anomaly follows common standard procedures. First, we make two corrections, one due to the tidal effect and the other relating to what is called drift of gravity meter. Second, we make Free air, Bouguer, and Terrain corrections. Free air correction is calculated by assuming a normal vertical gradient of 0.3088 mgal/m. Density of rocks for Bouguer and terrain corrections is estimated 2.50 g/cm^3. Map of Bouguer anomaly is shown in Fig.37. Two and half-dimensional subsurface model was constructed for north-south traverses using Talwani method as shown in Fig.38.

Gravity anomaly map (Fig.37) shows gradually decrease to the peak of Merapi. Starting from 45 mgal at the foot slowly down to -40 mgal at the summit area. The steeper the slopes are, the denser are the contour lines. It indicates that the influence of topography still remains. Comparet to the regional gravity pattern, however, the results are still consistent. The regional trend of gravity value increases southward. Based on the model (Fig.38), there are three density values of Merapi;

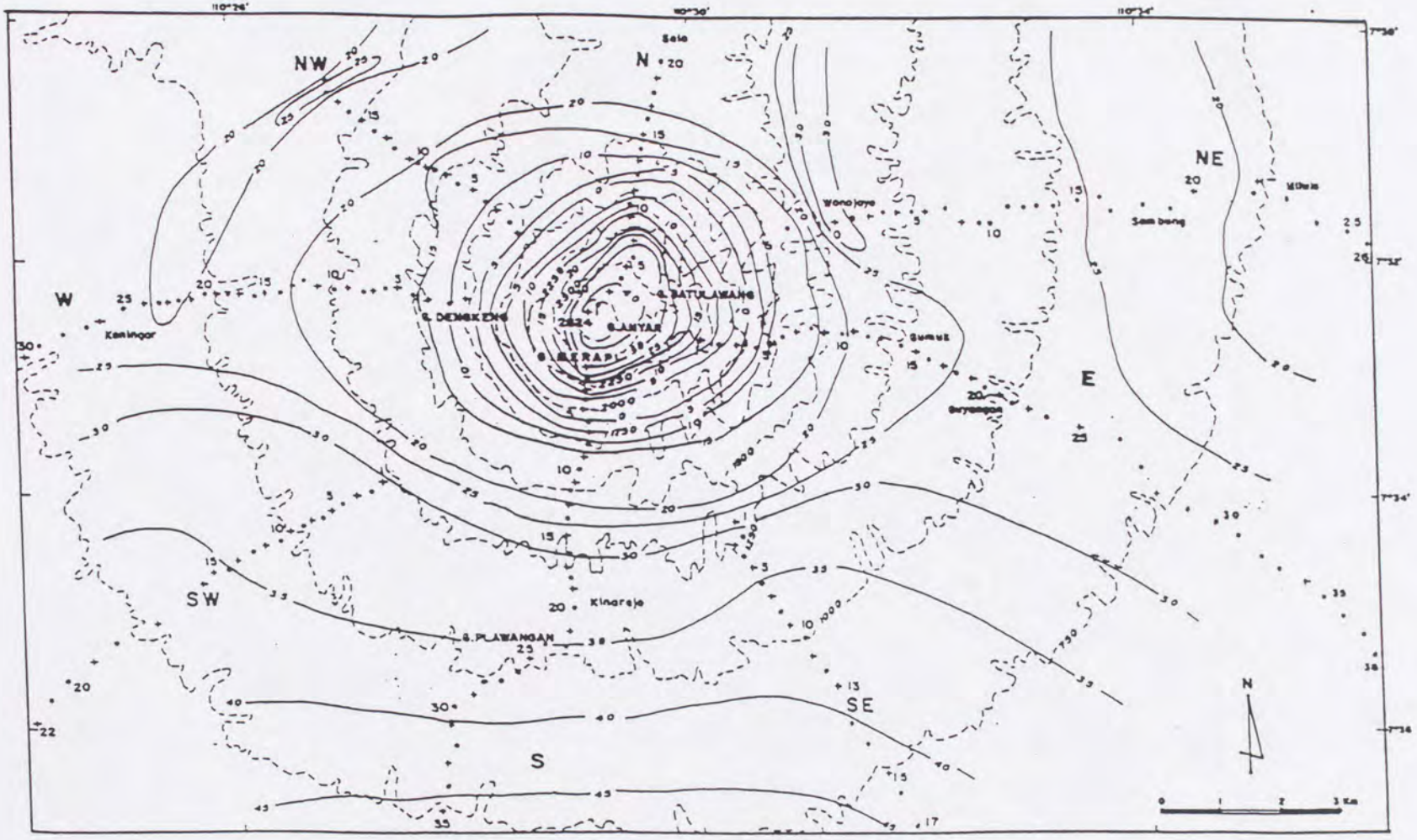

Fig.37. Bouguer anomalies map of Merapi volcano. Contour topographic interval is 250 meters, contour gravity interval is 5 mgal. Solid circle is the coincided ELF-MT, gravity, and magnetic measurement site. Cross sign is the site without ELF-MT measurement.

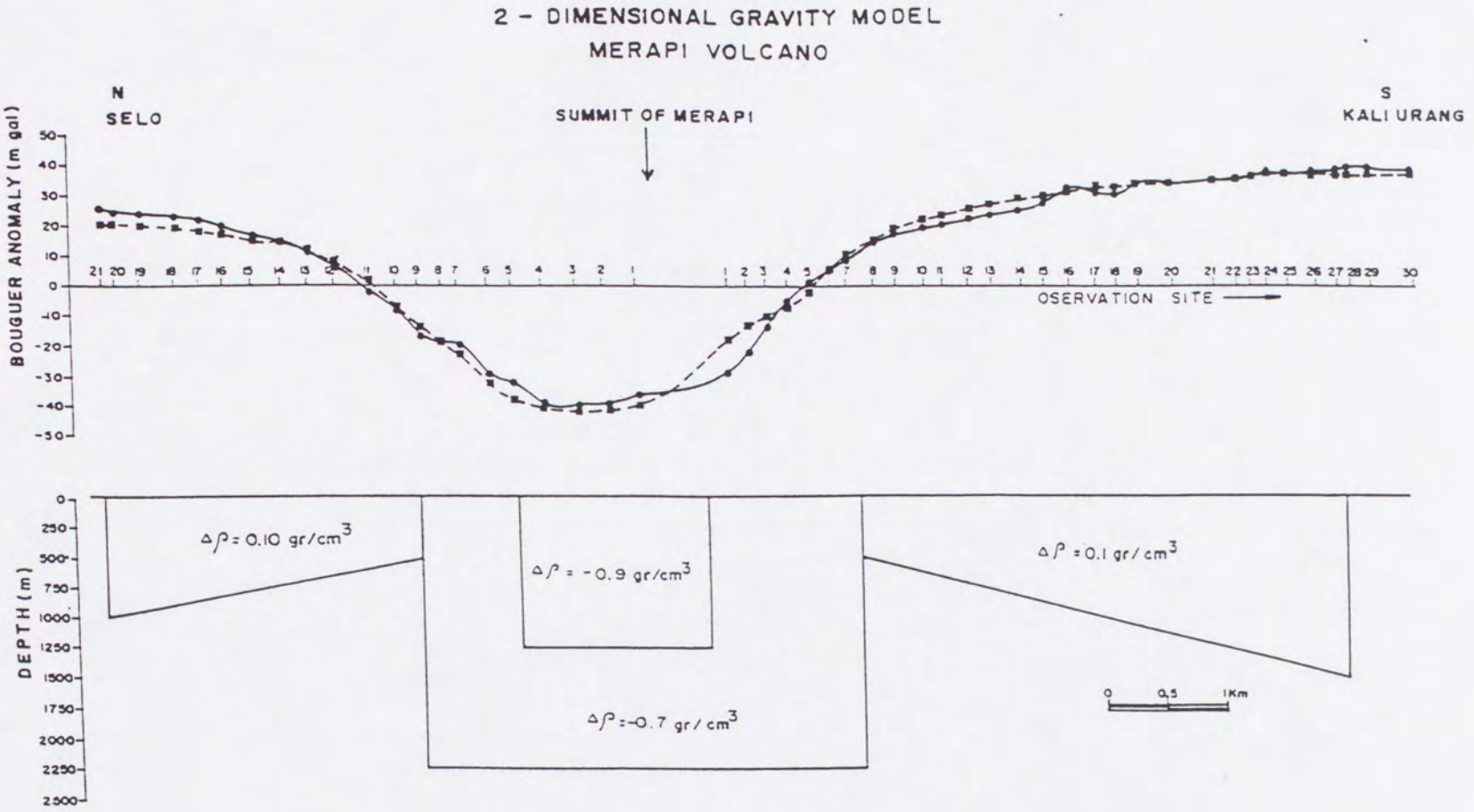

Fig.38. 2-D gravity model of Merapi volcano. Solid line is observed value and dash line is calculated value.

2.60 g/cm^3 around the foot, 1.80 g/cm^3 in the mid-body, and 1.60 g/cm^3 in the summit area. This model is calculated by assuming density value of the regional 2.50 g/cm^3. The rocks in the summit area is composed of sand, tuff, lava fragments and lava dome.

Magnetic survey

Observation points of geomagnetic survey were coincident with observation points of gravity measurement. Because there was only one geomagnetic instrument, the measurements were carried out by loop-moving method. This method is used to eliminate or to correct the diurnal variation at each station. Scintrex Digital Fluxgate Magnetometer model MFD-4 which measures the vertical component of earth's magnetic field was used in the survey.

Geomagnetic anomaly is calculated by subtracting each of observed value with regional magnetic value (Parkinson, 1983) at its observed point. Geomagnetic anomaly pattern as shown in Fig.39 is dominated by two values; 0-1000 nT and 1000-2500 nT. The first value covers the western part and second value covers the eastern part of Merapi body. These anomalies of vertical force suggest to be strongly controlled by young and old Merapi products. The western part of Merapi consists of young products and eastern part consists of old products (Furuya, 1989).

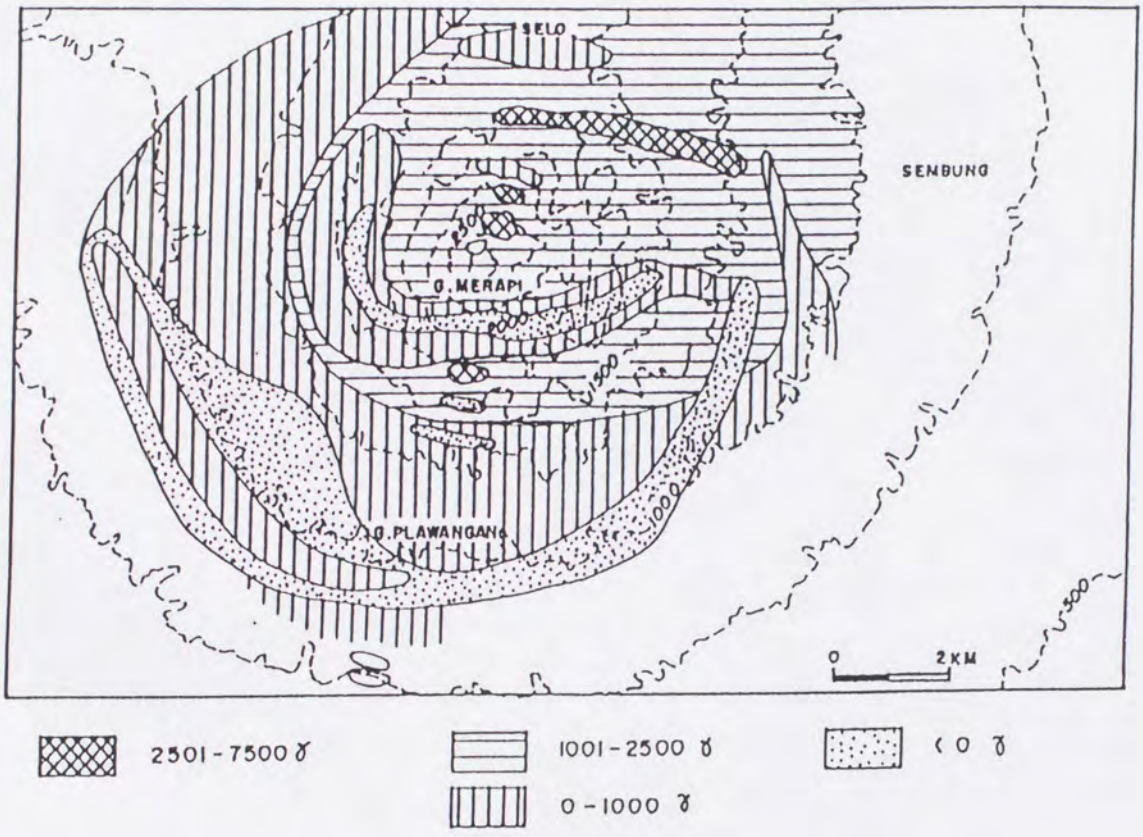

Fig.39. Geomagnetic anomaly (vertical force) of Merapi volcano.

3.4. ELF-MT survey

ELF-MT measurements at Merapi volcano were carried out using narrow-band channel to pick up signals of the Schumann resonance band in 1989, 1990, 1991, 1992 and 1993. The instrument is basically the same as the one used at Sakurajima volcano. Slight modification has been developed to pick up more Schumann resonance frequencies, 39 Hz of ELF, 15.5 and 23.4 kHz of VLF. The total frequencies measured in the survey are 7.8, 14.0, 20.4 and 39.0 Hz of Schumann frequencies and 15.5, 17.4 and 23.4 kHz of VLF. Because the tropical region is a main source for Schumann resonance, the additional frequencies are sufficiently effective in the Indonesian region. It has been proven in delineating the active Sumatra fault (Arsadi et al., 1989).

The total MT observation sites are 173 which are 123 sites on the body of volcano (Fig.36.a), 27 sites in the east side and 23 sites in the west side of Merapi. The distribution of MT sites on the body of Merapi volcano runs along the eight traverses namely, N, NE, E, SE, S, SW, W, and NW traverses. Rope meter and compass were used for positioning and at some possible locations GPS (Global Positioning System) was used as well. Interval spacing of each station is 500 meters, where the N-S traverses connect through the summit of Merapi. In other traverses, however, the summits were inaccessible because of the very steep slope and loose materials. EM and WM traverses are the two of MT measurement with spacing 2 km along the road which are located in the east and west sides of Merapi (Fig.36.b). During MT measurement, the

orientation of the sensor was set to the summit direction for magnetic field and perpendicular to magnetic orientation for electric field sensor with assumption that the main structures around Merapi are radial pattern. The distance of electric sensor varied from 10 to 30 meters.

South-north line of the MT measurements represents the topographic feature of Merapi volcano (Fig.36.a). The profile consists of 34 MT sites through the summit area. The MT measurements start from the Salam village in south side (site S-24) with altitude about 400 m above sea level. Measurement were carried out along the road where the altitude gradually increases until Kaliurang village (site S-16), after that it followed mountain paths. From Kaliurang to site S-01 (2,454 m) changes of altitude was relatively sharp particularly after site S-07 at which the lava flow accumulation forms a very steep slope. Site N-01 is located in the summit area with altitude about 2,900 m above sea level and the N-traverse goes down to the north (site N-11) in the Selo village with altitude 1,545 m. The line passes one of the old craters of Merapi, Pasar Bubrah, which is situated close to site N-02.

The MT measurement system consists of an amplifier, a computer, coils, and electrodes. The data is amplified, filtered, and AD onverted, and 90 data were selected by statistical testing. The measured frequencies are 7.8, 14, 20.4, and 39 for ELF, and 15500, 17400, 23400 for VLF.

Further analysis was carried out in laboratory to calculate and interpret the resistivity and its depth of each station. Simple 1-D resistivity structure was firstly estimated by applying Bostic transform (Goldberg, 1982). An example of 1-D inversion result is shown in Fig.40. The result

SITE=NMT.11 MODEL (INITIAL BY BOSTICK INVERSION)

	DEPTH (THICK)[m]		RESISTIVITY [Ohm.m]
1=	21(	21)	92.0
2=	21(	0)	0.3
3=	26(	5)	2.9
4=	535(	510)	170.0
5=	696(	161)	76.2
6=	759(	63)	7.9
			3.3

DMAX= 896

Residue= 18.4209 (%) ITER= 10

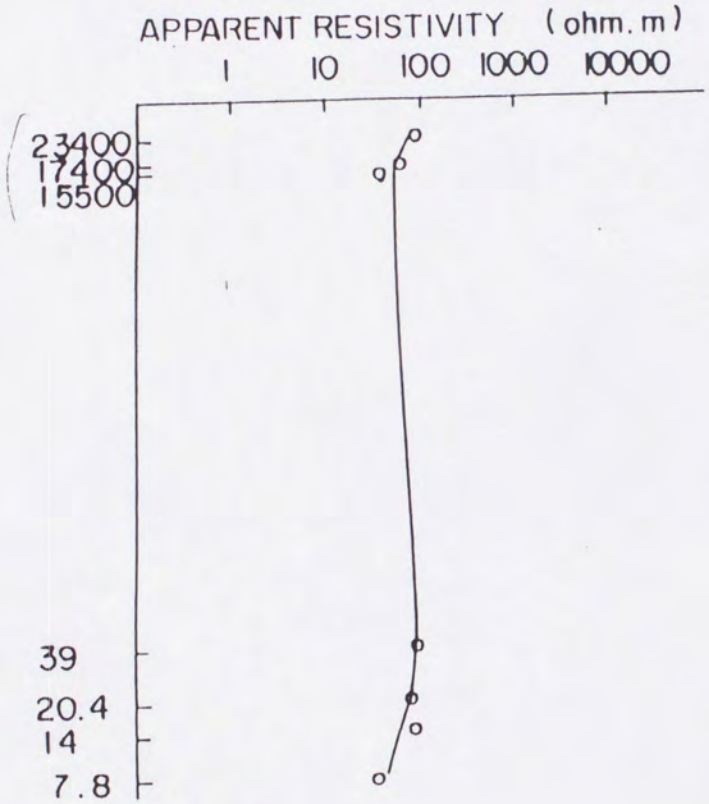

Fig.40. An example of 1-D inversion result of the ELF-MT survey at site N-11. The open circles are observed data and solid line is calculated value.

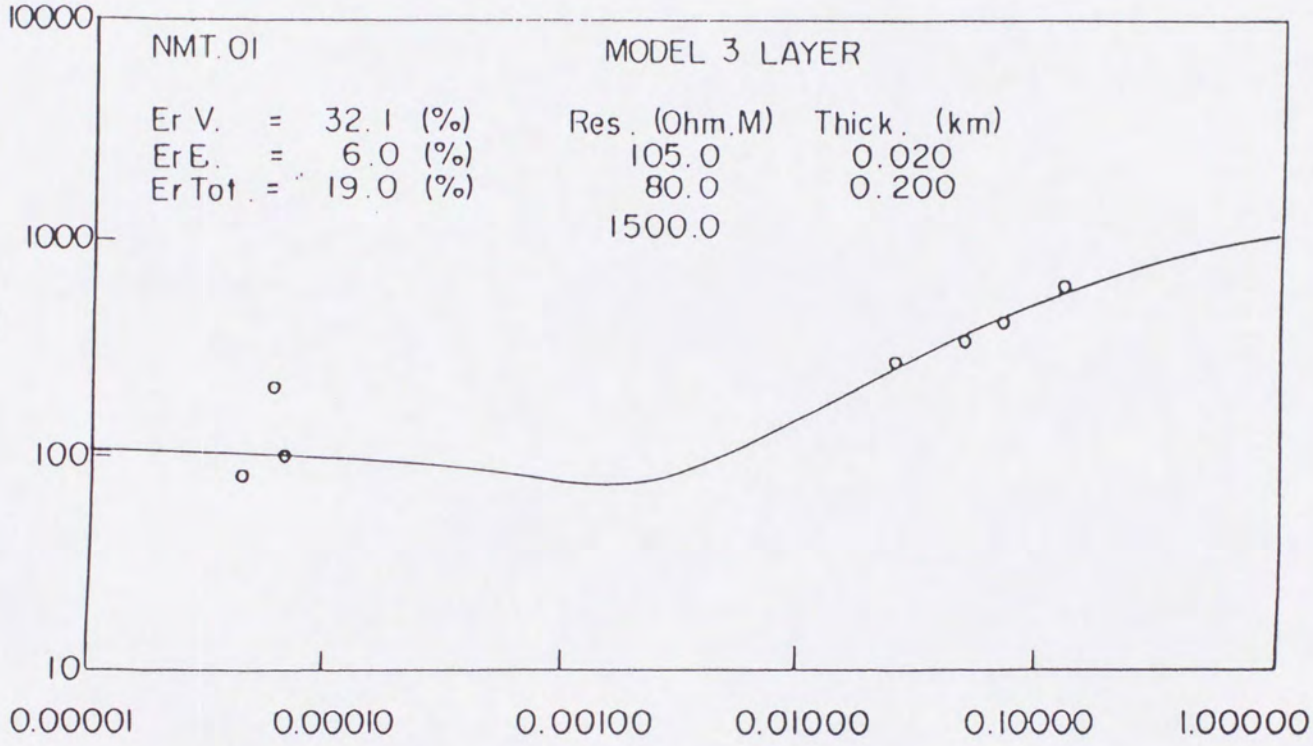

Fig.41. An example of 1-D inversion result of the ELF-MT survey at site N-01. The open circles are observed data and solid line is calculated value.

of Bostic inversion was used for the initial 1-D inversion analysis (Fig.41). The procedures of 1-D and 2-D analyses are the same as the procedures done in Sakurajima volcano (see section 2.3.5).

3.5. Resistivity structure beneath Merapi volcano

Apparent resistivity distributions of Merapi volcano and its adjacent area for frequencies 15.5 kHz, 39.0 Hz and 7.8 Hz are shown in Fig.42 to Fig.44. The resistivity values might be classified into three groups, high resistivity for value higher than 300 ohm-m, intermediate resistivity for value from 30 to 300 ohm-m and low resistivity for value lower than 30 ohm-m. The resistivity value of the 15.5 kHz represents a shallow resistivity layer. Two noticeable features of shallow resistivity layer are observed on the volcano. First, high resistivity layers are distributed from the summit to the southwest flank. Second, low resistivity layers are found at almost all sides of the foot of volcano (Fig.42.a). Conjunction with the MT data of east and west sides of Merapi, these conductive layers have wide distribution in the east, south and west sides of Merapi (Fig.42.b). The resistivity value of the 39.0 Hz (middle layer) is similar with the surficial layer and only a little changes both on volcano and adjacent area (Fig.43.a and Fig.43.b). Remarkable resistivity changes appear in the relatively deep layer of frequency 7.8 Hz. The high resistivity observed is concentrated around the summit, and in contrast the low resistivity is distributed more wider on the volcanic body and outer area of Merapi body (Fig.44).

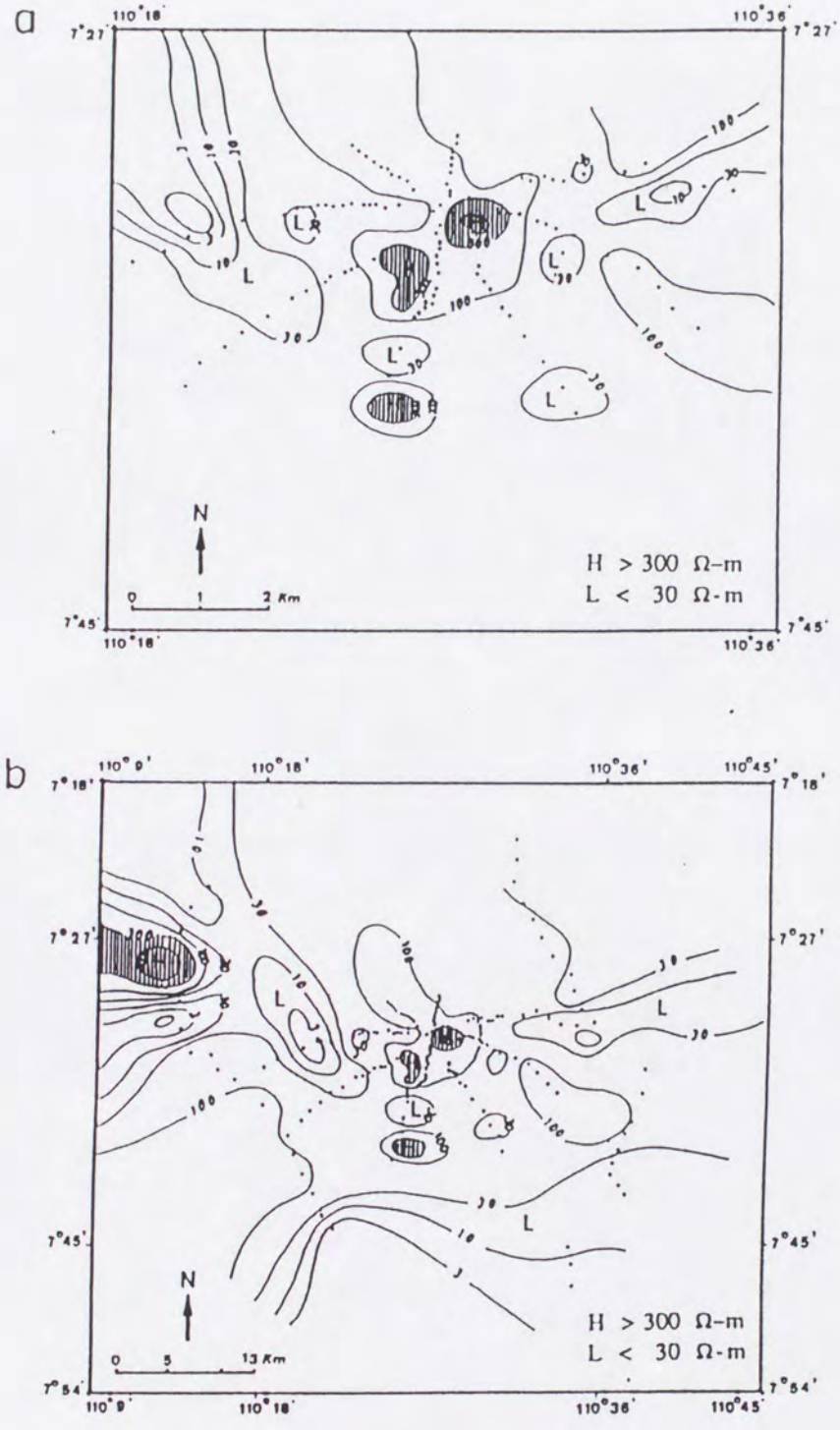

Fig.42. Apparent resistivity distribution Merapi volcano at frequency 15,500 Hz. a) Merapi volcano area, b) Merapi and its adjacent area.

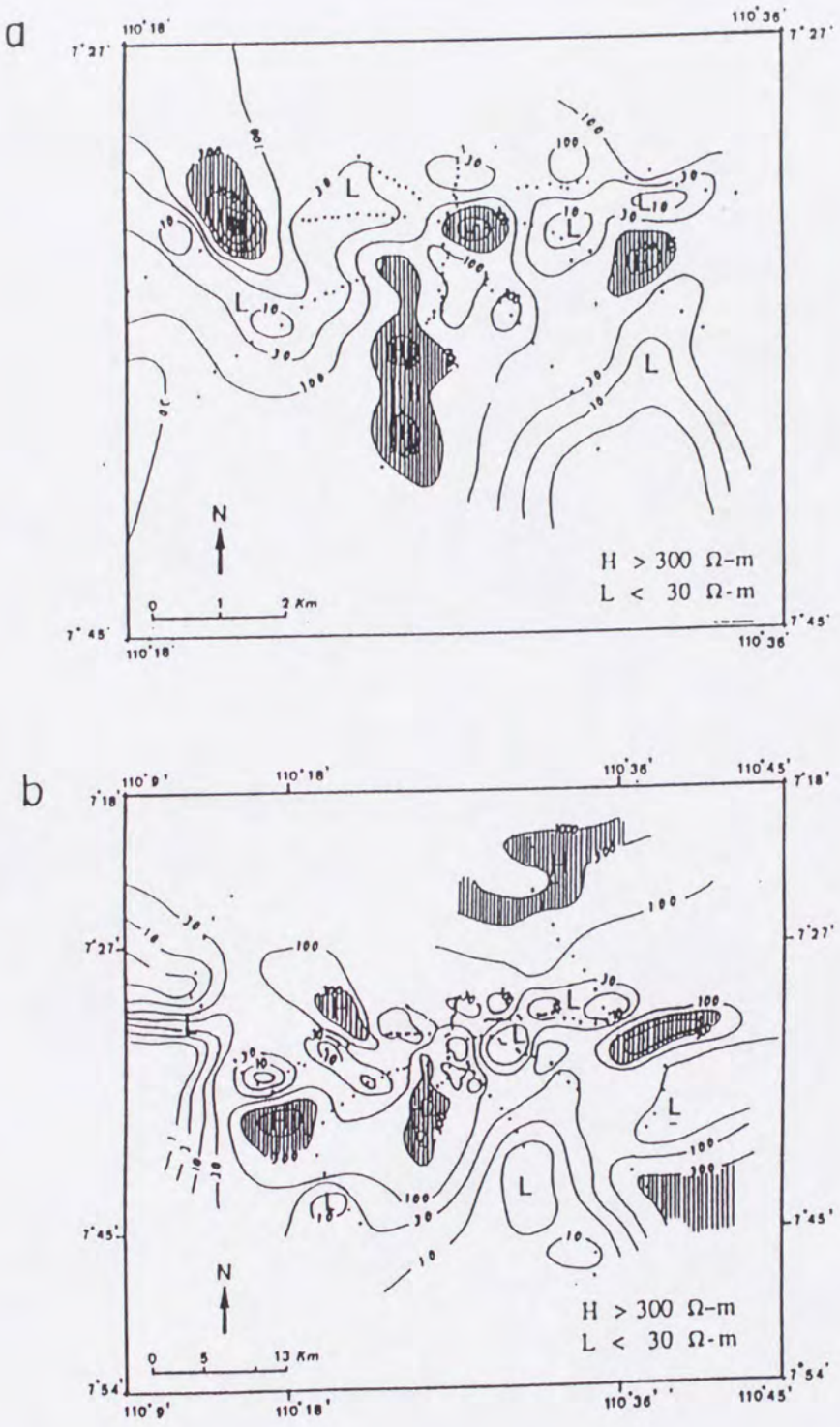

Fig.43. Apparent resistivity distribution Merapi volcano at frequency 39.0 Hz. a) Merapi volcano area, b) Merapi and its adjacent area.

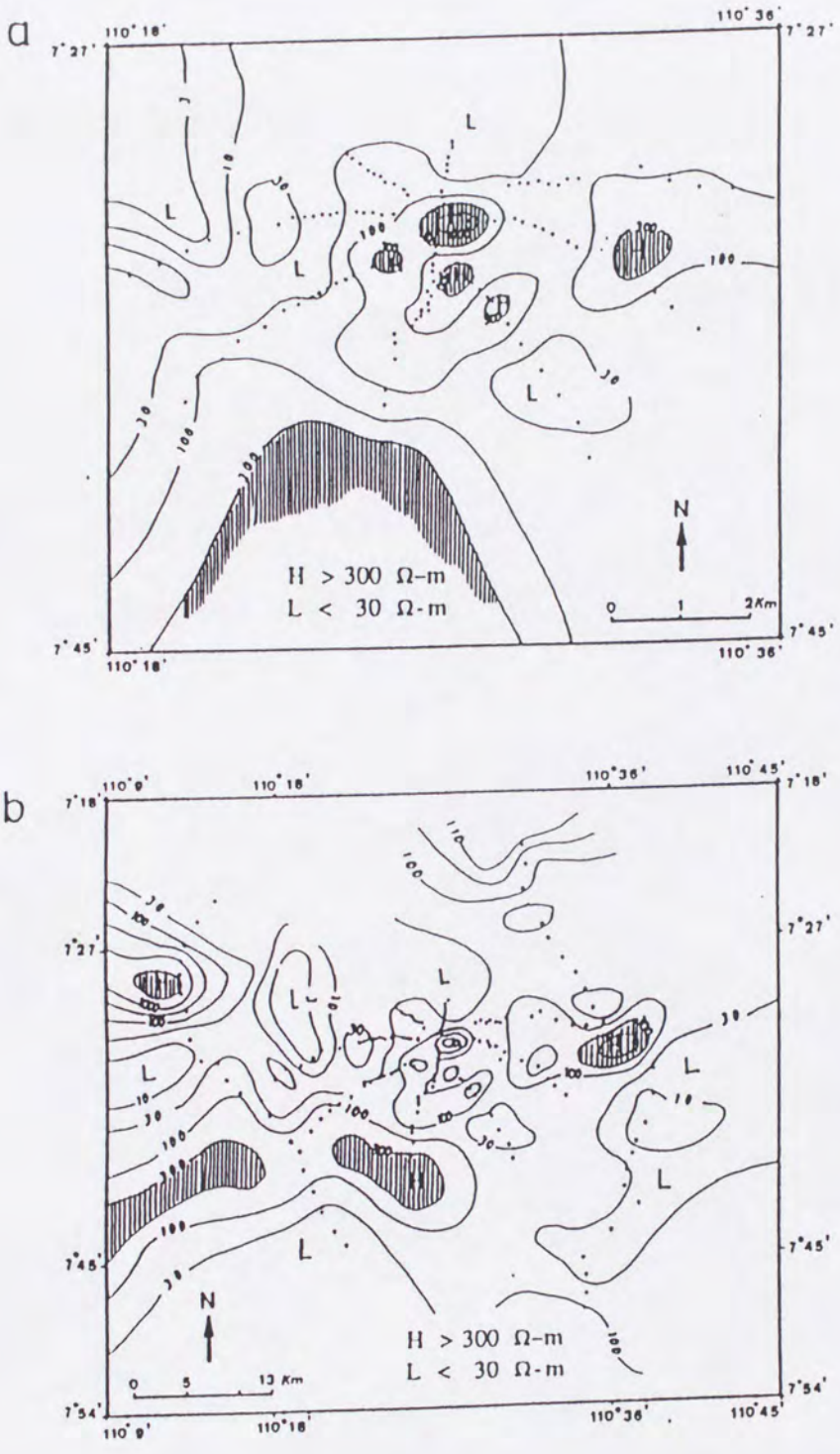

Fig.44. Apparent resistivity distribution Merapi volcano at frequency 7.8 Hz. a) Merapi volcano area, b) Merapi and its adjacent area.

Fig.45.a, b, c, d, e, and f are the resistivity structure beneath Merapi volcano based on 2-D analysis namely, S-N, SW-NE, W-E, NW-SE, WM and EM lines. The character of Merapi eruption is lava dome building. Every eruption is mostly terminated by lava dome or lava tongue. Based on 2-D analysis, the existence of remarkable high resistivity value, more than 1000 ohm-m, is observed around the summit area. This high resistivity value is suggested as an accumulated porous lava dome or lava flows in dry condition. The high resistivity value beneath site N-1 continues to the depth of about 2 - 3 km vertically beneath the summit (Fig.45.a). It might be a magma vent of Merapi volcano with diameter approximately about 500 meters. The distribution of high resistivity value is almost circular features with diameter approximately about 3 km and thickness about 500 to 750 meters.

Pasar Bubrah located near site N-2 is recognized as the old crater in the historical development of Merapi volcano. The resistivity anomaly, however, does not appear on the N-S resistivity structure (Fig.45.a). The volcanic products such as tuff, lava flows, lava fragments, and pyroclastic which built Merapi volcanic body are characterized by the resistivity value from 100 to 250 ohm-m. Different resistivity value is due to difference in water content or porosity of the materials. The boundary between old and young Merapi products is not clearly observed both from the resistivity distribution and the resistivity structure.

Merapi volcano is underlain by low resistivity basement with resistivity about 25-50 ohm-m which started from altitude about 600 m above sea level. The low resistivity value has wide distribution not only beneath Merapi volcano but also in the outer area of Merapi. Resistivity

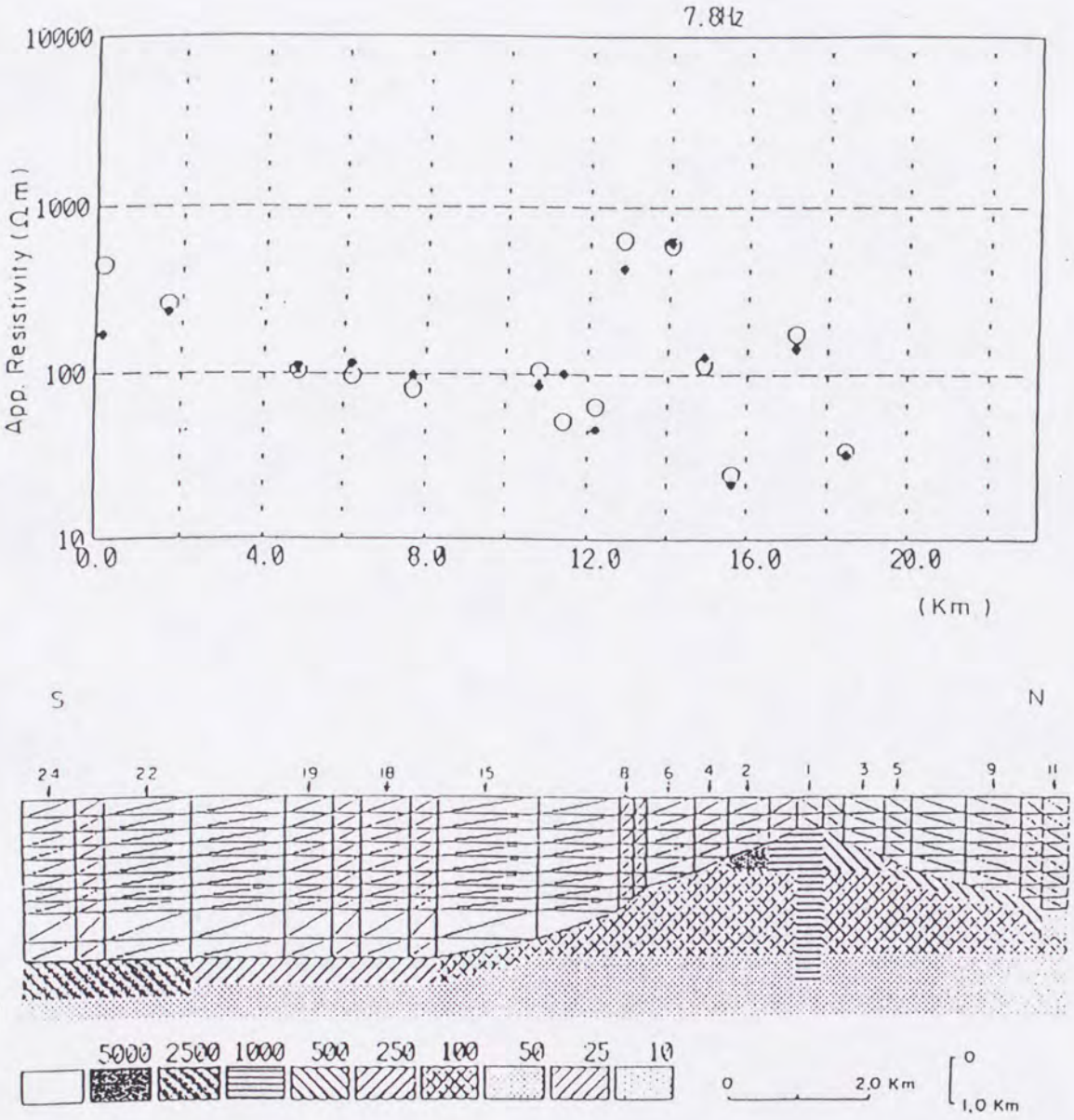

a

Fig.45. Resistivity structure of Merapi volcano inferred from ELF-MT 2-D model. a) south-north (S-N), b) southwest-northeast (SW-SE), c) west-east (W-E), d) northwest-southeast (NW-SE), e) east side of Merapi, and f) west side of Merapi. Numerals of legend denote resistivity in ohm-m. Open circles are observed value, solid circles are calculated value.

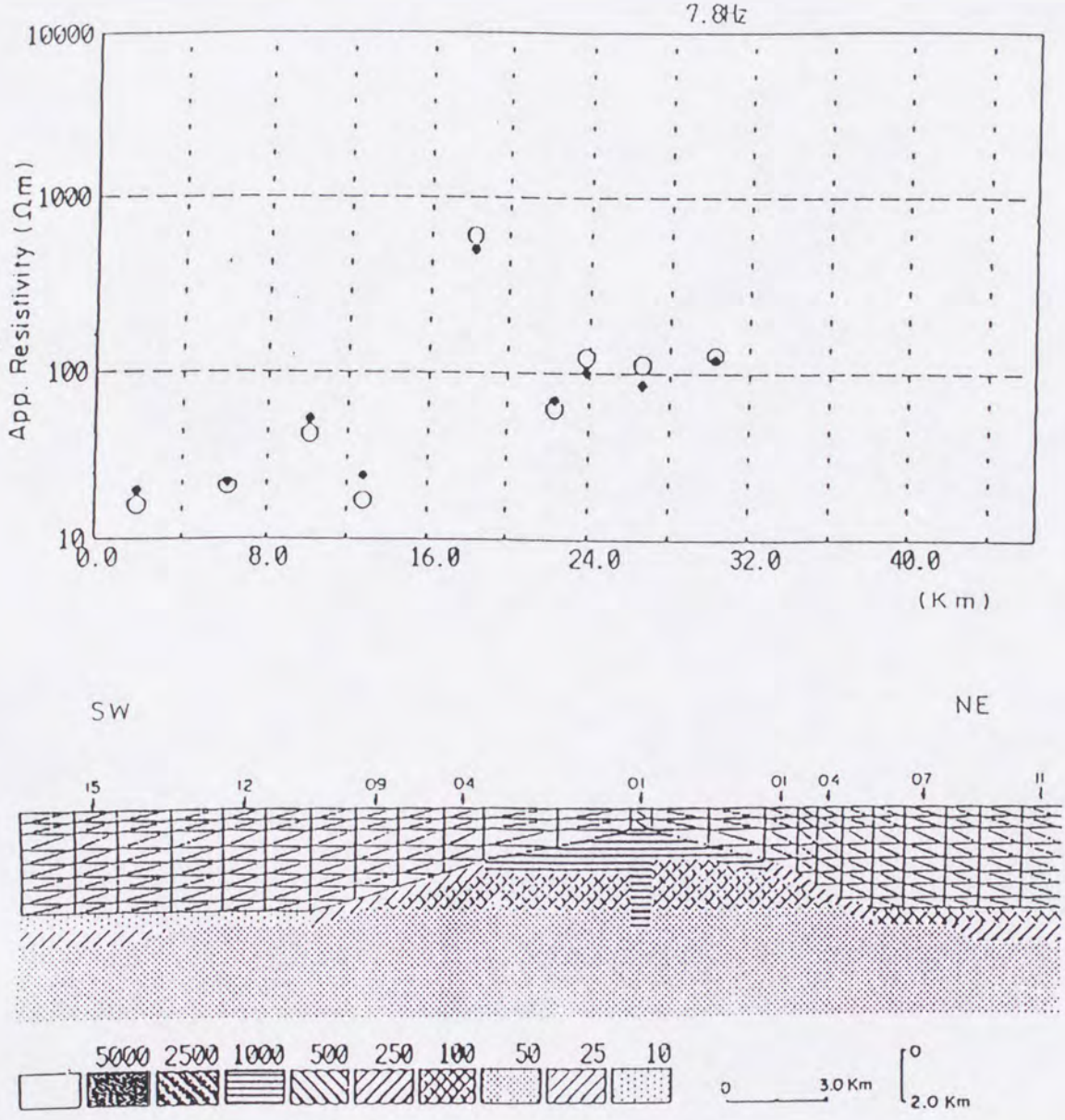
7.8Hz
10000
1000
100
10
App. Resistivity (Ω.m)
0.0
8.0
16.0
24.0
32.0
40.0
(Km)
SW
NE
15
12
09
04
01
01
04
07
11
5000
2500
1000
500
250
100
50
25
10
0
3.0 Km
0
2.0 Km

b

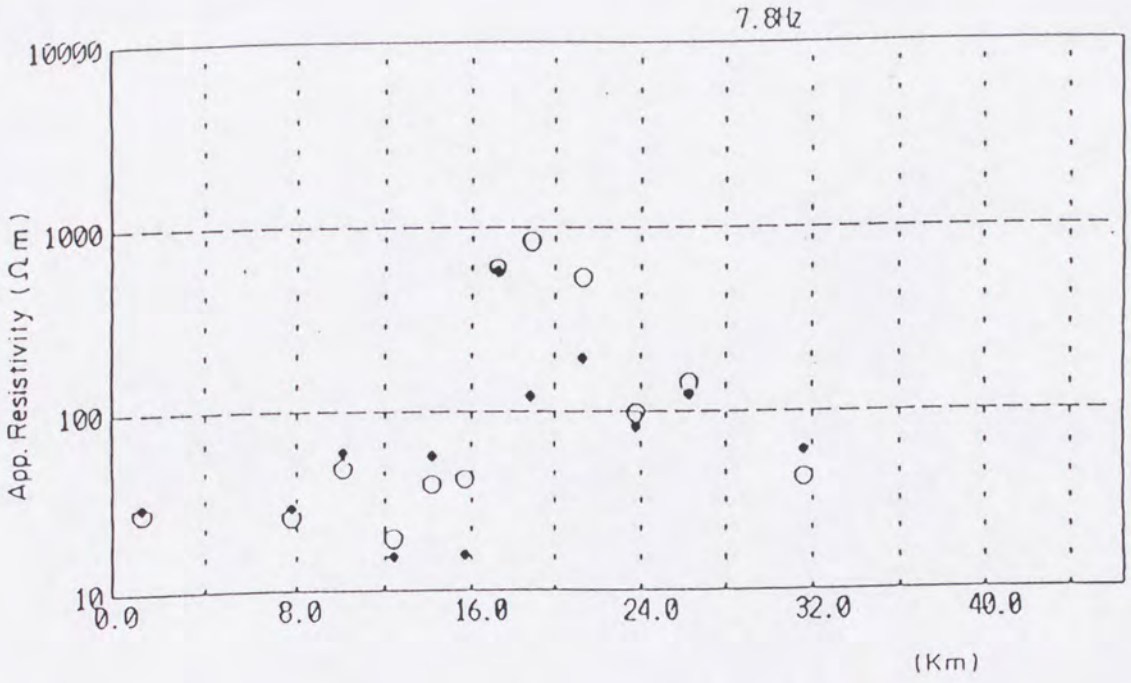
7.8Hz
100000
1000
100
10
App. Resistivity (Ω m)
0.0
8.0
16.0
24.0
32.0
40.0
(Km)

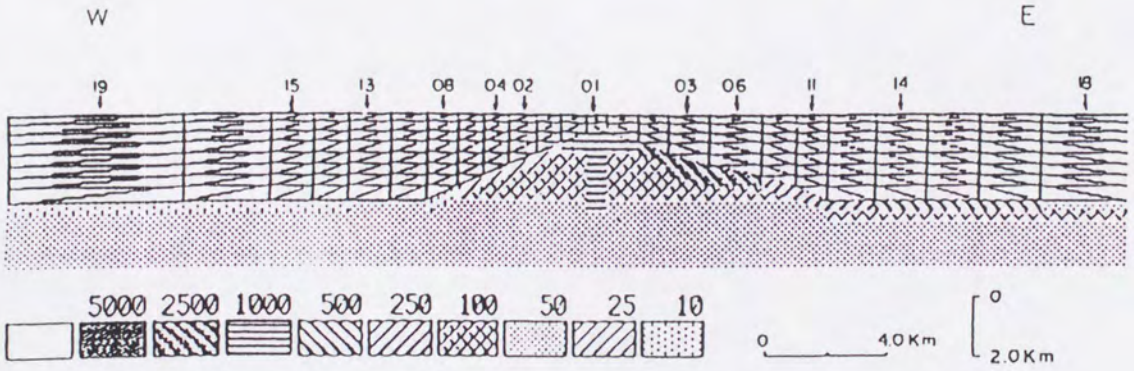
W
E
19
15
13
08
04
02
01
03
06
11
14
18
5000
2500
1000
500
250
100
50
25
10
0
4.0Km
0
2.0Km

C

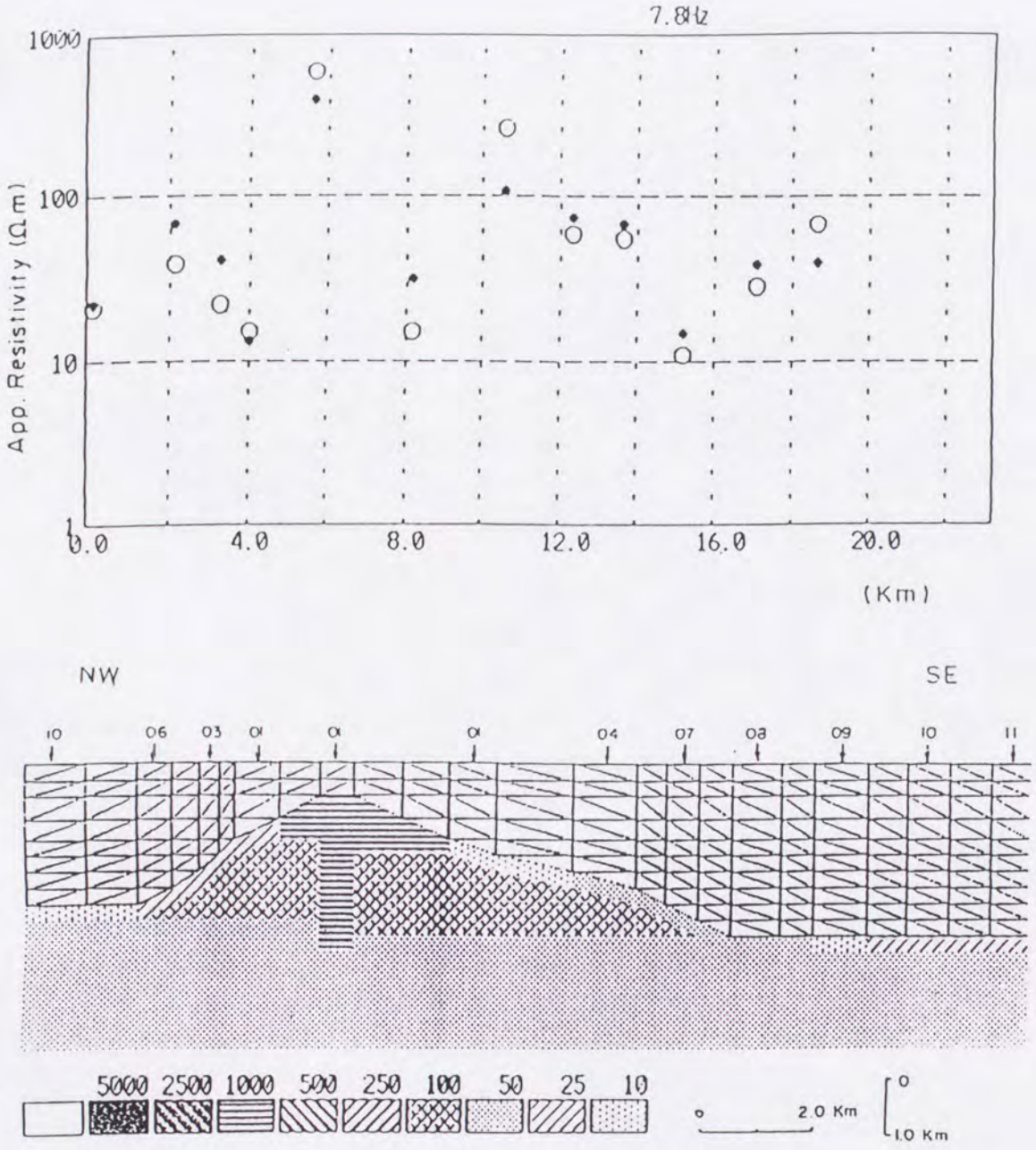
7.8Hz
App. Resistivity (Ω.m)
10000
100
10
1
0.0
4.0
8.0
12.0
16.0
20.0
(Km)
NW
SE
10
06
03
01
01
01
04
07
08
09
10
11
5000 2500 1000 500 250 100 50 25 10
0
2.0 Km
1.0 Km

d

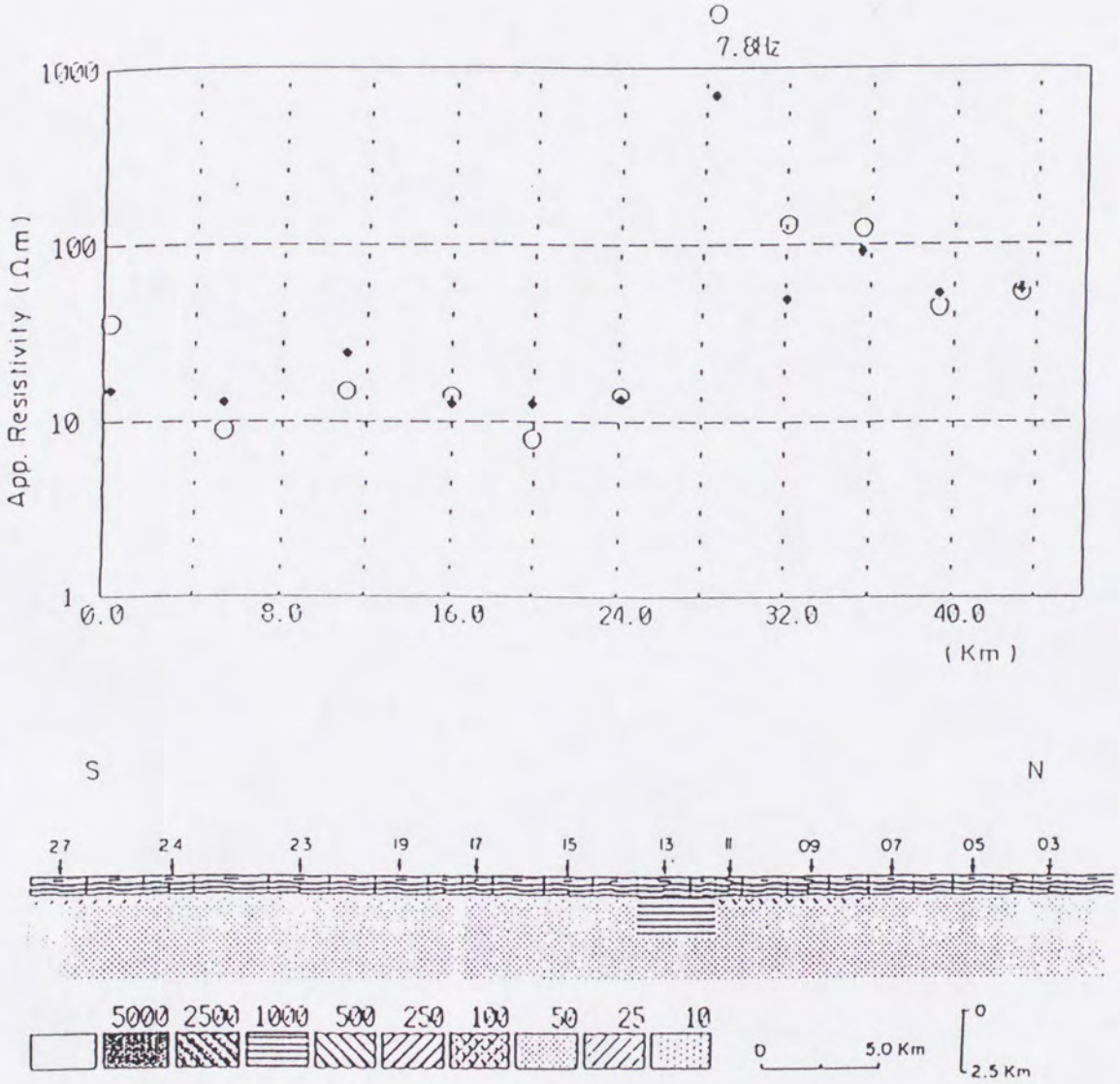
7.8Hz
10000
100
10
1
App. Resistivity (Ω.m)
0.0
8.0
16.0
24.0
32.0
40.0
(Km)
S
N
27
24
23
19
17
15
13
11
09
07
05
03
5000
2500
1000
500
250
100
50
25
10
0
5.0 Km
0
2.5 Km

e

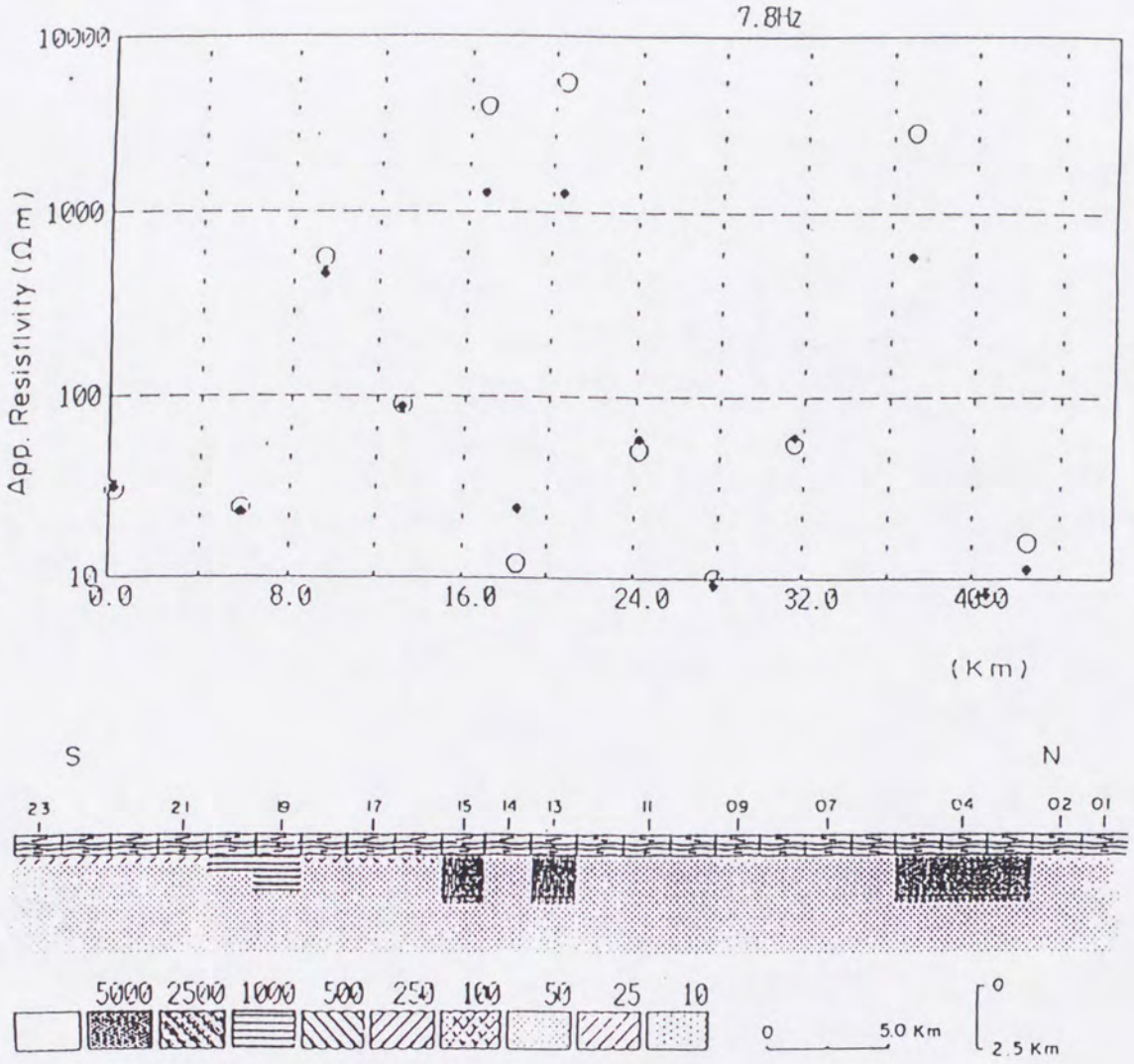
7.8Hz
10000
1000
100
10
App. Resistivity (Ω m)
0.0
8.0
16.0
24.0
32.0
(Km)
S
N
23
21
19
17
15
14
13
11
09
07
04
02
01
5000
2500
1000
500
250
100
50
25
10
0
5.0 Km
0
2.5 Km

f

structure of the east side of Merapi volcano, EM line (Fig.45.e), shows mainly low resistivity value, 25-50 ohm-m, except beneath site 13 with resistivity value about 1000 ohm-m. WM line (Fig.45.f) has similar resistivity structure with EM line. However, there are some locations with resistivity more than 1000 ohm-m at site 19, 15 and 13. The distribution of low resistivity value may have relation with heat transferred from magmatic reservoir and groundwater distribution.

3.6. ELF-MT survey during the 1992 active stage

3.6.1. The 1992 eruption

The chronological processes of the 1992 eruption of Merapi volcano quoted from Tjetjep et al. (1993) is as follows:

January 20, 1992: First glowing lava avalanche in the south-west flank of volcano was observed from Babadan and Ngepos observatory.

January 24, 1992 : First alert level was declared by the VSI.

January 31, 1992 : First glowing cloud occurred. It flowed down the south west flank to a distance of about 800 meters.

February 1, 1992 : After the occurrence of three times of glowing cloud reaching a maximum distance of about 900 meters, second alert level was declared by the VSI.

February 2,1992 : The number of the glowing lava avalanches increased and more frequent. The nuee-ardantes started almost uninterrupted.

12.31 : A series of seven times of nuee-ardantes began to a distance between 800 to 1500 meters. This completed at 13.54.

13.57 to 14.17 : Nuee- ardantes occured every minute, flowing until 2500 meters down.

14.20 to 14.52 : Nuee- ardantes continued, third alert level (one step before evacuation) was declared.

16.05 : First small eruption occurred in the summit during four minutes. The nue-ardantes flowed down to 4500 meters and the plume measures about 2600 meters high.

16.35 : A new explosion occurred within three minutes, the plume could not be estimated due to the cloudy weather.

18.42 : Small explosions were heard from the summit and followed by nuee-ardantes descending the south-west to west flank. All the activities ceased at 22.30, although the glowing lava avalanches still happened.

Feb. 3-9, 1992 : Lava avalanches continuously occurred, giving a red view in the night, sometimes followed by nuee-ardantes. On February 7, 1992, an important lava avalanches occurred, accompanied by nuee-

ardantes with the plume about 2.5 kilometers high above the summit.

Feb.. 12, 1992 : Alert level was returned back to second level.

March 8, 1992 : Alert level was returned back to first level.

July 16, 1993 : Normal active of volcano announced after the decreasing of all parameters activities.

3.6.2. Geophysical data during active stage

Tjetjep et al. (1993) discussed physical and chemical data of Merapi volcano during the 1992 eruption which is monitored by Merapi Volcanological Observatory (MVO). Some of geophysical data are seismic activity, deformation and geomagnetic data.

Seismic wave propagated from Merapi can be distinguished mainly into two classifications, low frequency (LF) and high frequency (HF) seismic signals. The high frequency events are produced by the faulting mechanism below the volcano due to an excessive pressure during magma movement. Two types of high frequency original seismic waves can be distinguished. The first is those originating from a depth of more than two kilometers below the summit. The second is those originating from a depth of less than approximately one kilometer. Hypocenters of high frequency are situated vertically below the summit with a maximum horizontal distance of one kilometer from the vent.

Before the 1992 eruption, an increase of intense seismic activities was clearly recorded in the seismogram at MVO since 1989 until the onset of the eruption on February 2, 1992. A special type of seismic signal, called multiphase earthquakes, was clearly observed after the 1984 eruption, during growing of a dome. This phenomenon, however, was not so significant during 1992 dome formation. The number of high frequency and low frequency events decreased just after the onset of the 1992 eruption. This fact proved that all the seismic activities which increased since 1989 were closely related to the magmatic up flow leading to the eruption.

A trilateration network consisting of twelve measurement points was installed around Merapi summit in 1988. Re-measurement was carried out on August 1991 using Electronic Distance Meter to compare with the first measurement on August, 1988. The preliminary result shows that surface deformations (extension) happened ranging from 0.01 to 0.07 percent oriented NW-SE. This extension indicates that there is a fissure crossing the crater where lava extrudes from a dome without destruction preexisting dome.

Three electronic tilt meter stations were installed on the west flank of Merapi summit on November 1992. The system has recorded two significant changes which closely related to the occurrences of pyroclastic flows. An inflation of about 15 micro radian per day had been observable since 15 days before the onset of pyroclastic flows on February 3, 1993. A similar pattern in a lower scale occurred also on April 8, 1993.

Geomagnetic monitoring has been applied on Merapi since 1977 and was improved on November 1989. Four magnetometer stations have been installed. Two stations are monitoring stations located about two and three kilometers away from the summit. Two stations are reference stations located about 9 and 19 kilometers away of the volcano.

A significant anomaly was observed at monitoring stations during the period of July-September 1990 measuring about 0.5 nT. This anomaly was estimated as related to seismic crisis on August 26, 1990. The later anomaly was observed in the period of May-August 1991 with an increasing total magnetic intensity of 4 nT. This variation was related to the increasing seismic energy released on September 1991. The increase of magnetic intensity was clearly observed in the period of January- February 1992 which than followed by eruption. Increasing magnetic intensity of volcano is closely related to the piezomagnetic effect so that it might have a correlation with the seismic energy release of shallow earthquakes.

3.6.3. Change of resistivity structure during active stage

The 1992 eruption of Merapi volcano was initiated by glowing lava avalanches on January 20, 1992 and the Merapi volcano was declared back to normal active volcano on July 16, 1993 (see section 3.6.1). Therefore, Merapi had been in the active stage during period from January 1992 to July 1993.

The ELF-MT re-measurement was carried out in order to examine resistivity change during the active stage of Merapi volcano. Eleven and twelve MT sites were measured on the north and the south flanks of Merapi. The survey was carried out on May 1992 for the north flank and on May 1993 for the south flank. The MT sites are coincident with the MT sites before the1992 eruption (Fig.46). The method and instrumentation which were used in the MT re-measurement are the same as the previous MT survey.

Fig.47 shows the result of MT measurement on the north and on the south flanks of Merapi before and during the active stage. The apparent resistivity of the north flank before the active stage is generally less than 300 Ohm-m, except those at site 1 and 2 about 600 to 800 ohm-m. The apparent resistivity changes are not clearly observed from site N-3 to the lowest altitude (site N-11) which is measured during the active stage both in ELF and VLF. Significant apparent resistivity changes observed at site 2 were about 6 to 12 times lower than before the increasing activities for frequencies 14.0 and 7.8 Hz. However, reverse results are found on the south flank. The apparent resistivity during the active stage at the lower altitude sites of the south flank (from site S-5 to site S-14) are relatively no high variation compared with before active . This case is almost the same as in the north flank. Remarkable resistivity changes were observed at site 3 and 4, (upper part of volcano) for all frequencies. At these sites, the resistivities during active stage are higher than before eruption, interesting phenomena. This phenomena may be explained as follows:

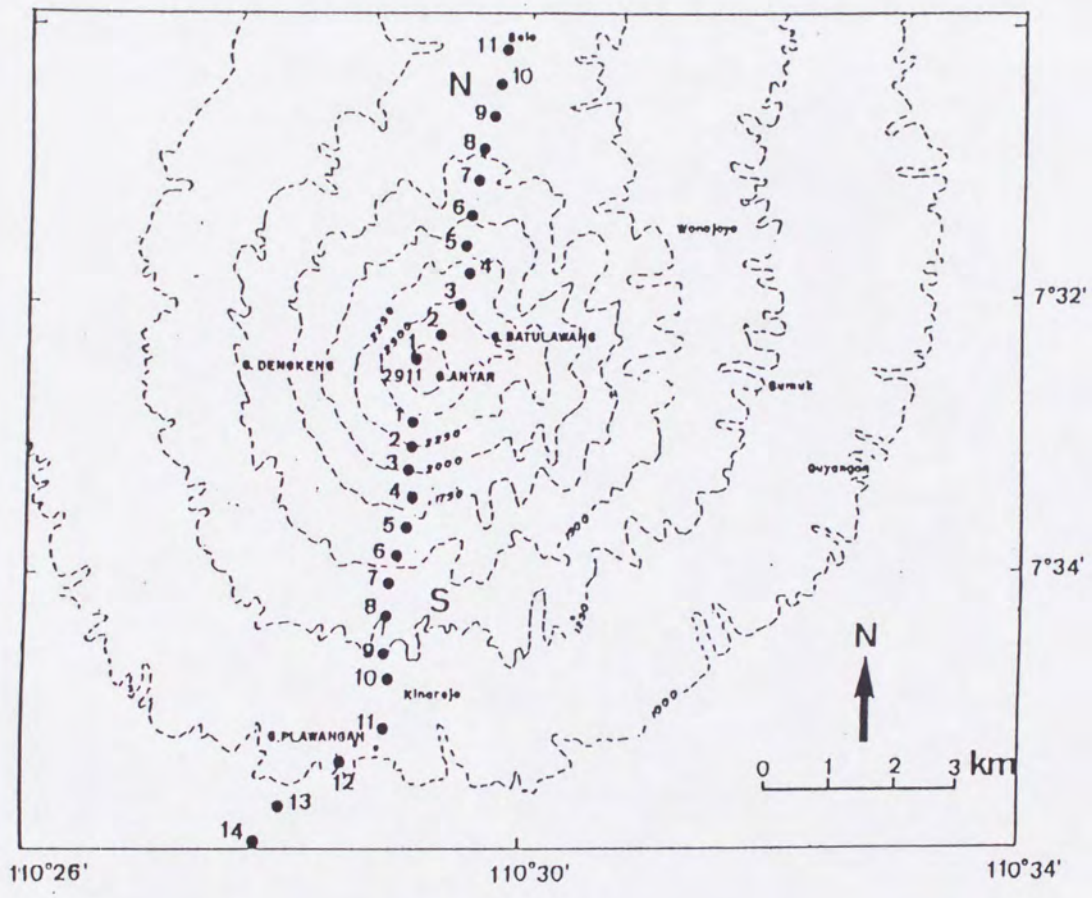

Fig.46. Location of ELF-MT re-measurement sites at the north and south flanks of Merapi volcano during the 1992 active stage.

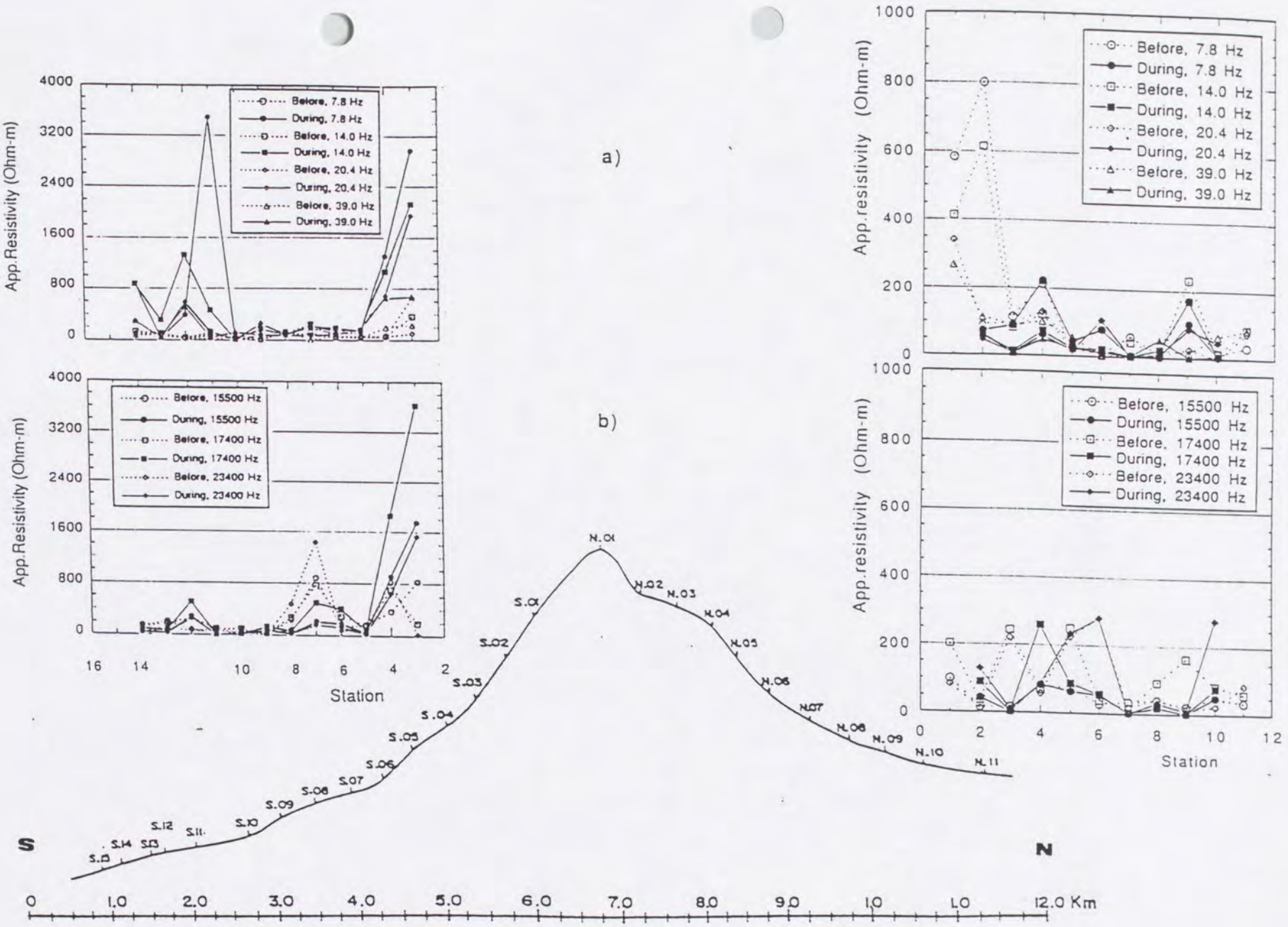

Fig.47. Apparent resistivity value of north and south flanks, before and during the 1992 active stage. a) ELF, b) VLF.

During the active stage of a volcano, high temperature magma rises up through magma vent foward the surface. The magma transfers the own heat into the surrounding rocks on the way of extrusion. The electrical resistivity of rock is highly dependent on temperature (Parkhomenko, 1967). When the temperature rises, the resistivity decreases. If the rock is subjected to melting, the decreasing of the resistivity is more drastic. Resistivity of the molten basalt in the lava lake of the Kilauea-Iki crater was obtained about 2.5 ohm-m. This is about 40 times lower than the resistivity of a sample of the same rocks immediately below the melting point (Keller and Rapolla, 1974). The resistivity also depends on the content of liquids in the rock. The liquid is usually ionized and their resistivity is low. Heating a rock usually works to reduce the resistivity. However, if the rock is heated beyond the boiling point of the contained fluid, the resistivity increase because of the resistivity of vapor is extremely high in contrast to its liquid state (Yukutake et al., 1990). If the rocks contain a bit of fluid, the area will dry up and resistivity of the rocks increase.

The site N-2 of the north flank is located at about 500 m from the central summit with altitude 2,628 m. Site S-3 of the south flank is located at about 1,250 m from the central summit with altitude 1,966 m above sea level. This situation matches that the site N-2 is located near the vent where the high temperature source coming and site S-3 is located in a little away from the summit or this site may be located in the dry area. Therefore, during the active stage the resistivity at site N-2 decrease and the resistivity at site S-3 increases.

Two-D resistivity structure before the 1992 eruption and during the active stage of the north flank are presented in Fig.48. The resistivity changes are clearly observed. The resistivity of accumulated lava dome and lava flow at the summit area decrease from 1000 to 3000 ohm-m before eruption to be 100 to 300 ohm-m during the active stage. The decreasing of resistivity value is approximately about 10 times. Change of the basement layer and the volcanic body resistivities during the active stage are also observed. The change is not so significant to compare with the summit area that is about 3 times lower than before eruption.

3.7. Discussion

Distributions of the low resistivity value around Merapi volcano is a related roughly with altitude. The lower the altitude is, the wider the distribution of low resistivity layer. The mean annual rainfall around Merapi volcano is about 3,500 to 4,000 mm/year. It produces the low resistivity value beneath Merapi volcano. The hydrogeological map around Merapi shows that the underground water table exists to about 1,500 meters above sea level beneath the Merapi volcano. At the foot of Merapi volcano, the water table is the level of 500 meters above sea level (Djaelani, 1982).

Collapses of volcanos happened frequently, in Java, as these volcanoes are located on soft, unconsolidated Late Tertiary sediments

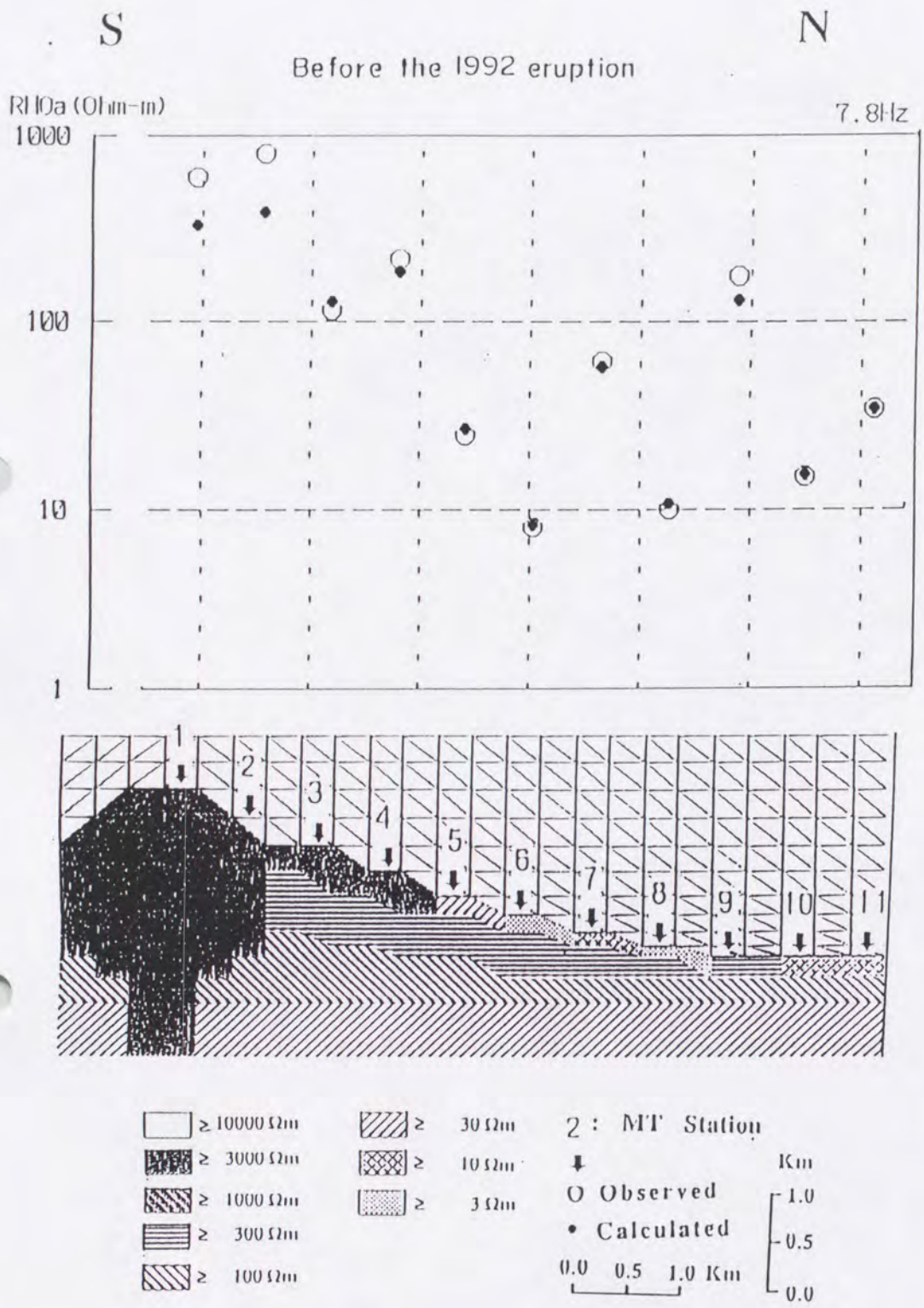

Fig.48-1. Resistivity structure of Merapi volcano inferred from ELF-MT 2-D model, before and during the 1992 active stage of the north flank. Numerals of legend denote resistivity in ohm-m.

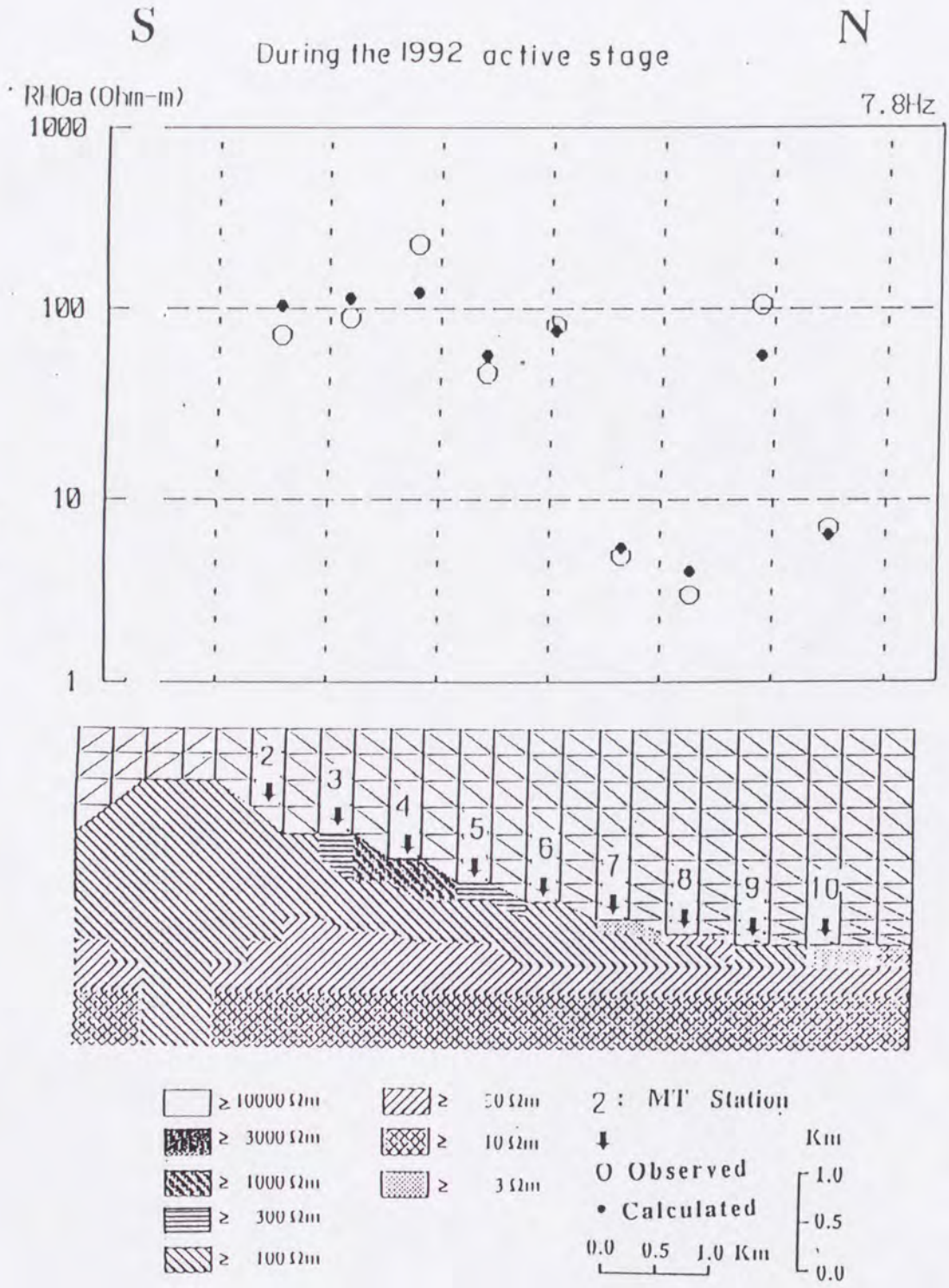

Fig.48-2. Resistivity structure of Merapi volcano during the 1992 active stage.

(Van Bemmelen, 1949). The existence of the unconsolidated sediments beneath Merapi and Merbabu volcanoes is related with the sharp decreasing of regional gravity profile along north-south trend (Yokoyama, 1974). Beneath Merapi volcano the low gravity zone is characterized by a concentric shape around the summit. This residual gravity anomaly is about -40 mgal, at the summit area (Arsadi et al, 1991). If it is assumed that soft and unconsolidated Late Tertiary sediments are founded beneath the Merapi volcano and has the low resistivity value caused in the case of saturated by groundwater.

However, analysis of A-type volcanic seismicity beneath the Merapi volcano reveals the existence of a shallow magma reservoir about 2-3 km depth (Ratdomopurbo, 1991). This depth coincides with the upper level of low resistivity layer. The evidence of hot spring at the level 1,000 m at the south and the west flanks of Merapi indicates that the conductive basement of Merapi volcano corresponds with the existence of high temperature body. The low resistivity basement layer is strongly suggested to be controlled by heat coming from magma reservoir or magma chamber especially beneath Merapi volcano with saturated underground water at the foot of meia. Ingham (1992) found that the low resistivity value under the crater is related to the hydrothermal system.

The influence of underground water with high temperature is to lower the resistivity of the formation. The temperature at the boundary between the second and the third layer may be estimated using Eq.(21). The temperature is about 218 to 298 °C assuming that the resistivity at reference temperature of 18 °C is in the range from 150 to 200 ohm-m and resistivity at the boundary layer is about 25 ohm-m. During

the active stage, the high frequency seismic activities are produced by the faulting mechanism below the volcano due to excessive pressure during magma movement. Hypocenters of high frequency earthquakes of Merapi are situated vertically below the summit with maximum horizontal distance of one kilometer from the vent (Tjetjep et al., 1993). This result is in agreement with the MT measurement during the active stage that no significant resistivity changes was observed at the sites located more than 2,000 m from the central summit. Ogawa et al. (1992) found difference in basement resistivity before and after the Izu-Oshima eruption in 1986. This phenomena is also evidence that change of resistivity value in an active volcano has strong relationship with the volcanic activities.

3.8. Summary

The resistivity structure of Merapi volcano before eruption is characterized by the high resistivity value, more than 1000 ohm-m, around the summit area. This high resistivity value has correspondence with an accumulation of lava dome, lava fragments and lava flow in dry condition. The magma vent of Merapi volcano has a diameter approximately about 500 meters which is recognized from high resistivity value at the site N-1 (Fig. 48-1).

The volcanic body of Merapi volcano which is composed of tuff, sand, lava flow and pyroclastic deposits has a resistivity value from 100 to 250 ohm-m. The low resistivity layer is assumed to be the basement

layer of Merapi volcano. This layer has wide distribution not only beneath the volcanic body of Merapi volcano but also in the adjacent area of Merapi volcano with resistivity value from 25 to 50 ohm-m. Heat from the magma reservoir is thought to have lowered the resistivity beneath Merapi, and the existence of grounwater may explain the low resistivity layer around Merapi area.

The magma movement during the active stage is closely related with the change of the resistivity value. However, the change in resistivity value of the volcanic material depends on the distance of observation site position from the magma vent. Resistivity of the volcanic material of Merapi volcano decreases about 10 times at site N-2 which located about 500 meters from the vent during the active stage (Fig.48-2). However, the resistivity of site S-3, located approximately 1,250 meter from the vent to the south, increases about 6 times compared to that before the 1992 eruption (Fig. 48-1). This change resulted by drying of the rocks with high temperature at the south of the dome.

These remarkable change of the resistivity during eruption can be used the monitoring the volcanic activity at Merapi.

4. COMPARISON BETWEEN SAKURAJIMA AND MERAPI VOLCANOES

Sakurajima and Merapi volcanoes have similarity in the global tectonic setting. Both volcanoes are erupted at the volcanic arc related to subduction. Sakurajima volcano is situated at the subduction of the Philippine sea plate under the Eurasian plate while Merapi volcano is located at the subduction of the Indian-Australian plate under the Eurasian plate. Sakurajima volcano existed in the graben-like structure of the Kagoshima Bay and formed as a volcanic island in the southern rim of the Aira caldera (Aramaki, 1984, Yokoyama, 1986). Merapi volcano is situated in the intersection of the two faults in the mainland of Java island (Bemmelen, 1949). Geologically, the basement complex at Sakurajima volcano is the Shimanto Group which is made up of highly deformed Mesozoic to Paleogene sediments of shale, sandstone, conglomerate and minor pillow lavas. The basement of Merapi volcano is soft and unconsolidated Late Tertiary marine sediments (Bemelen, 1949).

Both volcanoes are the strato volcano, classified as highly active and situated near dense populated cities. The diameter of Sakurajima is approximately 8 km with altitude 1,118 meters and Merapi has diameter about 12 km with altitude 2,986 meters above sea level. Eruption types and the chemical compositions of the lava flow extruded from the volcanoes are also different. Since, eruption type of Sakurajima volcano is characterized by emision of gas accompanied occasionally by lithic blocks and pumice but no lava flows, whereas Merapi volcano is characterized by formation of lava domes or lava tongues accompanied

by nuee ardantes. The rocks of Sakurajima are pyroxene andesite and dasite with SiO_2 content from 57 to 67 weight percent (Fukuyama and Ono, 1981). The rocks of Merapi volcano are in general pyroxene-hornblende, basaltic andesite with silica contents ranged between 50 to 57 weight percent (Merapi Volcano Observatory, 1990).

Yokoyama (1986) discussed the crustal deformation of Sakurajima caused by the 1914 eruption and interpreted it by assuming a model with two pressure sources or two magma chambers. One is shallow about 2 km deep directly below the volcano and the other one is about 8 km beneath the volcano. The interpretation of seismic data suggests that Merapi volcano has two magma reservoirs, about 2 to 3 km and about 7-8 km deep. These magma reservoirs are directly beneath the summit (Ratdomopurbo, 1991). Sakurajima volcano does not show any remarkable gravity anomalies (Yokoyama and Ohkawa, 1986). On the contrary, Merapi volcano is characterized by concentric low gravity anomalies. Observations of vertical ground deformation around Sakurajima show a more significant change of the ground surface related to the volcanic activity (Sakurajima volcano Observatory, 1988) than that around the Merapi volcano. These ground deformation is effected by the magma volume, plasticity of the magma chamber wall and magma temperature.

We found a four-layer resistivity structure beneath Sakurajima volcano inferred from MT survey. The first layer is about 250-3,000 ohm-m resistivity with 50-100 m thickness. The second layer has mainly 100-150 ohm-m resistivity and 200-300 m below the sea level. The third layer is about 300-1500 resistivity with 200-300 m thickness. The basement

layer of the resistivity structure has a resistivity smaller than 10 ohm-m. The first , second, and third layers are correlated to the lava flows of the Sakurajima volcano, unconsolidated pyroclastic deposits from the Aira caldera and the Kekura Formation, respectively. The fourth layer is also the Kekura Formation which coincides with the 800 m depth of the Koike borehole data. Different resistivity between the third and the fourth layers in the same formation (Kekura Formation) may be caused by the influence of the temperature resulting from magma activity and also the content of minerals. The resistivity of the southern part of the volcano is lower than the northern part. This si in agreement with the other data that the magma activity is concentrated in the southern part of the Sakurajima volcano.

Two-dimensional model analysis of the Merapi MT data shows that the resistivity structure beneath Merapi volcano is characterized by three layers. The first layer mainly represents the young lava flows of Merapi volcano with resistivity values ranging from 50 to 3,000 ohm-m and 50-150 m thickness. The second layer with 100-250 ohm-m resistivity corresponds to the volcanic products such as tuff, lava flows, lava fragments, and pyroclastics which built Merapi volcanic body. The thickness of the second layer coincides with the shape of the volcanic body. The resistivity of the basement layer beneath Merapi volcano is about 25-50 ohm-m situated at an altitude about 600 m above sea level. This low resistivity layer is distributed not only beneath Merapi volcano but also at the foot area of Merapi. Underground water distribution and heat transferred from magmatic activity are predicted to contribute in lowering resistivity of the basement layer. Estimated temperature at the

boundary of the second and the basement layers is about 218-298°C. The high resistivity value, more than 1,000 ohm-m, is observed before the 1992 eruption around the summit area. It is suggested as accumulated porous lava or dry lava. This laver is observed continuously to the depth of about 2-3 km vertically beneath the summit and might be a magma vent of Merapi volcano.

There are three noticeable differences in resistivity structure between Sakurajima and Merapi volcanoes. 1) The low resistivity zone related to magmatic activity is concentrated in the southern part of Sakurajima volcano while the Magmatic activity of Merapi volcano is vertically beneath the summit. 2) The resistivity of the bottom layer of Sakurajima volcano is higher than of Merapi volcano. 3) The magma vent of Merapi volcano is identified by high resistivity up to depths of 2-3 km.

The difference of volcanic eruption types of Sakurajima and Merapi volcanoes relating to their resistivity structure can be explained as bellow:

The viscosity of magma is one of the parameter that influences the eruption type of volcano. The viscosity of magma depends on several factors, including the chemical composition of the magma, the amount of the gas in it, the amount of solid load being carried by it, and its temperature.

Chemical compositions of rock samples of Sakurajima and Merapi volcanoes which were collected from the lava flows and lava bombs after 1955 eruption, show that the SiO_2 contents of Sakurajima volcano are 59-60 wt % , and of Merapi rocks, 53-56 wt %. Basic magma rich in Mg, Fe, and Ca are usually hot and fluid, while acid magma rich in

Al, and alkali-rich magmas, are cooler and much more viscous (Macdonald, 1972). Based on magma chemistry, the magma of Sakurajima volcano should be more viscous than the magma of Merapi volcano. However, the results of MT measurements show a reversed condition with the fact in the field.

The lava of Merapi volcano show porphyritic texture. Phenocrysts of plagioclase, pyroxene and opaque minerals having 2 mm maximum length are distributed randomly in the matrix (Arsadi et al., 1993). Anei (1779) and Taisho (1914) lavas of Sakurajima volcano contain microphenocrysts of olivine (Kobayashi, 1982). Even compared to the old lava of Sakurajima volcano, Merapi rocks are more porphyritic than Sakurajima volcano. The presence of lava fragments in the vent of Merapi volcano should contribute in increasing magma viscosity during eruption. The presence of high resistivity, more than 1000 ohm-m, in the vent of Merapi volcano which may be lava fragments in dry condition, are observed based on the ELF-MT survey before 1992 eruption.

Thermal data was not obtained for the Koike borehole down to 800 m depth at Sakurajima volcano (Aramaki, 1977) , because the borehole was made mainly for the stratigraphic study. Based on the thermal gradient map of the Japanese Islands (Okubo, 1993), the temperature gradient beneath Sakurajima volcano is higher than 10^{o}C/100 m. However, estimation of temperature beneath Sakurajima volcano is still difficult from this data. Unfortunately, there is no data related to thermal distribution or thermal gradient beneath Merapi volcano. The conductive layer beneath Sakurajima and Merapi volcanoes inferred from 2-D model analysis of ELF-MT data, exhibit different resistivity value, less than 10

ohm-m of Sakurajima and 25-50 ohm-m of Merapi, respectively. Thermal effect and mineral alteration caused by hydrothermal process are the common processes in decreasing resistivity in a volcanic area. If there are different thermal conditions in shallow magma chamber beneath Sakurajima and Merapi volcano, it is natural that the magma viscosity of Merapi volcano is higher than that of Sakurajima volcano.

REFERENCES

Abe, E., Katsura, K., Nishimura, S. and Eto, T., 1975. The Bouguer anomaly and their secular variation around Aira caldera, Kagoshima Pref. Rep. 1st Joint Obs. Sakurajima Volcano, Sakurajima Volcanol. Obs., Disas. Prev. Res. Inst., Kyoto Univ, 58-61. (in Japanese).

Aiken, C.L., Ander, M.E. and Fuentec, M.F., 1991. Geophysical investigations of the Platanares geothermal site, Honduras, Central America. J. Volcanol. Geotherm.Res., 45, 71-90.

Aramaki, S., 1977. Basement of Aira caldera and ejecta from Sakurajima volcano. Rep. 2nd Joint Obs. Sakurajima Volcano, Sakurajima Volcanol. Obs., Disas. Prev. Res. Inst., Kyoto Univ., 105-119. (in Japanese)

Aramaki, S., 1984. Formation of the Aira caldera, southern Kyushu, ~22,000 years ago. J. Geophys. Res., 89, 8485-8501.

Arsadi, E.M., Suwijanto, Nishimura, S., Nishida, J., 1989. Preliminary report on magnetotelluric (MT) survey crossing the Semangko fault. Geol.Indon., v.12, no.1, 215-226.

Arsadi, E. M., Anshori, Ch., Supriyanto, J., Sudrajat, Y. and Yusuf, M., 1991. Subsurface structure of Merapi volcano based on magnetotelluric, gravity and magnetic surveys. Interim report of R & D Centr. for Geotech., LIPI, no.11/PPPG/90.

Arsadi, M.E., Hie,K.T., Soempono,S.L.T. and Sudrajat, Y.,1993. MT measurement during active stage of Merapi volcano and rocks samples analysis. Intern report of Res. and Dev.Center for Geotech. no.05/01.06/04/PPPGT/93.

Ballestracci, R., 1982. Audiomagnetotelluric profiling on the volcano Stromboli, internal structure and mechanism of the Strombolian activity. J. Volcanol. Geotherm. Res., 12, 317-337.

Bemmelen, R.V. W., 1949. The Geology of Indonesia, The Hague,vol.1a.

Bendat, J.S. and Piersol, A.G., 1971. Random Data: Analysis and Measurement Procedures. John Willey and Sons Inc., New York, 407 pp.

Blank, H.R.Jr., Aramaki, S., and Ono, K., 1966. Aeromagnetic surveys of Kuttaryo and Aso caldera regions. Bull. volcanol.Soc.Jpn., 11, 40.

Cagniard, L., 1953. Basic theory of the magneto-telluric method of geophysical prospecting. Geophysics, 18, 605-635.

Cantwell, T. and Madden, T.R., 1960. Preliminary report on crustal magnetotelluric measurement. In: Vozoff, K. ed., Magnetotelluric Methods. Geophysics Reprint Series 5, Soc. Explo. Geophysicists, Tulsa, 516-519.

Chujo, J. and Murakami, F., 1976. The geophysical preliminary surveys of Kagoshima Bay. Bull. Geol. Surv. Japan, 27, 807-826. (in Japanese with English abstract).

Clarke, J. and Goldstein, N.E., 1982. Magnetotelluric measurement. In: Vozoff, K. ed., Magnetotelluric Methods. Geophysics Reprint Series 5, Soc. Explo. Geophysicists, Tulsa, 544-555.

Djaelani, A., 1982. Hidrogeological map of Indonesia, Sheet of Yogyakarta (Jawa), Scale 1:250,000. Directorat of Environmental Geology, Indonesia.

Ehara. S., 1992. Thermal structure beneath Kuju volcano, central Kyushu, Japan. J. Volcanol. Geotherm. Res., 54, 107-115.

Fukuyama, H., 1978. Geology of Sakurajima volcano, southern Kyushu. J. Geol. Soc. Japan, 84, 309-316.(in Japanese with Englishabstract)

Fukuyama, H. and Ono, K., 1981. Geological Map of Sakurajima Volcano 1:25,000, Geol. Map Volcanoes 1. Geol. Surv. Japan, Tsukuba.

Furuya, T., 1989. Geomorphology of Merapi volcano. Volcanic Sabo Technical Centre. Japan International Cooperation Agency.

Galanopoulos, D., Hutton, V.R.S. and Dawes, G.K.J., 1991. The Milos geothermal field: modeling and interpretation of electromagnetic induction studies. Physics of the earth and Planetary interiors., 66, 76-91.

Goldberg, S., Rotstein, Y. 1982. A simple form of presentation of magnetotelluric data using the Bostick transform. Geophysical Prospecting, 30, 211-216.

Goldstein, M.A., 1971. Magnetotelluric experiments employing an artificial dipole source. Ph.D Thesis, Univ.of Toronto.

Goldstein, M.A., and Strangway, D.W., 1975. Audio-frequency magnetotellurics with a grounded electric dipole source. Geophysics, 40, 669-683.

Gunawan, W.A.K., 1985. Analysis of the Gravity Free Air Anomaly of Merapi volcano and its adjacent area. B.Sc thesis of Physical Department, Gajah Mada University, Yogyakarta, Indonesia.

Handa, S. and Sumitomo, N., 1985. The geoelectric structure of the Yamasaki and Hanaori faults, southwest Japan. J. Geomag. Geoelectr., 37, 93-106.

Hasegawa, K., 1985., 1985. On the step response and the apparent conductivity for a stratified earth by a horizonta electric dipole. Butsuri-Tansa (Geophysics.Explor.), 38, 21-31 (in Japanese with English Abstract).

Hayasaka, S. and Oki, K., 1971. Geological consideration on the subsurface data from the deep wells drilled in Kagoshima City, south Kyushu, Japan. Rep. Fac. Sci., Kagoshima Univ., Earth Sci. Biol., 4, 15-30. (in Japanese with English abstract).

Honkura, Y., Nibblet, E. R. and Kurtz, R.D., 1976. Changes in magnetic and telluric fields in a seismically active region of eastern Canada: preliminary results of earthquake prediction studies. Tectonophysics, 34, 219-230.

Ingham, M. R., 1988. The use of invariant impedance in magneto-telluric interpretation. Geophysics.J., 92, 165-169.

Ingham, M. R., 1991. Electrical conductivity structure of the Broadlands-Ohaaki geothermal field, New Zealand. Physics of the earth and Planetary interiors., 66, 62-75.

Ingham, M. R., 1992. Audiomagnetotelluric soundings on White Island volcano. J. Volcanol. Geotherm. Res., 50, 301-306.

Ishihara, K., 1988. Geophysical evidences on the existence of magma reservoir and conduit at Sakurajima volcano, Japan. Ann. Disas. Prev. Res. Inst., Kyoto Univ., 31, B-1, 59-73. (in Japanese with English abstract).

Ishihara, K., Takayama, T., Tanaka, Y. and Hirabayashi, J., 1981. Lava flows at Sakurajima volcano (I)–Volume of the historical lava flows–. Ann. Disas. Prev. Res. Inst., Kyoto Univ., 24, B-1, 1-10. (in Japanese with English abstract).

Jupp, D.L.B. and Vozoff, K., 1976. Discussion on "The magnetotelluric method in the exploration of sedimentary basins" by Keeva Vozoff (Geophysics, February 1972, p.98-114). Geophysics, 41, 325-328.

Kamada, M.,1975. Volcanic activity and environment, Bull.volcanol.Socc.Jpn., Ser.II,20,355-262.

Kamo, K., Nishi, K., Furusawa, T., Akamatsu, J., Kikuchi, S., Ono, H., Sudo, Y., Takagi, A., Unno, N., Hori, S., Sato, Y. and Kakuta, T., 1977. On the seismicity and the detection of anomalous propagation of seismic wave around the Aira caldera. Rep. 2nd Joint Obs. Sakurajima Volcano, Sakurajima Volcanol. Obs., Disas. Prev. Res. Inst., Kyoto Univ., 13-20. (in Japanese).

Kamo, K., Nishi, K., Takayama, T. and Ueki, S., 1980. Seismicity and the anomalous propagation area of seismic wave at the south of Sakurajima. Rep. 3rd Joint Obs. Sakurajima Volcano, Sakurajima Volcanol. Obs., Disas. Prev. Res. Inst., Kyoto Univ., 11-15. (in Japanese).

Karaushi, K., Nakaya, K., Sakai, H., Ikeda, K., Sugawara, T., Owada, T., Fukushima, H., Yamamoto, T., Kato, S., Kuwashima, M., Agei, T., Tanaka, Y. and Masuda, H., 1989. Geomagnetic and geoelectrical observation in and around Sakurajima. Rep. 7th Joint Obs. Sakurajima Volcano, Sakurajima Volcanol. Obs., Disas. Prev. Res. Inst., Kyoto Univ., 47-58. (in Japanese).

Katsura, I., 1990. Block structure bounded by active strike-slip faults in the northern part of Kinki district, southwest Japan. Mem. Fac. Sci., Kyoto Univ., Geol. Mineral., 55, 57-123.

Kaufman, A.A. and Keller, G.V., 1981. The Magnetotelluric Sounding Method. Methods in Geochemistry and Geophysics 15, Elsevier Sci. Pub. Co., Amsterdam, 595 pp.

Keller, G.V. and Frischnect, F.C., 1966. Electrical methods in geophysical prospecting. Pergamon press, 197-250.

Keller, G.V. and Rapolla, A., 1974. Electrical prospecting methods in volcanic and geothermal environments. In: Civetta, L., Gasparini, P., Luongo, G. and Rapolla, A. eds., Physical Volcanology. Developments in Solid Earth Geophysics 6, Elsevier Sci. Pub. Co., Amsterdam, 133-166.

Kirbani, S.Bp., 1991. Analysis of volcanic tremor at Mount Merapi, Central Java, Indonesia. Thesis of Doctor degree at Department of Physics, Gajah Mada University, Indonesia.

Matsuzaki, T. and Utashiro, S., 1966. On the aeromagnetic surveys in the Kagoshima Bay and its vicinity. Rep. Hydrogr. Res., Mar. Safe. Agen. Japan, 1, 23-25. (in Japanese with English abstract).

Merapi volcano observatory, 1990. Annual report of volcanology, special edition of Merapi volcano, Volcanological Survey of Indonesia.

Mogi,T., Miyoshi,F., Kinoshita,K. and Zyomory,A., 1986. A geological structure survey by the ELF-MT method at the Zyoso terrace, Ibaraki prefecture, Central Japan. Butsuri tansa (Geophysical exploration), 39, 3 (in Japanese with English abstract).

Mogi, T., Arsadi, E.M., Nishimura, S., Katsura, I., Nishida, J. and Kusunoki, K., 1988. Resistivity structure beneath Sakurajima volcano inferred from ELF-magnetotellurics and controlled source audiofrequency-magnetotellurics prospecting. Proc. Kagoshima International Conference on Volcanoes 1988, 268-271.

Mogi, T., Katsura, I. and Nishimura, S., 1991. Magnetotelluric survey of an active fault system in the Kinki district, southwest Japan. J. Structural Geol., 13, 235-240.

Mogi, T. and Nakama, S., 1993. Magnetotelluric interpretation of the geothermal system of the Kuju volcano, southwest Japan. J. Volcanol. Geotherm. Res., 56, 297-308.

Nekut,A.G., 1987. Direct inversion of time domain electromagnetic data, Geophysics, 52, 1431-1435.

Nelder, J.A. and Mead, R., 1965. A simplex method for function minimization, Computer J., 7, 308-313.

Newman, G.A., Wannamaker, P.E. and Hohmann, G.W., 1985. On the detectability of crustal magma chambers using the magnetotelluric method. Geophysics, vol.50, no.7.

Nishi, K., 1978. On the focal mechanism of volcanic earthquakes in Sakurajima volcano. Ann. Rep. Disas. Prev. Res. Inst., Kyoto Univ., 21, B-1, 145-152. (in Japanese with English abstract).

Nishi, K. and Iguchi, M., 1983. Preliminary report on the seismicity in south Kyushu. Ann. Disas. Prev. Res. Inst., Kyoto Univ., 26, B-1, 23-29. (in Japanese with English abstract).

Nishimura, S. and Mogi, T., 1986. The magnetotelluric survey around Sakurajima volcano, southern part of Kyushu, Japan. Ann. Rep. Disas. Prev. Res. Inst., Kyoto Univ., 29, B-1, 13-21. (in Japanese with English abstract).

Nishimura, S., Nishida, J. and Mogi, T., 1986. Gravity and magnetotelluric interpretation of the southern part of the Fossa Magna region, central Japan. J. Phys. Earth, 34, 171-185.

Nishimura, S., Abe, E. and Katsura, K., 1988. The secular variation of vertical gradient of gravity around Aira caldera. Rep. 6th Joint Obs. Sakurajima Volcano, Sakurajima Volcanol. Obs., Disas. Prev. Res. Inst., Kyoto univ., 55-62. (in Japanese).

Nishimura, S., Abe, E., Nishida, J. and Katsura, K., 1989a. The secular variation of gravity in Sakurajima. Rep. 7th Joint Obs. Sakurajima Volcano, Sakurajima Volcanol. Obs., Disas. Prev. Res. Inst., Kyoto Univ., 41-45. (in Japanese).

Nishimura, S., Arsadi, E.M., Katsura, I., Yamada, Y., Mogi, T., Nishida, J. and Kusunoki, K., 1989b. Resistivity structure of Sakurajima volcano inferred from ELF-MT and CSA-MT methods. Rep. 7th Joint Obs. Sakurajima Volcano, Sakurajima Volcanol. Obs., Disas. Prev. Res. Inst., Kyoto Univ., 59-63. (in Japanese).

Ogawa, T., Tanaka, Y. and Yasuhara, M., 1969. Schumann resonances and worldwide thunderstorm activity-Diurnal variations of the resonant power of natural noises in the earth-ionosphere cavity–. J. Geomag. Geoelectr., 21, 447-452.

Ogawa, T., Kozai, K., Kawamoto, H., Yasuhara,M. and Huzita, A., 1979. Schumann resonances observed with a balloon in the stratosphere. J. Atmos. Terr. Phys., 41, 135-142.

Ogawa, Y. and Takakura, S., 1990. CSAMT Measurement across the 1986 C Craters of Izu-Oshima Island, Japan. J Geomag. Geoelectr., 42, 211-224.

Ogawa, Y., Takakua, S. and Soya, T., 1992. Wideband Magnetotelluric across Izu-Oshima volcano. J.Geomag. Geoelectr., 44, 561-566.

Okubo, Y.,1993. Temperature gradient of the Japanese islands, Journal of the Geothermal Research Society of Japan, v.15 no.1, pp.1-21.

Ono, K., Ito, K., Hasegawa, I., Ichikawa, K., Iizuka, S., Kakuta, T. and Suzuki, H., 1978. Explosion seismic studies in south Kyushu, especially around the Sakurajima volcano. J. Phys. Earth, 26 suppl., S309-S319.

Ortiz, R., Aran~a, V., Astiz, M. and Gracia, A., 1986. Magnetotelluric study of the Teide (Tenerife) and Timanfaya (Lanzarote) volcanic areas. J. Volcanol. Geotherm. Res., 30, 357-377.

Padilha, A.L., Vitorello, I., Trivedi, N.B., Ribeiro, M. J. and Gross, J.M., 1992. Seasonal variation in apparent resistivity probably associated with drastic rainfall changes in Southern Brazil. J. Geomag. Geoelectr., 44, 651-660.

Parkhomenko, E.I., 1967. Electrical properties of rocks. Plenum, New York, N.Y., 314 pp.

Parkinson, W.D., 1983. Introduction to geomagnetism. Scottish Academic Press, 220-346.

Ratdomopurbo, A., 1991. Seismicity and vulcanic system of Merapi volcano. Interim report of Merapi volcanological observatory, Volcanological Survey of Indonesia, (in Indonesian).

Reddy, I.K. and Rankin, D., 1974. Coherence functions for magnetotelluric analysis. Geophysics, 39, 312-320.

Reddy, I.K. and Rankin, D., 1975. Magnetotelluric response of laterally inhomogeneous and anisotropic media Geophysics, 40, 1035-1045.

Sakurajima Volcano Observatory, 1988. Disaster Prevention Research Institute, Kyoto University.

Sentman, D.D., 1987. Magnetic elliptical polarization of Schumann resonance. Radio.Sci., 22,4,595-606.

Shibata, K., Ono, K., Hayasaka, S., Oki, K. and Yamamoto, M., 1978. K-Ar age of the Terukuni pyroclastic flow underlying Kagoshima City, southern Kyushu. J. Geol. Soc. Japan, 84, 551-553. (in Japanese).

Shimoizumi, M., Mogi,T., Suzuki, K., and Jomori,A., 1991. Development of TDEM instrunent using Fluxgate magnetometer, Boll.Condct.Anomaly Res.Group, 9-17.

Sims, W.E., Bostick,Jr., and Smith, H.W., 1971. The estimation of magnetotelluric impedance tensor element from measured data. Geophysics, 36, 938-942.

Siswowidjoyo, S., 1989. Mitigation of disasters caused by lahar on active volcanoes of short interval of dormancy with Merapi volcano in Central Java as the case of study. ISEV"89, Yogyakarta, Indonesia. S15.

Skokan, K.C.,1993. Overview of electromagnetic methods applied in active volcanic areas of western United States. J. Volcanol. Geotherm. Res., 56, 309-318.

Sumitomo, N. and Noritomi, K., 1986. Synchronous precursors in the electrical earth resistivity and the geomagnetic field in relation to an earthquake near the Yamasaki fault, Southwest Japan. J. Geomag. Geoelectr., 38, 971-989.

Swift, C.M. Jr., 1967. A magnetotelluric investigation of an electrical conductivity anomaly in the southwestern United States. In: Vozoff, K. ed., Magnetotelluric Methods. Geophysics Reprint Series 5, Soc. Explo. Geophysicists, Tulsa, 156-166.

Takasugi, S., Tanaka, K., Kawakami, N. and Muramatsu, S., 1992. High spatial resolution of the resistivity structure revealed by a dense network MT measurement. A case study in the Minamikayabe area, Hokkaido, Japan. J.Geomag.Geoelectr., 44, 289-308.

Ting, S.C. and Hohmann, G.W., 1981. Integral equation modeling of three-dimensional magnetotelluric response. Geophysics, 46, 182-197.

Tjetjep,W.S.,Ratdomopurbo,A.,Suharno,M.Ch.,Supriati,D.A., Subandriyo, and Sri Sumarti, 1993. Preliminary account of the 1992 eruption of Merapi, Central Java, Indonesia. Proceedings of the 22nd annual convention of the Indonesian Association of Geologists (IAGI), v.I, 241-257.

Untung,M. and Sato,Y., 1978. Gravity and geological studies in Java, Indonesia. Geological Survey of Indonesia and Geological Survey of Japan. A joint research program on regional tectonics of Southeast Asia Institute for transfer of Industrial technology project.

Utada, H. and Shimomura, T., 1990. Resistivity structure of Izu-Oshima volcano revealed by the ELF-VLF Magnetotelluric method. J.Geomag. Geoelectr., 42, 1969-194.

Vozoff, K., 1972. The magnetotelluric method in the exploration of sedimentary basins. Geophysics, 37, 98-141.

Widarto, D.S., 1993. Controlled Source Electromagnetic Studies in the vicinity of Waita volcano, Central Kyushu, and Its Geothermal Significance. D.Sc. Thesis of Department of Geology and Mineralogy, Kyoto University.

Wirakusumah, A.D., Juwarna, H. and Loebis, H., 1989. Geologic map of Merapi volcano, Central Java, scale 1: 50,000. Volcanological survey of Indonesia.

Yokoyama, H., Nakatsuka, K., Abe, M. and Watanabe, K., 1983. Temperature dependency of electrical resistivity of water saturated rocks and the possibility of underground temperature estimation. J. Geotherm. Res. Soc. Japan, 5, 103-120.

Yokoyama, I., 1961. Gravity survey on the Aira caldera, Kyushu, Japan. Nature, 191, 966-967.

Yokoyama, I., 1974. Geomagnetic and Gravity anomalies in volcanic areas. In: Civetta, L., Gasparini, P., Luongo, G. and Rapolla, A. eds., Physical Volcanology. Developments in Solid Earth Geophysics 6, Elsevier Sci. Pub. Co., Amsterdam, 167-193.

Yokoyama, I. and Ohkawa, S., 1986. The subsurface structure of the Aira caldera and its vicinity in southern Kyushu, Japan. J. Volcanol. Geotherm. Res., 30, 253-282.

Yokoyama, I., 1986. Crustal deformation caused by the 1914 eruption of Sakurajima volcano, Japan and its secular changes. J. Volcanol. Geotherm. Res., 30, 283-304.

Yukutake, T., Yoshino, T., Utada, H., Kawamura, M., Nagano, T., Kato, Y., Baba, H., Nakaya, K., Tanaka, Y. and Masuda, H., 1980. Electrical survey at Sakurajima. Rep. 3rd Joint Obs. Sakurajima Volcano, Sakurajima Volcanol. Obs., Disas. Prev. Res. Inst., Kyoto Univ., 55-62. (in Japanese).

Yukutake, T., Yoshino., T., Utada H., Watanabe, H., Hamano, Y. and Shimomura, T., 1990. Changes in the electrical resistivity of the central cone, Miharayama, of Oshima volcano observed by a direct current method. J.Geomag. Geoelectr., 42, 151-168.

Xu, S.Z., 1986. Quantitative estimation of an annual variation of apparent resistivity, J. Geomag. Geoelectr., 38, 991-999.

Zonge, K.L. and Hughes, L.J., 1991. Controlled Source Audio-frequency Magnetotellurics, in Nabhigian, M.N., Ed., Electromagnetic method in applied geophysics, vol.2, Soc.Explor.Geophysics., pp 713-809.